UNIVERSITY OF BIRMINGHAM

POWER SMOOTHING AND OSCILLATIONS SUPPRESSION BY CONTROLLING INERTIAL ENERGY OF WIND ENERGY SYSTEMS

by

XIANXIAN ZHAO

A thesis submitted to
The University of Birmingham
for the degree of
DOCTOR OF PHILOSOPHY

Department of Electronic,
Electrical and Systems Engineering
School of Engineering
The University of Birmingham
March 2018

To my parents and my supervisor

ACKNOWLEDGEMENTS

First of all, I would like to express my deepest gratitude to my supervisor, Prof. Xiao-Ping Zhang. It is a great honor for me to have Prof. Xiao-Ping Zhang as my supervisor for my PhD study. He has always been very patient, supportive, and encouraging. His generosity to share with me his understanding and visions of power systems and renewable generation allows the completion of this research work.

The PhD study was sponsored by the University of Birmingham Li Siguang Scholarship, the China Scholarship Council and UK EPSRC. I would like to greatly express my gratitude for the financial support.

I would like to thank Mr. Zuanhong Yan for his advices and help at the initial stage of my PhD study, and Dr. Ying Xue for his advices and inspiring discussions. The collaboration with them places a good basis for my further research. I would also like to thank Dr. Jianing Li, Dr. Conghuan Yang, Mr. Rui Guan, Mr. Jiajie Luo, Mr. Yang Liu, Mr. Min Zhao, Mr. Cong Wu and Mr. Kanghui Gu in the Electrical Power and Control Systems Group. It was very enjoyable working with them.

I must express my great appreciation to my family and my beloved Dr. Jianglin Lan, for their support, encouragement and understanding.

ABSTRACT

The thesis consists of three parts. The effectiveness of the proposed schemes is evaluated on Real Time Digital Simulator (RTDS).

In the first part, an economic scheme to smooth short periodic and heavily fluctuating wave power is proposed by controlling the inherent large amount of inertial energy of nearby offshore wind turbine systems (WTSs). The smoothing principle is that these WTSs are controlled to absorb the fluctuations of the wave power or release power opposite to them. The control challenge is that two objectives have to be achieved simultaneously: the rotor speed of a WTS has to be controlled against smoothing requirement whilst controlled to follow changes of wind speed to achieve wind power capture close to the maximum. To resolve this issue, Integrated Compensation Control (ICC) is developed by adding two supplementary terms into the original maximum power point tracking (MPPT) control.

In the second part, a method for short-term wind power smoothing is proposed by controlling wind turbines inertial energy. To achieve this, the structure of the power reference of ICC is applied, but through different derivation procedures considering in the specific wind power self-smoothing situation. The designed power reference of a WTS for wind power smoothing includes two components: one component can approximately recover the original power trajectory of the MPPT control and the other can compensate the fluctuations of the former.

In the third part, a new scheme to isolate and suppress forced oscillations is proposed. It controls the inertial energy of wind farms using ICC to timely release or absorb power opposite to the forced oscillating power from perturbation area(s). Thus, the forced oscillations are prevented from propagating to the rest of power grid - isolated and the oscillating power in the disturbed area(s) is also reduced - suppressed.

TABLE OF CONTENTS

LIST OF FIGURES

LISTS OF TABLES

LIST OF ABBREVIATIONS

WTS	Wind Turbine System
MPPT	Maximum Power Point Tracking
ICC	Integrated Compensation Control
DCC	Direct Compensation Control
WEC	Wave Energy Converter
OWC	Oscillating Water Column
AWS	Archimedes Wave Swing
PMSG	Permanent Magnetic Synchronous Generator
DFIG	Doubly Fed Induction Generator
FSIG	Fixed Speed Induction Generator
PCC	Point of Common Coupling
MAF	Moving Average Filter
RTDS	Real-Time Digital Simulator

CHPTER 1 INTRODUCTION

1.1 Research Background

1.1.1 Development of Renewable Generation

Fossil fuels have been the driving force for industry and economic growth all over the world since the dawn of the Industrial Revolution. This can be seen from Figure 1-1 that fossil energy has grown exceptionally in the last 200 years, and it is expected to continue growing in the future with worldwide economic growth and development. Nevertheless, the increasing world energy demand of fossil fuels contributes a significant part in air pollution and the upward trend in greenhouse gas emissions, especially CO_2 emissions. Figure 1-2 shows that the annual CO_2 emissions from fossil fuels combustion have increased from around zero, before the Industrial Revolution, to nearly 33 gigatons in 2015 [1]. It is well known that CO_2 is one of the main greenhouse gas emissions that contribute to global warming which results in various environmental impacts, e.g. glaciers melting, sea levels increasing and changes in the traditional agriculture productivities. It is commented in paper [2] that if we stay on our present course, the global emissions of CO_2 are projected to triple by 2040.

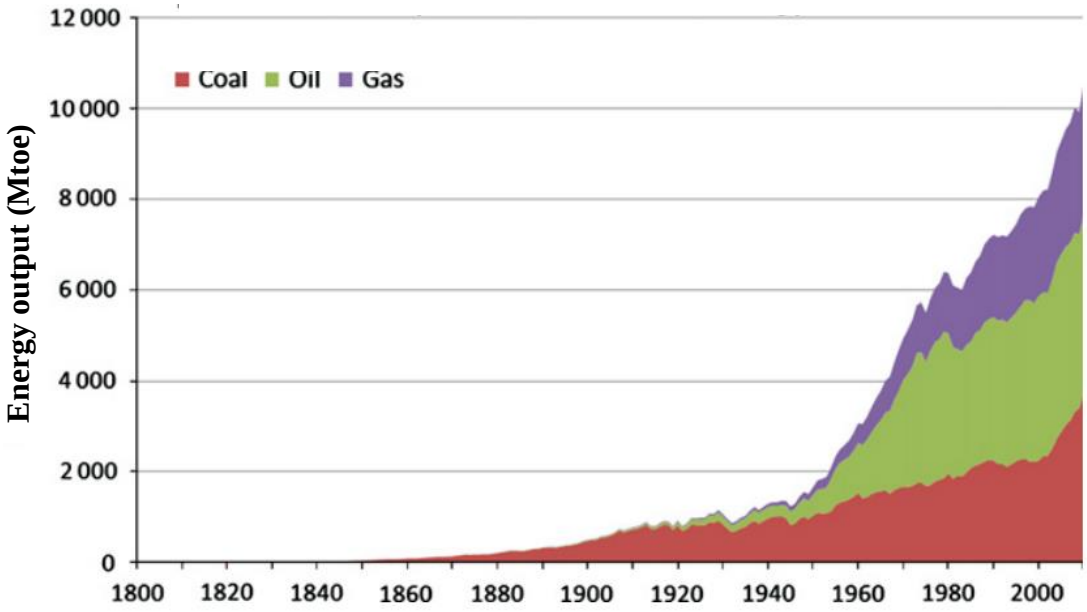

Figure 1-1 Worldwide fossil fuels production from 1800 to 2010 [3].

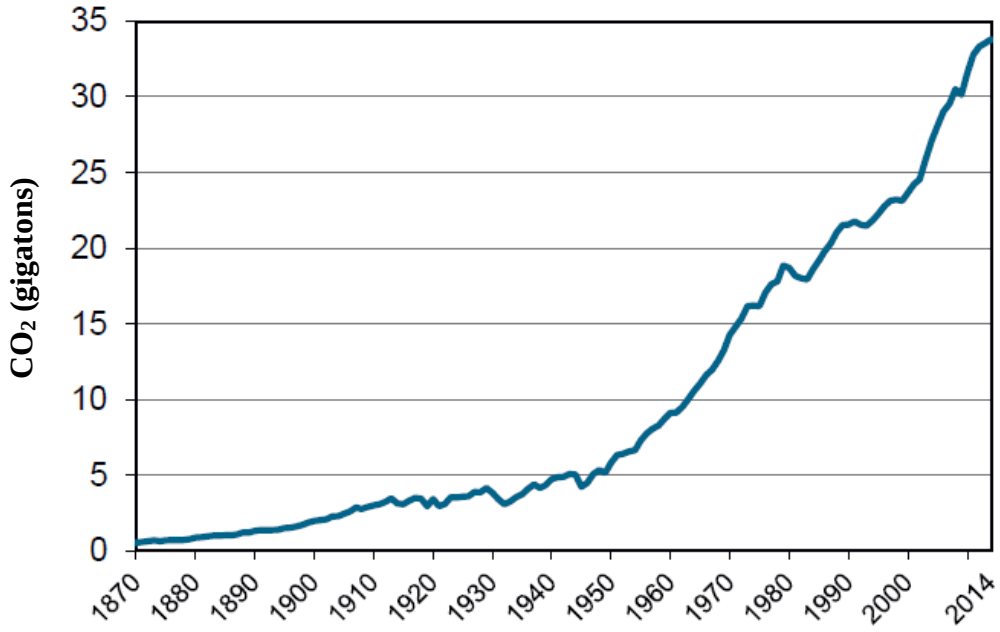

Figure 1-2 Trend in CO_2 emissions from fossil fuels combustion from 1870 to 2014 [4].

Among all economic sectors contributing to the global CO_2 emissions from fossil fuels combustion, electricity and heat generation are considered to be the largest sector, which accounts for 42% in 2015, as seen in Figure 1-3. With anticipated continuous growth of electricity demand (see Figure 1-4) [5], the electricity supply is under pressure to achieve

reduction in CO_2 emissions and thus seeking for renewable generation. The necessity of reducing CO_2 emissions via de-carbonization of electricity sector has been demonstrated by the International Panel on Climate Change (IPCC) [6] and has been discussed from an economic perspective in the Stern Report [7]. It is also reported in [8] that power system is a core factor for worldwide energy transition. In [8], a comparison is made for three Shared Socio-economic Pathways (SSPs) scenarios: SSP1 (A green growth strategy with sustainable development proceeding at a reasonably high pace), SSP2 (Intermediate road between SSP1 and SSP3) and SSP3 (A regional rivalry road where unmitigated emissions are high due to moderate economic growth, a rapidly growing population, and slow technological change in the energy sector, making mitigation difficult). SSP1 is characterized as a transition from a fossil-fuel dominated system (with around 90% of energy supply in 2010), towards an energy system where renewable energy is the key part. If SSP2 scenario is taken, by 2100 the total fossil fuels consumption will be substantially less than today's amount of fossil fuel use (see Figure 1-5) and renewable energy will become the major part of energy generation, accounting for 65% of the total supply (see Figure 1-6).

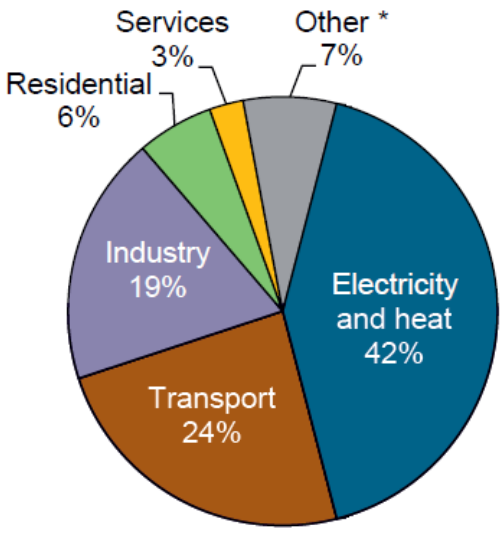

Figure 1-3 Worldwide CO_2 emissions from fossil fuels combustion by different economic sectors in 2015 [4].

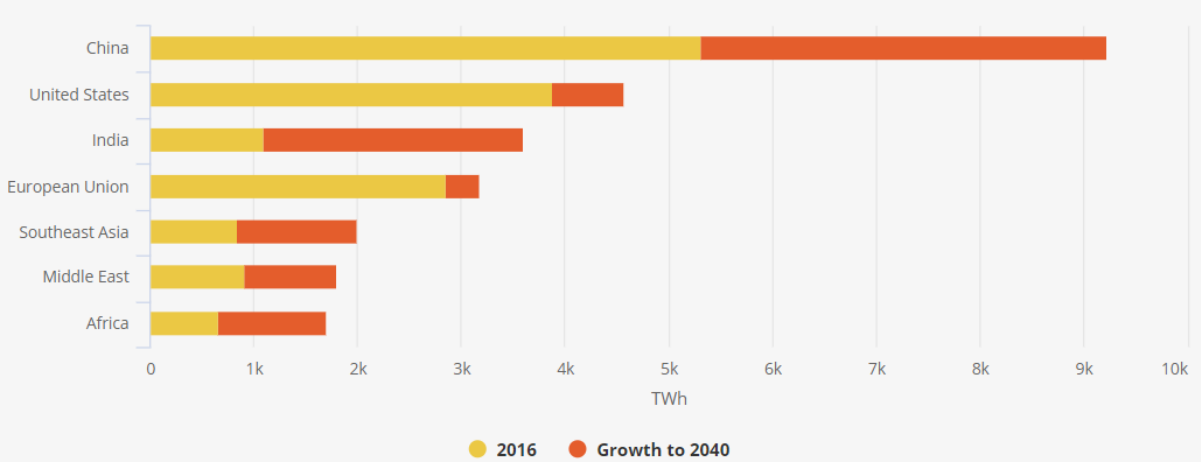

Figure 1-4 Electricity demand in 2016 and its future growth to 2040 in different regions [5].

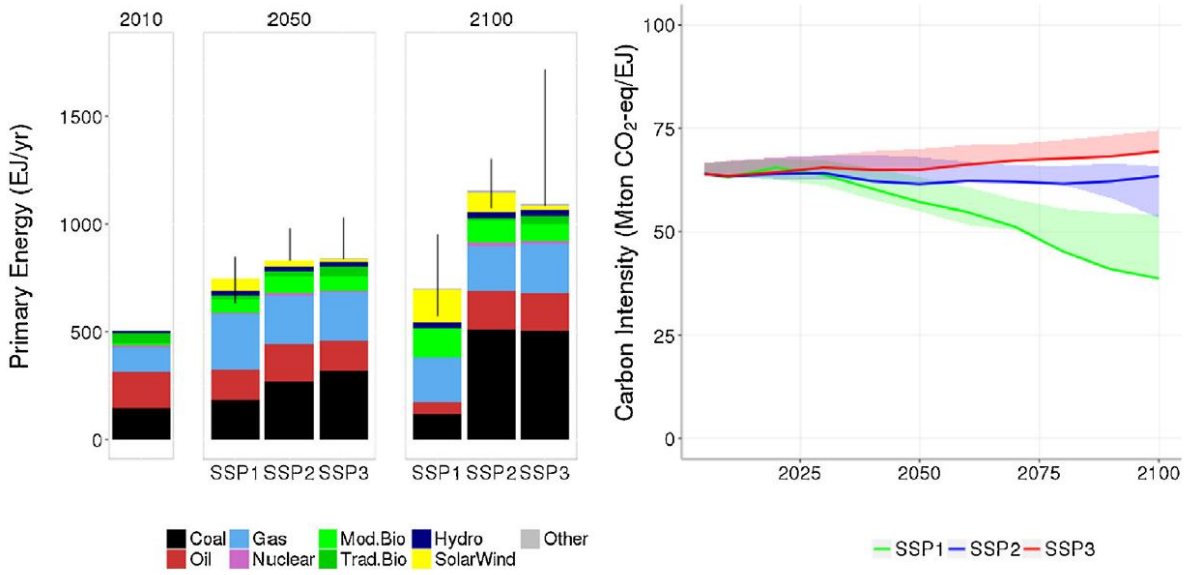

Figure 1-5 Global primary energy use per energy carrier and CO_2 emissions per unit of primary energy [8].

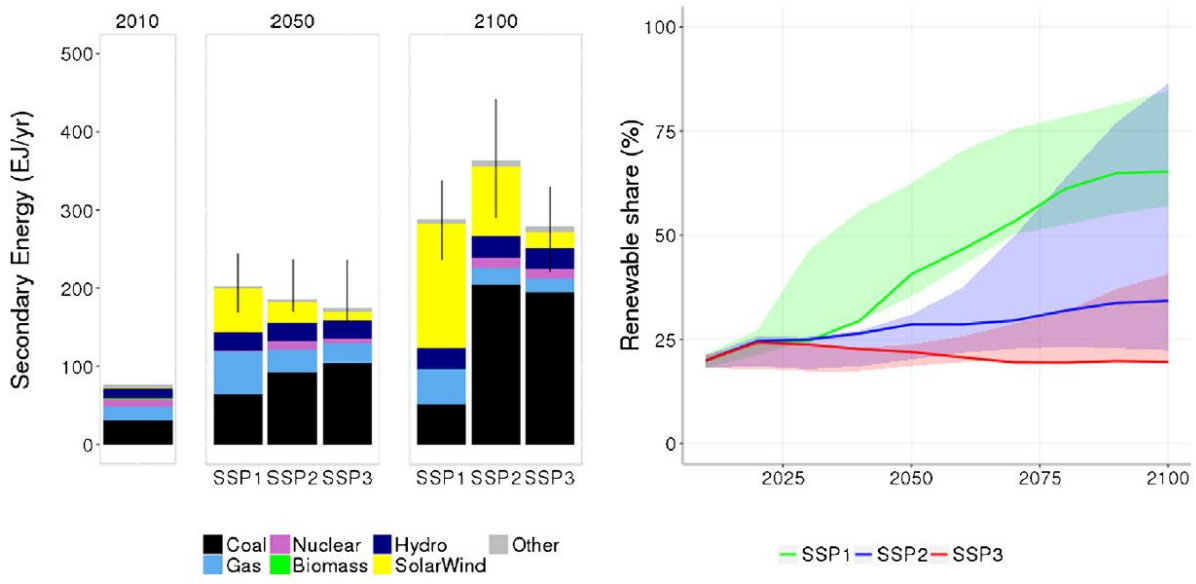

Figure 1-6 Power system development and renewable resources share [8].

In response to de-carbonization of electricity generation, different countries have been making great efforts in developing renewable generation. It was reported in 2014 [9] that in Denmark 60% of electricity generation was from wind, solar, and biomass. In Portugal, about 30% of electricity was supplied by non-hydropower renewable resources. And in Spain, 29% of electricity was supplied by renewable generation. In China, as observed from Figure 1-7, although the electricity is mainly generated from fossil fuels until now, renewable generation will increase significantly and accounts for around 40% of the total electricity generation by 2040. In the United States (US), renewable generation has seen a large increase since 2015, and it is expected to continue increasing at this rate till 2050, mainly due to the contribution of solar and wind energy generation, as seen in Figure 1-8.

The Gone Green 2011 scenario shows that in the United Kingdom (UK) 31% of the electricity generation would be contributed by renewable energy resources, mainly by wind, in 2020 [10]. And by 2020, carbon emission is expected to cut by 34% at 1990 levels. Meanwhile, the Scottish Government's 2020 renewable energy target is that renewables would meet the equivalent of 100% of Scotland's electricity demand [10].

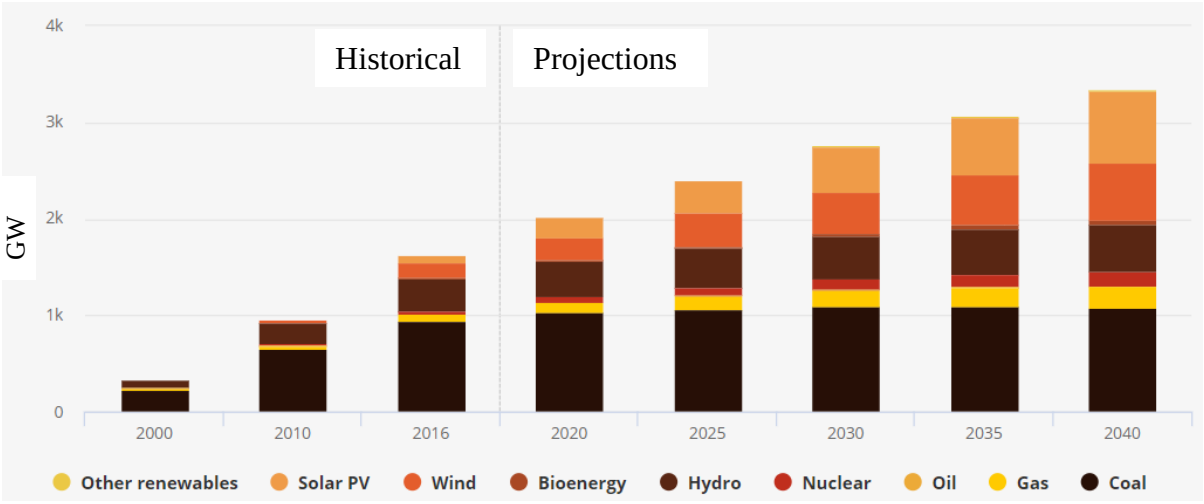

Figure 1-7 Installed capacity of different electricity generation technologies in China and its future trend [5].

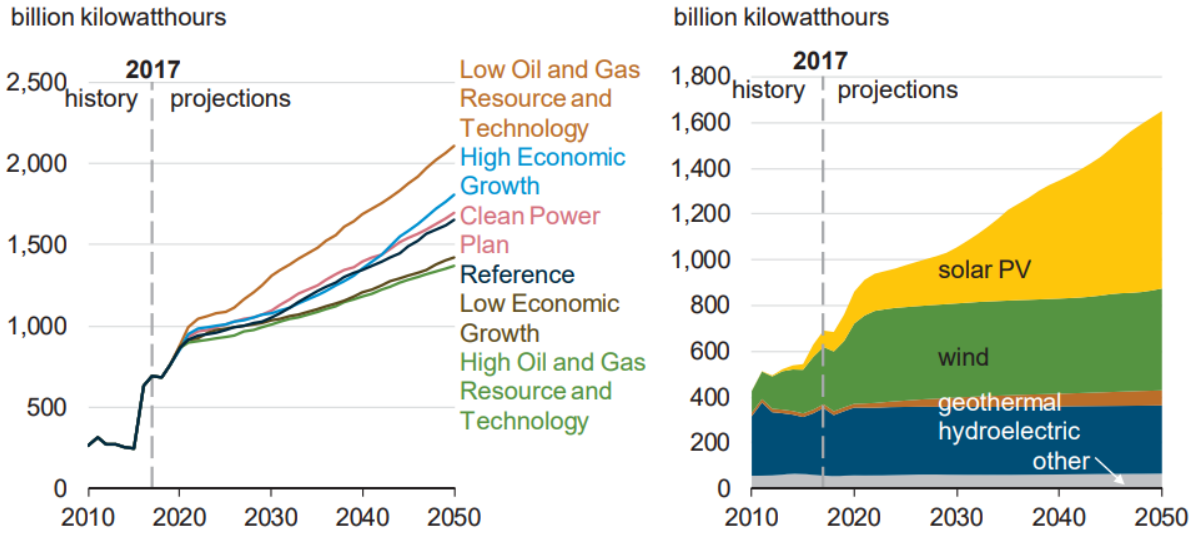

Figure 1-8 US electricity generation history and future trend [11]. Total renewables generation (left) and renewable electricity generation based on reference case (right).

1.1.2 Fluctuating Characteristics of Wave Power

Wave is a clean renewable energy resource and wave energy is huge. The existing research studies show that there is more than 2 TW of wave power potentially available on the 60m

bathymetry [12], which is equal to more than 10% of the average power consumption all over the world in 2010 [13].

Compared to other renewable generation technologies such as wind and solar energy, wave energy generation technology is relatively new and currently is of less economically competitive [14-16]. However, wave energy has many advantages over other renewable energies [14-16] :

(1) It has significantly higher energy density;

(2) It is more predictable, which can be predicted several days in advance;

(3) It is available at much longer time, almost throughout day and night;

(4) It has lower hourly variations;

(5) Compared with offshore wind power, resource locations with high wave power in many regions of the world are around the coastlines that are close to major load centres, e.g. the US [15] and the UK [17].

These features make wave energy generation a promising option of renewable generation, which has attracted a surge of attention from many countries, such as the US [15], many European countries, e.g. the UK [18], Portugal, Ireland, Norway, Sweden and Denmark [16], as well as China [19].

Unlike wind turbines which has a single standard design, a wide variety of wave energy converters (WECs) have been developed, by using different ways to absorb energy from waves. According to the working principle, the existing WEC technologies can be classified into three categories: (1) oscillating water columns (OWCs); (2) oscillating bodies with a hydraulic

system or a direct-drive linear generator; (3) overtopping devices. More details of the working principles and the output power characteristics of the WECs can be found in [18, 20-22].

Due to the fact that ocean wave power undergoes zero twice within each wave period, the electrical wave power generated by most of the WECs mentioned above, especially by those using linear generators, fluctuates heavily at typical periods of 5~12 s.

As for overtopping devices, the water reservoirs capture waves and store their energy as potential energy. Therefore an overtopping WEC has a strong smoothening effect [22].

For an OWC, the inertia of the Wells turbine can be used to smooth the output electrical wave power. However, the smoothing effect depends on the amount of moment of inertia. In order to improve wave energy capture efficiency, it is better to design a low inertia OWC system. For example, in [23], the authors propose a low inertia Wells turbine-based OWC in order to improve the capture efficiency. Figure 1-9 shows the output electrical power of the low inertia OWC under the optimal speed control mode. It can be seen that the electrical wave power is highly fluctuating. In order to further prove that the output power of an OWC device is highly fluctuating under the low-inertia situation, Figure 1-10 shows the time series of the equivalent electrical power based on the experimental electrical power data of a quarter-scale OWC prototype for the European FP7 project CORES [24]. During this time period, the generator was operated under the low inertial energy storage control mode.

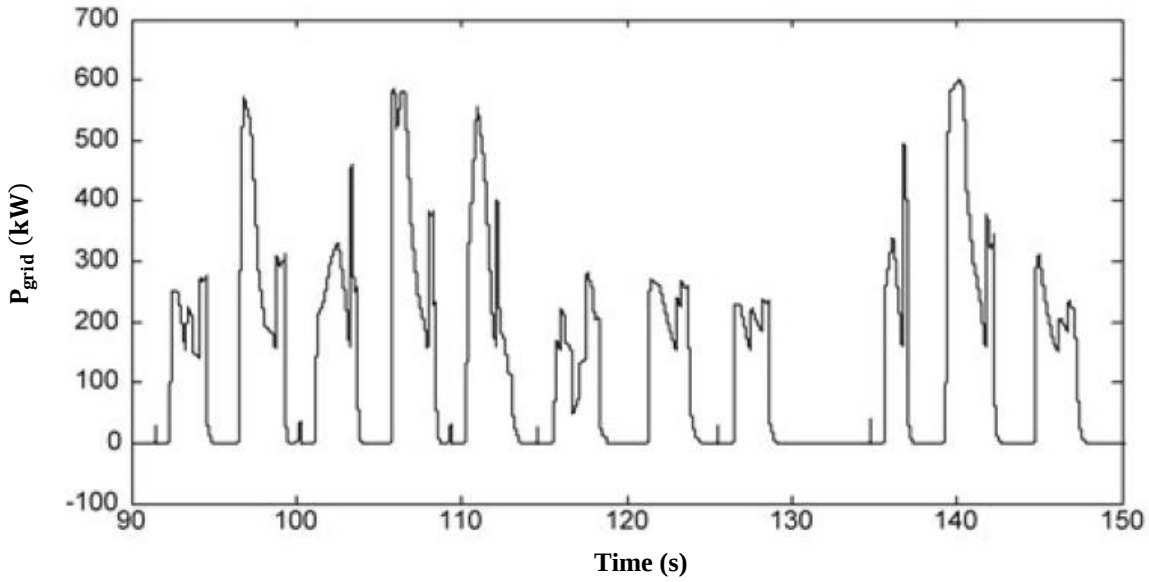

Figure 1-9 Output electrical wave power of a low inertia well turbine-based OWC [23].

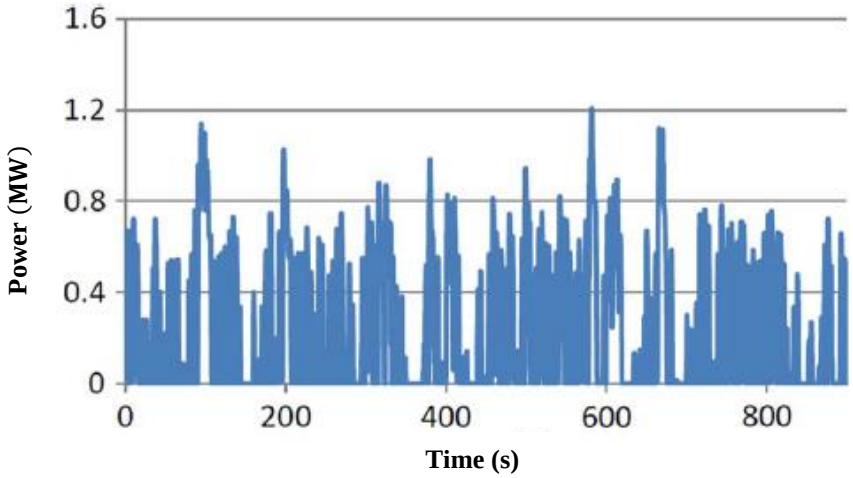

Figure 1-10 Electrical power profile of an OWC based on the European FP7 project CORES [24].

For oscillating bodies using hydraulic systems, the high-pressure accumulators are energy buffers that can smooth the output wave power. However, similar to the relationship between the amount of moment of inertia and energy capture efficiency in an OWC, there is a compromise between the structure of a high-pressure accumulator and wave energy capture efficiency. Usually a high-pressure accumulator with more complicated structure and bigger size means more development and maintenance costs [25].

For oscillating bodies which use direct-driven linear electrical generators, e.g. Archimedes wave swing (AWS), the generated electrical power fluctuates from zero to several times of the average [22, 26, 27]. This is because the captured mechanical energy is directly converted into electrical power and there is no energy buffering in such devices. Figure 1-11 shows the output current and power of AWS for its first test [22]. Figure 1-12 shows the experimental results of three phase voltage where a direct-drive linear generator-based point absorber is connected to a 20Ω load [27]. These two figures verify that the output power of a linear generator is highly fluctuating.

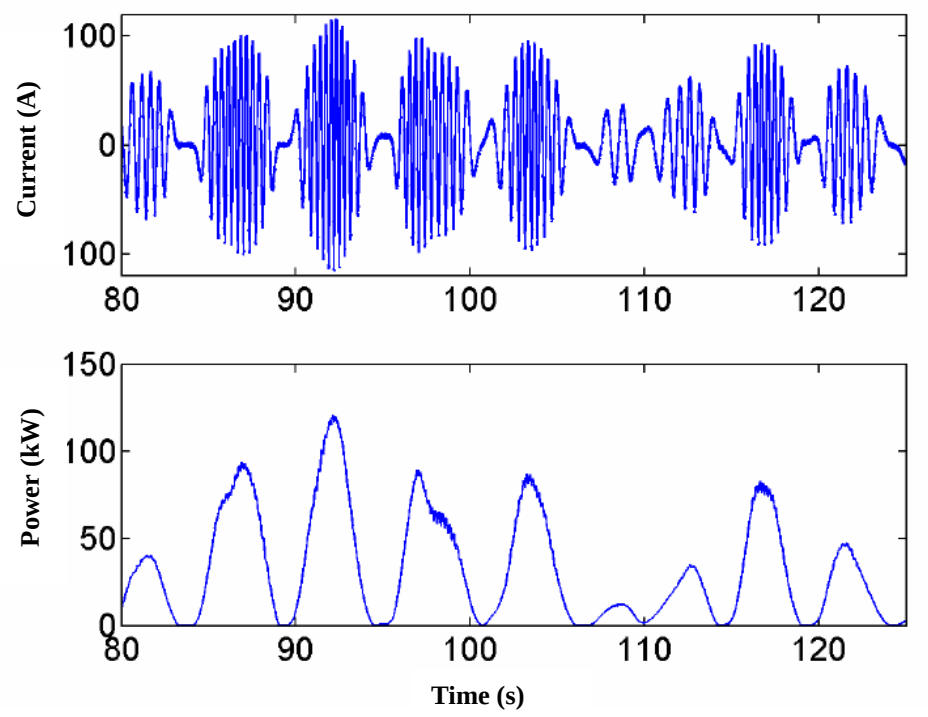

Figure 1-11 Output current and power of AWS during its first test [22].

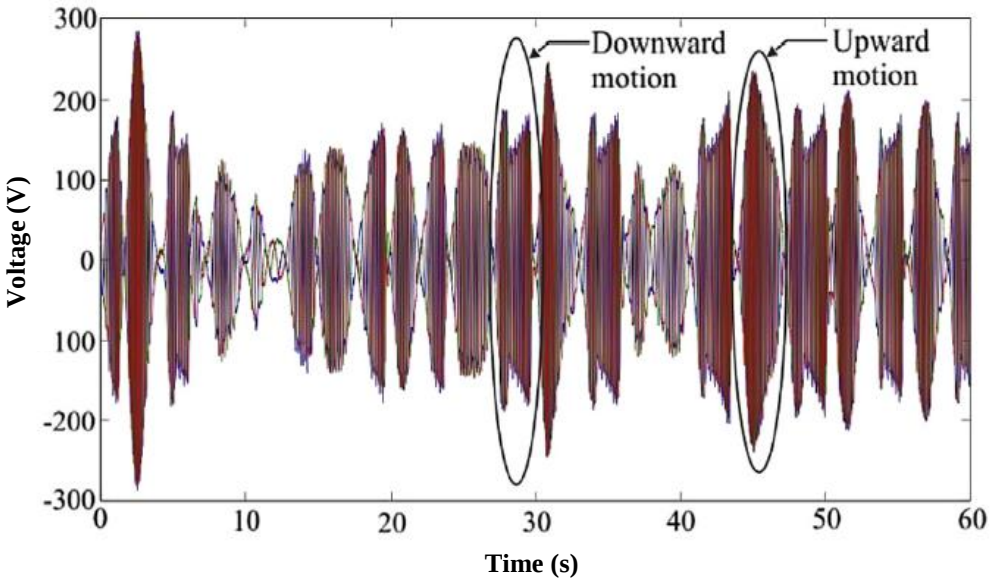

Figure 1-12 Experimental data of three phase voltage where a linear generator-based point absorber is connected to a 20Ω load [27].

If heavily fluctuating wave power is directly transmitted into a power grid before being smoothed, it will cause many problems, e.g., flicker, variations in voltage and frequency, harmonics, thermal excursions [22, 24, 26, 28] and increased power losses, which become even worse in weak grids [29, 30] and microgrids [31]. Although aggregating many WECs in a wave farm has a smoothing effect [14, 32], wave power smoothing is still of great importance and it is challenging when a power grid is integrated with high level of wave energy production [18, 26]. To demonstrate this view, Figure 1-13 shows that the total active power output at the point of common coupling (PCC) in a 20 MW wave farm is still oscillating heavily [33]. The reference of the wave farm model is from the real test case Biscay Marine Energy Platform (*bimep*), which consists of 10 linear permanent magnetic synchronous generator (PMSG)-based point absorbers.

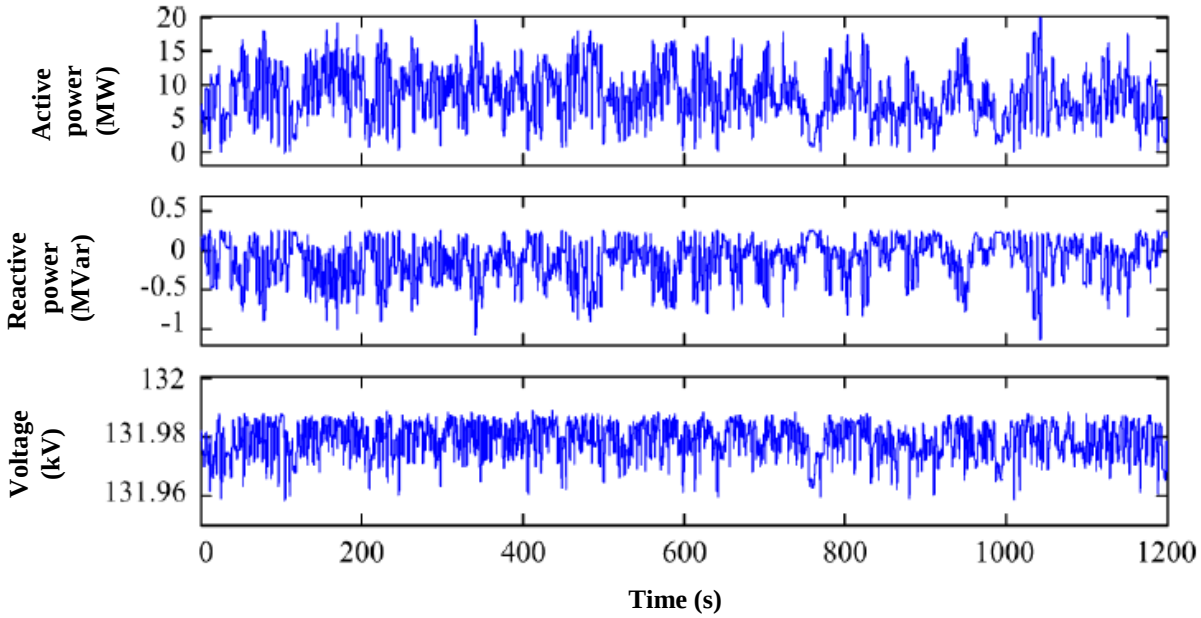

Figure 1-13 Time series of active, reactive power and voltage at the PCC in a 20 MW wave farm consisting of 10 linear-generator-based point absorbers from the real test case *bimep* [33].

1.1.3 Wind Energy Generation and its Variation Characteristics

1.1.3.1 Development of Wind Energy Generation

Nowadays, wind power is considered to be the most economically viable renewable solution, apart from hydro power [34]. Figure 1-14 outlines the global annual and cumulative installed wind capacity from 2001 to 2017 [35]. It shows that by 2017, the global installed wind capacity has arrived 539GW, which is 22.6 times of that in 2001. It is anticipated that, by the end of 2030, installed wind capacity will reach 2000 GW, supplying about 16.7% to 18.8% of the total electricity produced worldwide [36]. Figure 1-15 shows the newly and cumulative installed wind capacity of the top 10 countries in the world by the end of 2017 [35]. It can be observed that China and the US have become the first and second countries for cumulative wind capacity installed by 2017, respectively, followed by Germany.

Figure 1-16 shows the worldwide net electricity generation from renewable power between 2010 and 2040 from *International Energy Outlook 2017*. It can be seen that wind power accounts for the biggest renewable generation except hydropower [37] by the end of 2015, and it is projected to continue this status by the end of 2040. According to the report in *World Energy Outlook 2017* [5], renewables in the European Union are projected to be 80% of new capacity of electricity generation. Also wind power will become the leading source of electricity soon after 2030 due to the rapidly increase of both onshore and offshore wind energy generation. Table 1-1 shows wind power targets in different countries [38].

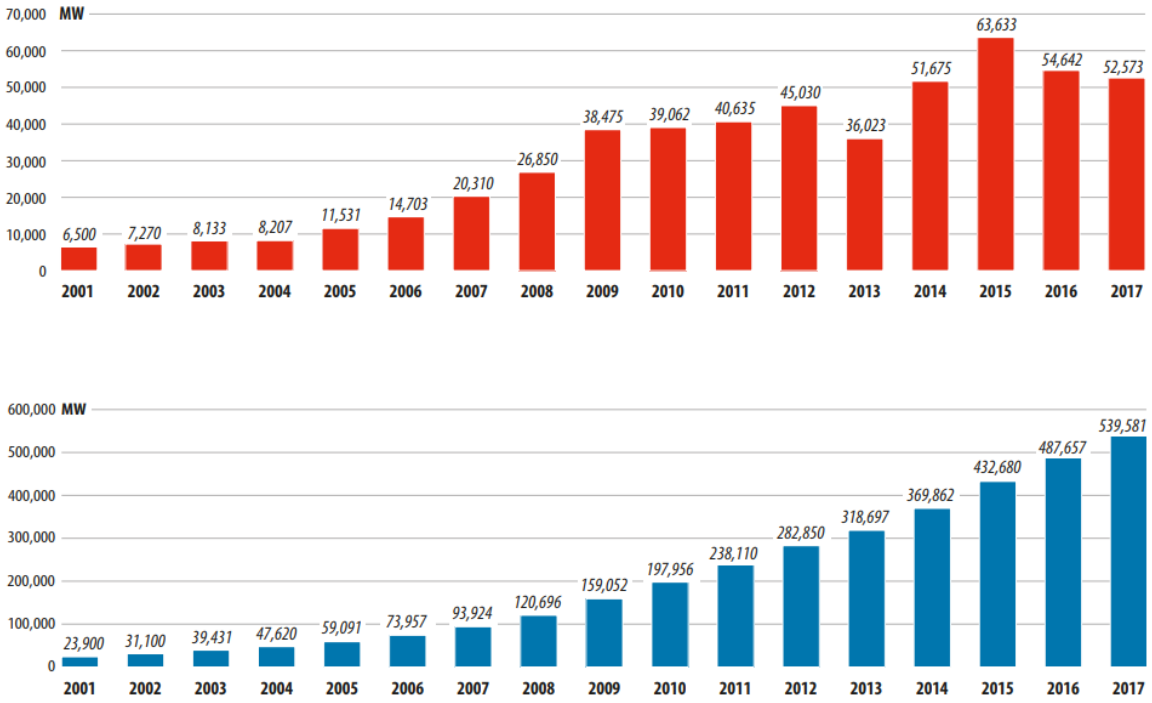

Figure 1-14 2001 – 2017 global annual (above) and cumulative (below) installed wind capacity [35].

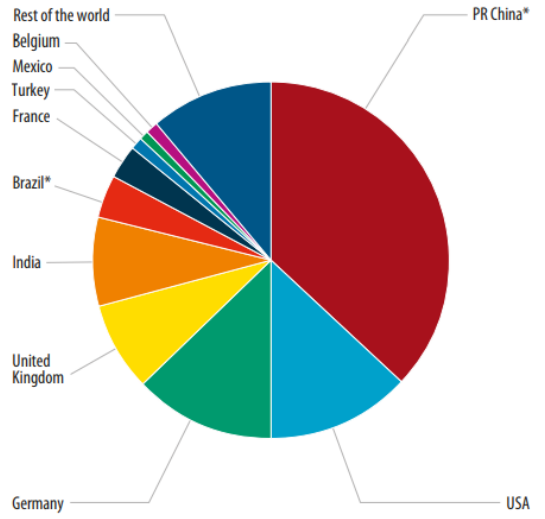

Country	MW	% Share
PR China*	19,500	37
USA	7,017	13
Germany	6,581	13
United Kingdom	4,270	8
India	4,148	8
Brazil*	2,022	4
France	1,694	3
Turkey	766	1
Mexico	478	1
Belgium	467	1
Rest of the world	5,630	11
Total TOP 10	**46,943**	**89**
World Total	**52,573**	**100**

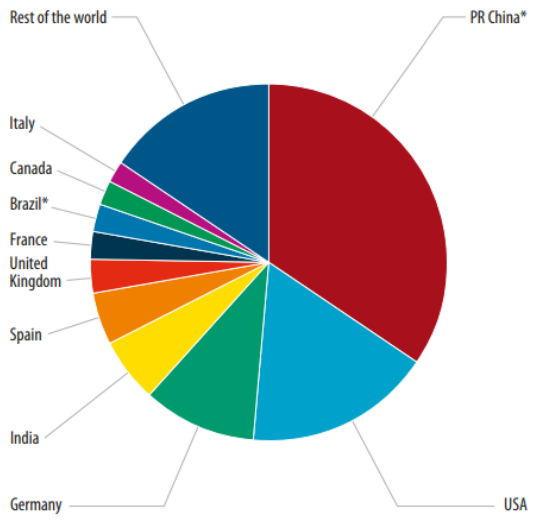

Country	MW	% Share
PR China*	188,232	35
USA	89,077	17
Germany	56,132	10
India	32,848	6
Spain	23,170	4
United Kingdom	18,872	3
France	13,759	3
Brazil*	12,763	2
Canada	12,239	2
Italy	9,479	2
Rest of the world	83,008	15
Total TOP 10	**456,572**	**85**
World Total	**539,581**	**100**

Figure 1-15 The newly (left) and cumulative (right) installed wind capacity of the top 10 countries by the end of 2017 [35].

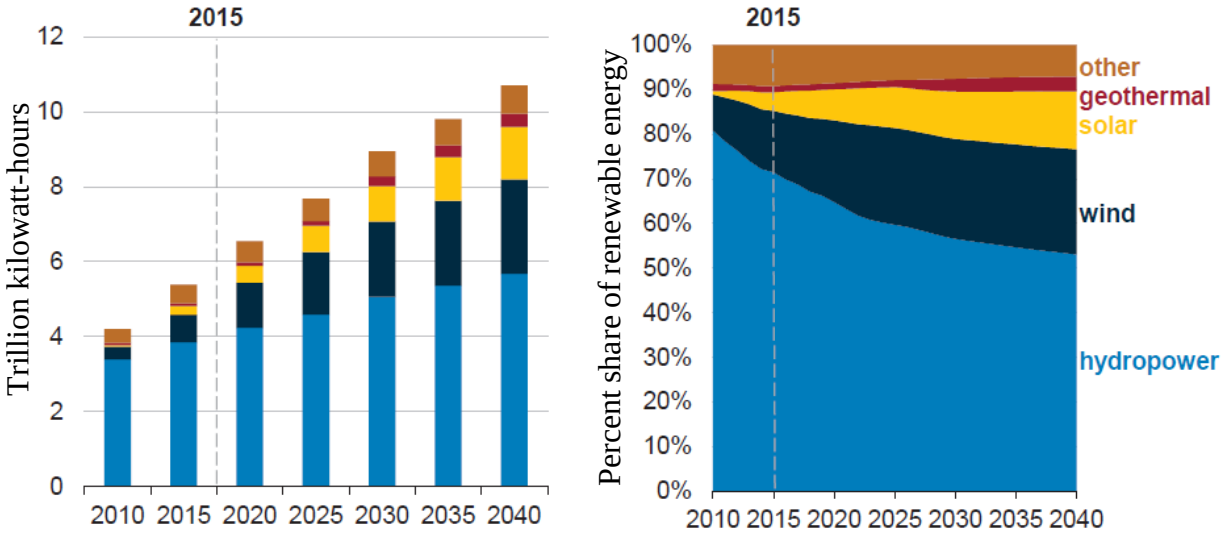

Figure 1-16 Worldwide net electricity generation from renewable power [37].

Table 1-1 Wind energy policy in different countries [38].

Country	CO_2 Emission Deduction compared to 1990 level	Wind Energy Target
China	45%, 2020	200 GW, 2020
US	25%, 2025	25% of supply, 2025
Germany	20%, 2020	35% of supply, 2020
Brazil	38%, 2020	10% of supply, 2021
India	20%, 2020	83 GW, 2030
Canada	20%, 2020	20% of supply, 2025
England	34%, 2020	15% of supply, 2020
Denmark	50%, 2030	200GW, 2030
Australia	60%, 2050	10 GW, 2020
Egypt	-	7.2 GW, 2020
Portugal	20%, 2020	39% of supply, 2020
Spain	20%, 2020	35 GW, 2020

With the exponentially increase of wind energy installed capacity over the past three decades, the size of commercial wind turbines has also seen an exponentially increase since larger wind turbines can capture higher power with less installation and maintenance costs. Figure 1-17 shows the evolution of the size of commercial wind turbines [39].

Figure 1-18 shows the main components of a fixed speed wind turbine [40]. The state-of-the-art and emerging wind energy conversion technologies from the electrical engineering perspective are comprehensively studied in [39].

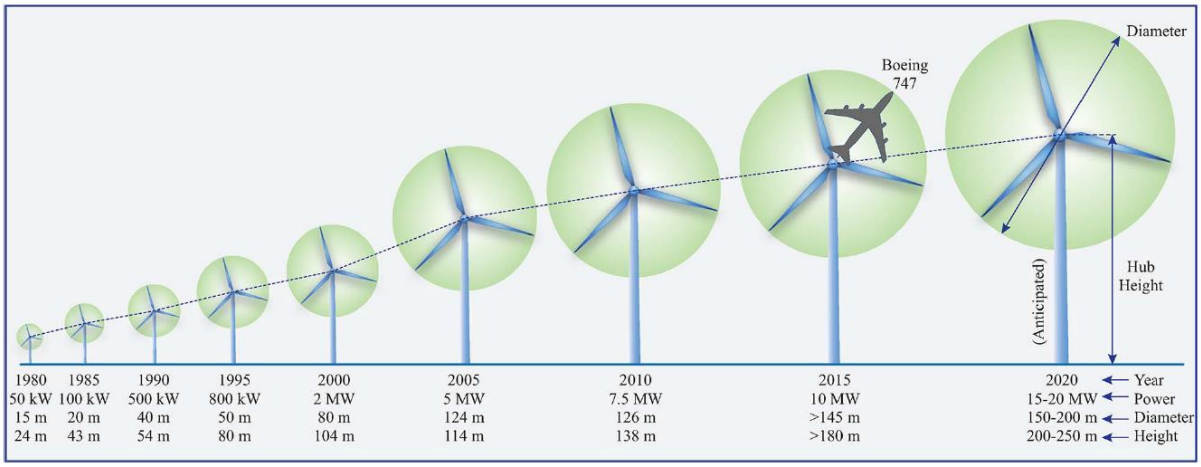

Figure 1-17 Evolution in the size of commercial wind turbines [39].

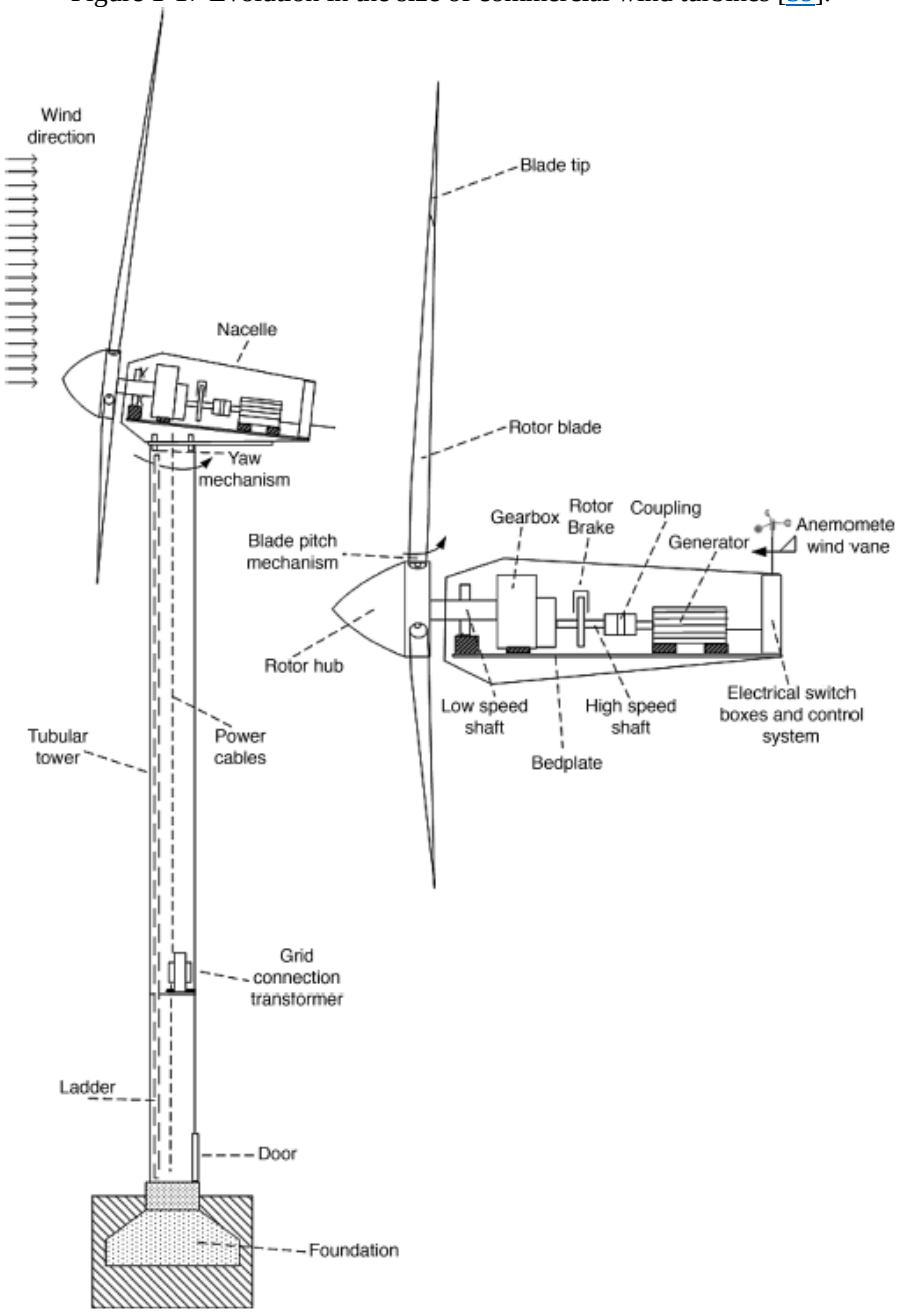

Figure 1-18 Main components of a fixed speed wind turbine [40].

A fixed-speed induction generator (FSIG)-based WTS without power converter interface is shown in Figure 1-19, where the squirrel-cage induction generator (SCIG) is connected to the grid through a soft starter and step-up transformer [41-43]. The generator speed varies within 1% around the corresponding synchronous speed at different wind speeds, and thus this configuration is called fixed-speed WTS. Since a FSIG is directly connected to the grid without electronics control, when grid frequency decreases or increases, the *slip* speed of the rotor increases or decreases, causing the power output increase or decrease. In this way, the FSIG provides inertial response to the power grid, helping to decrease the rate of change of frequency, like induction motors.

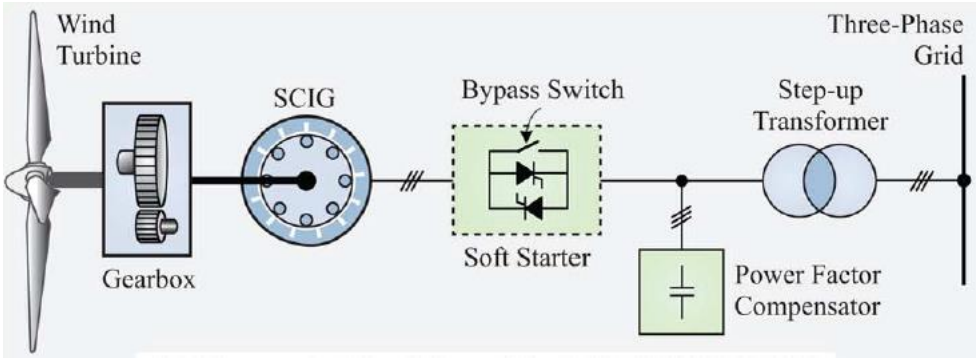

Figure 1-19 Configuration of a FSIG-based WTS [39].

To improve wind power capture efficiency, variable speed wind WTSs are developed. A variable speed doubly fed induction generator (DFIG)-based WTS is shown in Figure 1-20, where the power from the generator is fed to the grid through both stator and rotor windings [40]. The power converter employed in the rotor side allows bidirectional power flow in the rotor circuit, which is approximately 30% of the rated generator power [39]. In Figure 1-20, the rotor side voltage source converter (VSC) performs maximum power tracking point (MPPT) control to maximize wind energy capture [44]. The grid side VSC is to transfer the power from the rotor side VSC to the grid by keeping the DC-link voltage constant [44]. Due to the MPPT control, the rotor speed of a DFIG is always controlled at the optimum point under

each wind speed. Thus, during a frequency event, the output power of a DFIG does not change. Therefore, a DFIG does not provide inertial support to power grid.

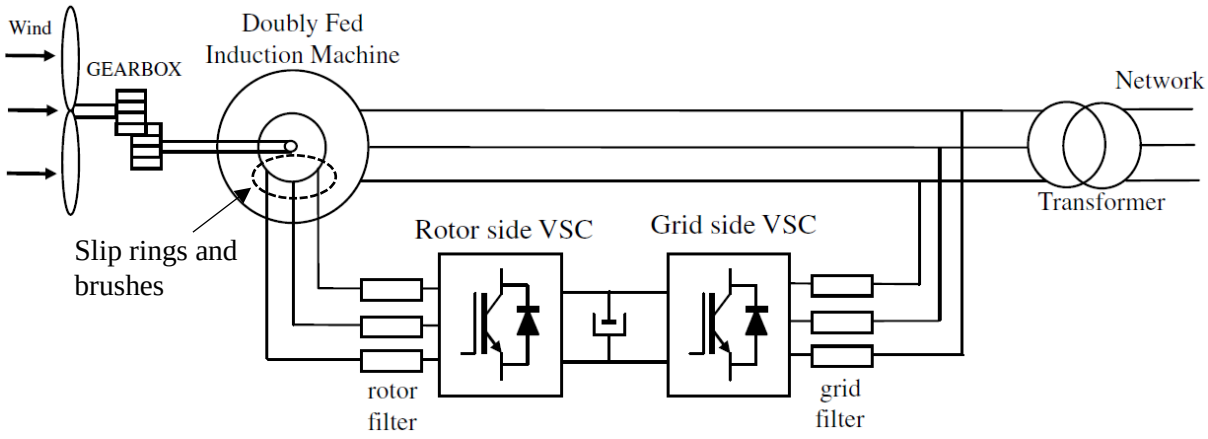

Figure 1-20 Configuration of a variable speed DFIG-based WTS [40].

With the increasingly higher penetration of wind energy generation and the domination of variable speed WTSs, a rising issue is the decrease in overall system inertia and thus the increase in the rate of change of system frequency [45-51]. Thus, to provide inertial response, the so-called "virtual" inertial control in variable speed WTSs is proposed by modifying the original MPPT control.

Generally, virtual inertial control by WTSs can be classified into two types. One type of virtual inertial control is realized by adding an extra torque term ($K_{in}\frac{df}{dt}$) into the existing torque reference of the MPPT control [49, 50]. This type of virtual inertial control requires the measurement of grid frequency. The other type, which does not need a prior knowledge of grid frequency, is realized by replacing the existing space vector control based on the widely used phase-locked loop synchronizing technique, with direct power control in the converters to mimic synchronous generator [51, 52]. In this way, the WTS can perform inertial response like a traditional synchronous generator without knowledge of the frequency.

It should be noted that the frequency control or frequency regulation by variable speed WTSs also include primary frequency regulation besides just inertial response, although both of them are using the kinetic energy stored in a WTS.

1.1.3.2 Variation Characteristics of Wind Power

Although the global wind energy generation is experiencing unprecedentedly growing, it also brings a series of technical and economic problems to power systems, due to two main factors: the high inter-temporal variation and limited predictability of wind power [38, 48]. Specifically, the impacts on power systems brought by the high variation and limited predictability of wind power include: generation unit commitment and dispatch [53]; power systems design and operation; the need for ramping and reserve capacities [54]; scheduling, frequency regulations, and system stabilization requirements, etc.. Figure 1-21 outlines these impacts by time and spatial scales [55]. The primary reserve here denotes the reserves activated in seconds, while the secondary reserve represents the reserves activated in 10~15 min.

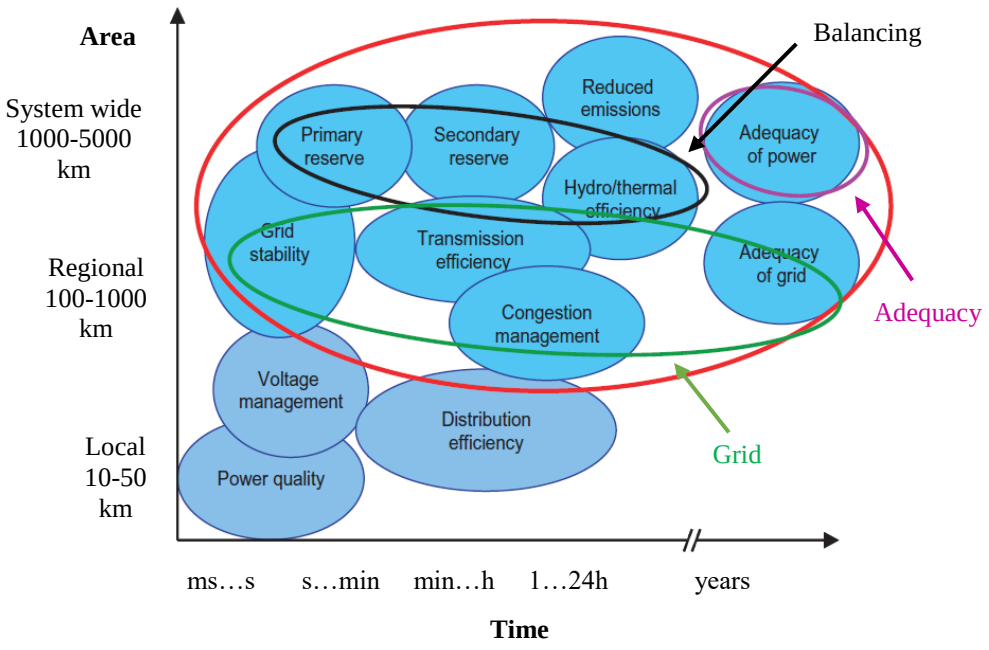

Figure 1-21 Impacts of wind power on power systems shown by time and spatial scales [55].

As a result, actions should be taken to mitigate the grid impacts of wind power variability with different time scales and restrictions [56]. Since this thesis only focuses on smoothing wind power with variations less than tens of seconds, wind power with variations beyond this time scope are not discussed in detail.

Wind power variations at less than tens of seconds are mainly due to the variations in wind speed fluctuations, wind shear and tower shadow effect, and wind turbulence.

Wind speed generally increases with height and this variation is termed wind shear. The torque and power oscillate due to the different wind conditions at different heights encountered by each blade as it rotates through a complete cycle. If a wind turbine has three blades, the distribution of wind is altered by the presence of the tower. For upwind rotors, the wind directly in front of the tower is redirected and thereby it reduces the torque at each blade when in front of the tower. This effect is called tower shadow. If a wind turbine has three blades, a power drop will appear three times per revolution. This frequency is normally referred to as $3p$ frequency. This is the reason why the wind shear and tower shadow effect can produce a periodic fluctuating power at the so-called $3p$ frequency [57].

Figure 1-22 shows the torque variations of a DFIG-based WTS due to the wind shear and tower shadow effect under a constant wind speed [58]. It can be seen that the torque variations caused by the wind shear and tower shadow effect is periodic and has a fixed form.

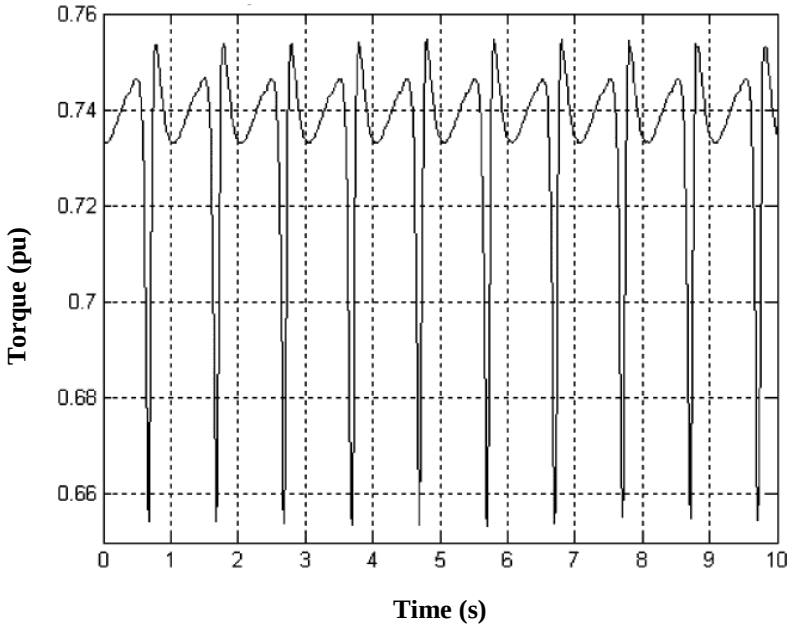

Figure 1-22 Torque variations of a DFIG-based WTS due to the wind shear and tower shadow effect under a constant wind speed [58].

Another factor that causes variations of generated wind power is wind turbulence. Figure 1-23 shows the wind speed variations due to the wind turbulence with 9.5m/s in average and 15% turbulence intensity, which is generated by the turbulent wind simulator (TurbSim) developed by the National Renewable Energy Laboratory (NREL) using the Kaimal turbulence model [59]. It can be seen that the wind speed variations caused by the wind turbulence is stochastic with longer changing periods than that caused by the tower shadow effect.

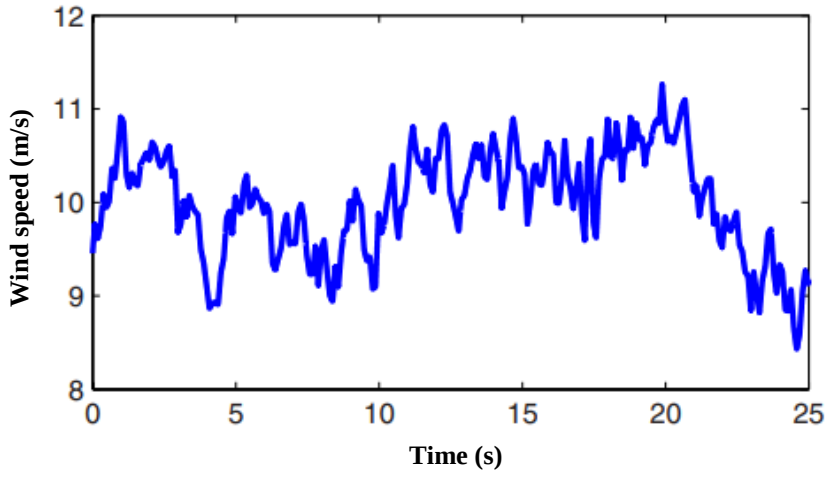

Figure 1-23 Wind profile generated by TurbSim using the Kaimal turbulence model [59].

Although a power grid may have many wind farms and each wind farm has many WTSs, the total output power from these wind farms is much smoother than that from a single WTS, output power from these wind farms is still fluctuating and needs to be smoothed. The wind power with variations at less than tens of seconds brings many problems, especially when the wind energy generation in the power system is high. Particularly, the resulted voltage flicker is mainly due to the wind shear and tower shadow effect [60, 61]. Moreover, since the wind shear and tower shadow effect can produce a periodic power at the $3p$ frequency, when the $3p$ frequency is close to the frequency corresponding to the inter-area oscillations of a power system, significant tie-line power resonance, namely forced oscillations, may be excited [62, 63].

Other problems caused by wind power with variations less than tens of seconds of a wind farm are: (1) grid frequency fluctuating [64]; (2) instability problems in power systems, especially where there are many loads that are sensitive to voltage and frequency variations; (3) increasing the power loss and capacity of transmission lines; (4) increasing the operation cost of transmission devices; (5) degrading the reliability of wind power conversion devices [65]. The above problems will become more significant when a power grid is integrated with high level of wind energy production, especially for small or isolated medium systems, e.g. Ireland.

In order to show the impacts of wind power variations on power grid frequency, Figure 1-24 provides the bode diagram of transfer function $G(f_W) = \Delta\omega_g(f_W)/\Delta P_{WF}(f_W)$ for a small power system with three thermal plants integrated with a wind farm [66], where $\Delta\omega_g(f_W)$ is the frequency deviation from the $60Hz$ standard frequency and $\Delta P_{WTS}(f_W)$ is the net power fluctuations from the wind farm at fluctuating frequency f_W. Regions A, B, and C denote the jurisdictions of the automatic generation control (AGC), governor systems, and inertia,

respectively in this small thermal plants system. It can be seen from Figure 1-24 that the thermal plants power system in region B has the weakest smoothing effect.

Figure 1-25 (a) shows the wind speed profile taken from a 600s wind speed data measured from a specific wind turbine location. Figure 1-25(b) shows the fast Fourier transform of the wind speed variations. The wind speed variations in region A have the highest spectral magnitude and are mainly attenuated by AGCs, which is not the focus of this thesis. The variations in region B are the focus of this thesis and have a spectral magnitude which is not small. In [67], it says that although in a grid system composed of many wind farms and each wind farm has multiple WTSs, the aggregated spectrum will be smoother than that in Figure 1-25(b), but the aggregated fluctuating components of wind power still lie in the same frequency range.

According to the above analysis for Figure 1-24 and Figure 1-25, it is concluded that the thermal power plants system has the worst smoothing effect for wind speed variations in region B and the variations in region B have a spectrum amplitude which is not small. These imply that wind power variations in region B which is less than tens of seconds should be smoothed by extra forces.

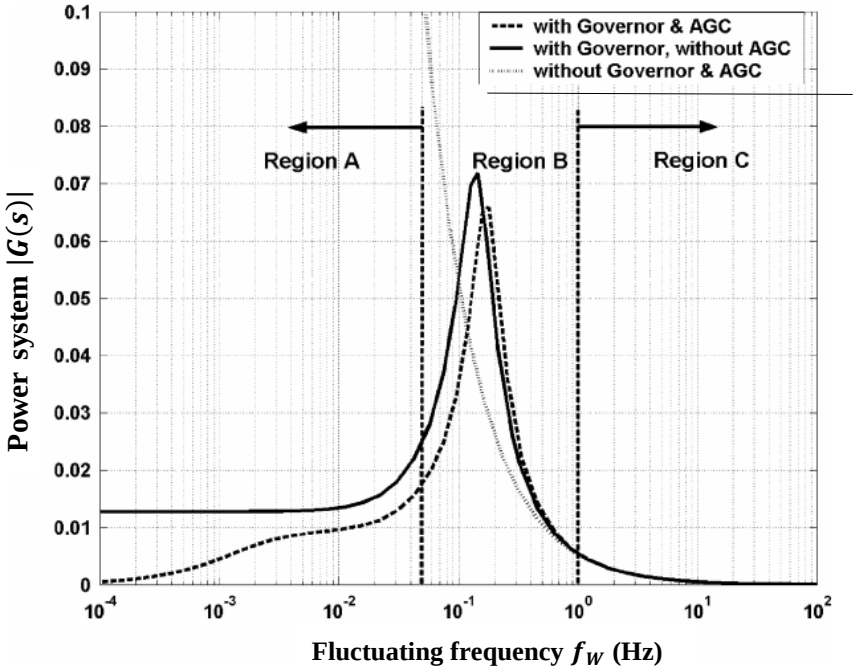

Figure 1-24 Bode diagram of transfer function $G(f_W) = \Delta\omega_g(f_W)/\Delta P_{WF}(f_W)$ for a small thermal plants system integrated with a wind farm, to show the impacts of wind power variations on power system frequency [66].

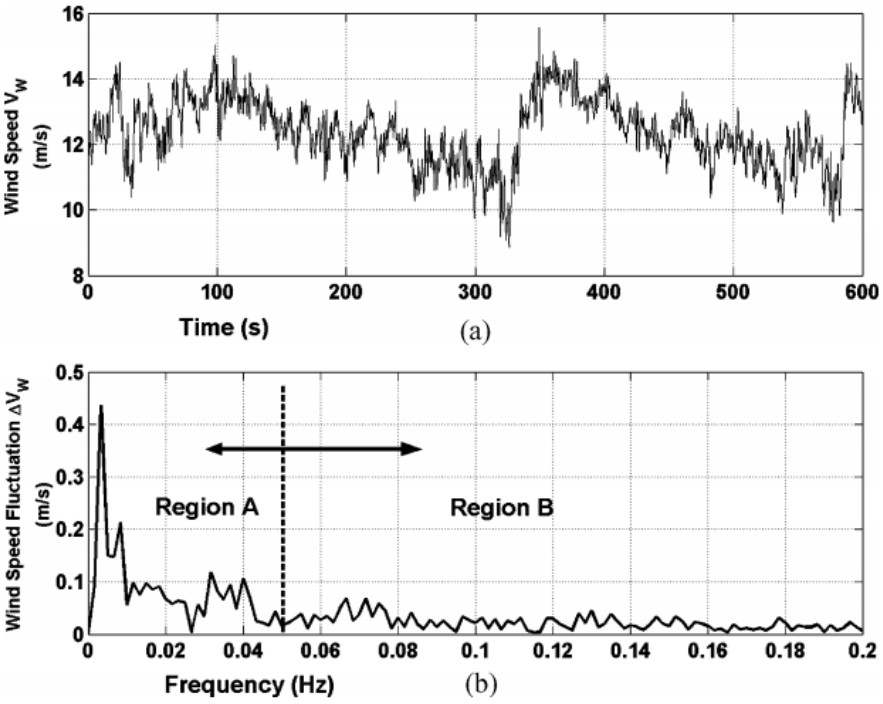

Figure 1-25 (a) Wind speed profile taken from a specific wind turbine location. (b) Fast Fourier transform of the wind speed variations [66].

1.1.4 Forced Oscillations Phenomenon and its Unique Characteristics

A forced oscillation is a resonance phenomenon of a power system, which can be excited when there exists a periodic external perturbation at the frequencies that are close or equal to the natural frequencies of system modes [68-72]. Forced oscillation phenomenons have been found in several power systems, e.g. the western North American power system and the China Southern Power Grid [70, 71, 73]. The paper [74] summaries the worldwide reported forced oscillations.

Unlike natural (or modal) oscillations caused by low or negative damping [75] of a power system, forced oscillations are excited by persistent external periodic perturbations. These external perturbations can be classified into four types: (1) Cyclic loads [76-79]; (2) Electrical oscillations caused by malfunctions of power system stabalizers (PSSs) in power plants [68]; (3) Mechanical oscillations of synchronous generator turbines [69, 80]; (4) Periodically fluctuating wind power due to tower shadow effect [57] and vibrations of floating offshore wind turbines [81]. Compared with natural oscillations, forced oscillations exhibit much higher amplitude and may cause catastrophic consequences, especially under poorly damped operating conditions [70]. Two examples about forced oscillations are given as follows.

Paper [82] discusses a forced oscillation event occured in western American power system in November 29, 2005. The 200 MW forced oscillation on the California—Oregon inter-area lines was caused by a 20 MW external perturbation in Alberta, which shows the forced oscillation is ten times of the external perturbation. This paper also indicates that the large amplitude tie-line forced oscillation was the resonance excited by interactions between the external periodic perturbation and the 0.25 Hz inter-area western system mode. Moreover, [82] verifies that forced oscillations occur even when the power system is well damped. Figure 1-26 shows the active power flow on Captain Jack—Grizzly line due to the forced oscillation event.

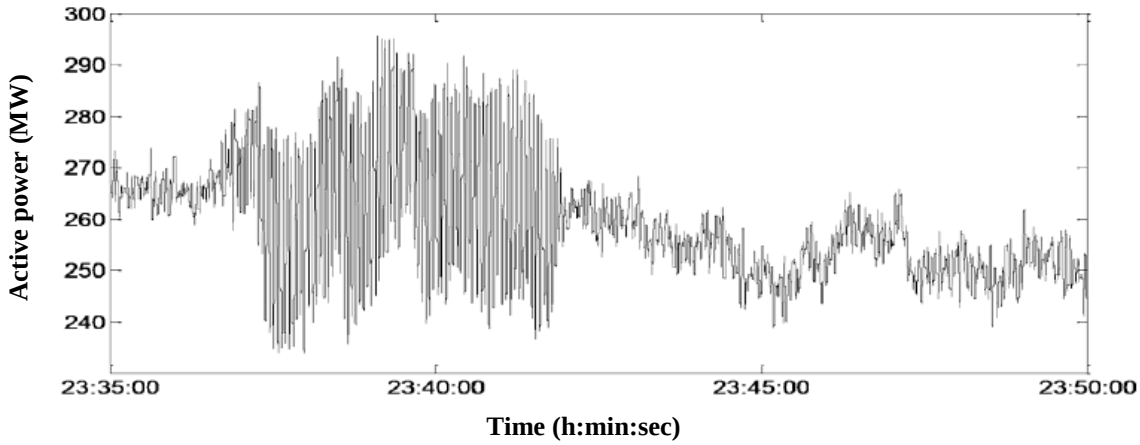

Figure 1-26 Active power flow on Captain Jack—Grizzly line [82].

On February 26, 2011, the China Southern Power Grid also found a significant tie-line forced oscillation, which had a peak to peak variation of 48 MW with a frequency around 0.20-0.36 Hz [83]. After investigation, it was shown that this forced oscillation was not resulted from the traditional poor inter-area modes but from the external turbo-pressure pulsation of a steam turbine in Guizhou province of China.

Since forced oscillations are significantly different from the origins and nature of natural oscillations, it is of importance to take unique countermeasures to eliminate or mitigate them.

1.2 Literature Review

1.2.1 Wave Power Smoothing Methods

As explained in Section 1.1.2, the generated electrical wave power from WECs fluctuates heavily over short time scales of 5~12 s. This presents a challenge to transmission system operator as it affects power grid stability, reliability, and operation. Therefore, smoothing output electrical wave power becomes an important and necessary requirement.

Existing wave power smoothing methods can be divided into three categories: (1) Proper design or control of the physical components in WECs; (2) Proper arrangement of the geometrical layout of WECs in a wave farm; (3) Using short-term electrical energy storage devices.

(1) Proper design or control of the physical components in WECs

As mentioned in Section 1.1.2 the high-pressure hydraulic accumulators in a hydraulic-systems-based oscillating body and the inertia in an OWC are naturally short-term energy storage [20, 84, 85]. Generally, the bigger size they are, the better the smoothing effect of wave power will be. However, bigger size means higher installation cost, lower energy capture efficiency, more frequent maintenance, more limitation in installation location, and etc. [86, 87], especially in a harsh ocean environment.

Paper [25] designs an OWC by using two segmented chambers which transfer power with a phase difference to the turbines so that the output wave power can be smoothed. This kind of methods suffers from the two drawbacks: it is site oriented, and the successive chambers require specific design.

Instead of designing two complementary chambers, paper [88] proposes a complementary control using the exiting physical components of an OWC system, in which the airflow control of the turbine and the kinetic energy control of the generator are complementary so that the output electrical wave power can be smoothed. The drawbacks of this method are that it can only be used in OWC devices and requires a compromise between the wave power smoothing effect and energy capture efficiency.

(2) Proper arrangement of the geometrical layout of WECs in a wave farm

The second type of methods to smooth fluctuating wave power is through optimizing WECs locations in a wave farm [32]. This method is able to smooth wave power to some extent and reduce required capacity from energy storage. However, the smoothing effect is subject to weather change and specific spatial conditions in an ocean environment.

(3) Utilizing short-term electrical energy storage devices

The third category of methods is to install short-term energy storage devices for smoothing generated electrical wave power. These energy storage devices include batteries [89], supercapacitors [90-92], flywheels [93], super conducting magnetic energy storage systems (SMES) [94], or hybrid energy storage [95], which have high ramp rates of power. However, a harsh offshore environment needs to be taken into account when installing additional energy storage devices. Because compared with onshore environment, offshore environment makes it more difficult to consider the following factors: frequent replacement of batteries due to limited battery charge cycles, large installation space for capacitors, and installation and maintenance of required electronic converters and associated hardware.

Instead of installing extra energy storage to smooth wave power, the low voltage-side local DC-link capacitor in a wave energy conversion system is used in papers [17, 96]. The

drawbacks of this method are: (1) The smoothing capability of the DC capacitor is limited and (2) The DC voltage is varying under the smoothing condition.

Considering the above background, it is of great importance to develop a new smoothing scheme that is of low investment cost and little maintenance, especially when taking into account a harsh ocean environment.

1.2.2 Wind Power Smoothing Methods

As mentioned in Section 1.1.3, wind power with variations at less than tens of seconds causes many problems if it is directly transmitted to power grids before being smoothed. Therefore, smoothing wind power in this time scale becomes an important and necessary requirement.

Many different schemes have been used for smoothing wind power variations in this timescale. Paper [97, 98] classify the methods of wind power smoothing into two categories: (1) with extra energy storage and (2) without extra energy storage.

(1) Wind Power Smoothing with Extra Energy Storage

Wind power smoothing methods based on different energy storage technologies in different time periods can be found in the review papers [99-101]. However, the most suitable energy storage technologies for smoothing wind power with variations less than tens of seconds are batteries [56, 102-104], supercapacitors [105-108], SMESs [109-114], flywheel energy storage systems [115-120], or combination of them [118, 121], due to their high ramp rates of power [99, 116, 122, 123].

However, implementation and maintenance of energy storage devices are expensive and the thermal excursions of the power conversion devices in WTSs are still not improved [124].

(2) Wind Power Smoothing without Extra Energy Storage

The second category of methods for wind power smoothing are those without installing extra energy storage devices, including the pitch angle control [64, 125-127], using the DC-link capacitors in PMSG-based WTSs [128], and using kinetic energy stored in WTSs [129, 130]. Since a DC-link capacitor has a very limited energy storage capability, it is always utilized together with the pitch angle control [131] or with both the pitch angle and kinetic energy control [132].

The pitch angle control to smooth wind power discards extractable wind energy, which is not economical and it increases blade pitching which will reduce the lifetime of wind turbines [97, 125, 131].

Compared with the two methods of using DC-link capacitors and pitch angle control, the method of utilizing the rotating kinetic energy of WTSs to smooth wind power is preferred in many works [124, 130, 132-137]. This is because the kinetic energy is usually quite large. Therefore little wind power procurement will be lost if the WTSs are well controlled.

It has been discussed in [135] that smoothing wind power variations of a certain time period can be achieved by controlling WTSs inertial energy in which the WTS power reference is properly designed as a function of the rotor speed. In [135], comparative results were provided for the following three methods: the maximum power point tracking (MPPT) control, constant power control, as well as linear slope approach. The simulation results demonstrated that a WTS can be unstable if the power reference for smoothing is not designed well. Paper [134] provided a smoothing method which is easy in implementation, by just designing the power reference as $K_{opt}\overline{\omega_r}^3$ compared with $K_{opt}\omega_r^3$ of the MPPT control, $K_{opt}\omega_r^3$ where $\overline{\omega_r}$ is the average rotor speed over time. This approach can smooth the wind power well under the simulated wind speeds. However, the smoothness of the given power reference $K_{opt}\overline{\omega_r}^3$ is affected by the rotor speed under the smoothing situation and it is no longer as smooth as the

average of that under the MPPT control. This is because under the wind power smoothing condition, the rotor speed and its average will change more dramatically than that under the MPPT control. A way for wind power smoothing which is similar to that in [134] is also used in [124]. But in [124] the rotor speed instead of the electrical torque is given as the control reference and the rotor speed reference is calculated based on the filtered output electrical power of a WTS. An optimized proportion integration (PI) controller for the rotor speed control is deliberately designed to maintain the WTS stable. However, the way of designing the filter time constant has not been discussed. In [132] a fuzzy logic smoothing controller is used. However, the requirement of measuring mechanical torque in [132] is not practical and the simulation results show that the smoothing capability is limited. In [133] a new control structure is proposed to achieve the suboptimal filtered power output. However, systematic procedures for designing the coefficient of the suboptimal power output control and the filter time constant are not provided. In both [130] and [136] the trade-off between the wind power capture and smoothing performance is considered, but different control strategies are used. In paper [137] the wind power smoothing problem is converted into an optimization problem. However, it is difficult to implement in practice since the accurate electrical model of a WTS is required.

According to the above background, an economical way which can smooth wind power variations less than tens of seconds is still waiting to be developed.

1.2.3 Forced Oscillations Suppression Methods

Considering the origins and characteristics, countermeasures of forced oscillations are different from that of natural oscillations. Generally, there are three categories of methods to minimize the grid adverse impacts from forced oscillations: (a) Elimination of forced oscillations; (b) Damping of forced oscillations; (c) Isolation and suppression of forced oscillations. The first

category of methods aims to completely eliminate forced oscillations by removing persistent external periodic perturbations [70, 138]. However, this removal is difficult and sometimes even impossible to realize due to two reasons. (1) It requires timely and accurate online locating of external periodic perturbations, which is difficult to obtain by the current locating methods [138-140]. (2) The external perturbation sources can be small or just within some critical power plants or loads making it neither practical nor economical to remove [71].

In the second category of methods, instead of complete elimination of forced oscillations, paper [58] proposes the methods of improving system damping by using power system stabilizers (PSSs) or flexible alternating current transmission systems (FACTS)-based stabilizers. However, unlike natural oscillations are attenuated quickly for a system with good damping performance, forced oscillations can still occur and be sustained [82, 141].

The third category of methods aims to isolate and suppress forced oscillations, so that the propagation of forced oscillations from disturbed area(s) to the rest of power grid is stopped. And subsequently the forced oscillations of the disturbed area(s) can be reduced. Paper [71] proposes an E-STATCOM approach to isolate and suppress forced oscillations by incorporating an energy storage unit into a static compensator (STATCOM). The disadvantages of this scheme are twofold: (1) Extra power electronic hardware and energy storage devices are required, and the cost and maintenance requirements of the associated devices must to be considered. (2) Resonant controllers are adopted that requires a priori knowledge of the frequencies of the external perturbations. Reference [142] proposed the installation of an extra flywheel in a wind farm to suppress forced oscillations excited by the oscillating wind power with the $3p$-frequency due to the tower shadow effect. Instead of using resonant controllers like paper [71], reference [142] proposes a power compensation method in which the flywheel is controlled to generate fluctuating power opposite to the forced

oscillating power. Instead of installing an extra flywheels, reference [63] utilizes the DC-link capacitor in a PMSG-based WTS with the same power compensation control as that in [142] to suppress forced oscillations. The method proposed in [142] is not economically viable and the one in [63] has limited suppression capability since the capacity in DC-link capacitor is small.

Based on the above background, economical and convenient approaches for isolation and suppression of forced oscillations still remain open.

1.3 Research Objectives and Contributions

The research objectives of this thesis are to improve the power quality of the output power from wave and wind farms, and improve power systems stability by isolating and suppressing oscillations. The three objectives are achieved through controlling the inherent large amount of inertial energy stored in wind farms. Specifically, the objectives are: (1) Smoothing the heavily fluctuating wave power from a wave farm; (2) Smoothing the output wind power with variations less than tens of seconds from a wind farm; (3) Isolating and suppressing forced oscillations and inter-area oscillations.

It should be noted that this thesis uses the existing inertial energy of WTSs to smooth wave and wind power before being transmitted to a power grid, which can help to reduce the frequency fluctuations caused by wind and wave power fluctuations. However, this is different from the way of using "virtual" inertial energy of WTSs to smooth frequency fluctuations [49, 50, 51, 52]. The methods proposed in this thesis does not use frequency measurement as a feedback signal while the "virtual" inertial energy control methods directly use frequency as a feedback signal. Hence, compared with the "virtual" inertial energy control methods, the methods in this thesis are considered to be an indirect ways to smooth grid frequency.

1.3.1 Smoothing Wave Power

Nowadays, the vast exploitation of offshore wind recourses has drawn great attention in the world and many offshore wind farms are being planned or under construction [143]. By 2030 the installation capacity of offshore wind farm in the North Sea and the Baltic Sea is expected to rise to 20–25 GW [143]. This is because offshore wind energy resource has many intrinsic advantages, compared to its opposite onshore wind energy resource. Offshore wind farm has stronger and more constant wind speed, less noise and visual pollution, more economical viable

in terms of using far larger turbines, closer to major population centers e.g. the US and etc. [144].

It is known that wave and wind resources overlap in nature since waves are generated by wind blowing [18]. Combined exploitation of offshore wave and wind resources has attracted increasing research attention and has been supported by several EU projects, such as MERMAID, TROPOS, H2OCEAN, ORECCA and MARINA [145]. Figure 1-27 shows a floating wave and wind energy combined conversion system, proposed by Pelagic Power AS.

Figure 1-27 A design concept of a floating wave and wind energy combined conversion system [145].

There exist many advantages of a combined offshore wave and wind farm, e.g., shared infrastructure, operation and maintenance, enhancement of energy production, reduction of operation and maintenance costs, smoothing of generated electrical power [145-148]. These benefits are analyzed and verified in [145-148], which implies that combined exploitation of wave and wind energies is a promising direction. In this way, using the large inertia of offshore WTSs (whose turbines are much larger than onshore wind turbines) as kinetic energy storage to achieve smoothing of wave power is possible and economic viable. Thus it is proposed in

this thesis. Meanwhile, Integral Compensation Control (ICC) is deduced for those WTSs in which only two supplementary terms are added into the control reference of the original MPPT control. ICC is able to regulate WTSs rotor speeds to use the WTSs as kinetic energy storage to smooth wave power. At the same time ICC makes the WTSs running close to the optimal rotor speeds points under varying wind velocities to minimize the loss of wind power procurement.

The rotor speeds of these WTSs have to be controlled at the related optimums at different input wind velocities so that the WTSs can maximize wind energy capture. However, the rotor speeds also need to be changed timely as kinetic energy storage so that the WTSs can generate fluctuating power that is opposite to the fluctuations of the wave power. The two objectives are not only irrelevant but also in conflict. Therefore, in order to realize the two objectives, the integral torque supplementary term of the two supplementary terms is introduced in ICC.

The contributions of the proposed wave power smoothing strategy are summarized below.

- Heavily fluctuating wave power is smoothed by controlling the inertial energy of nearby offshore WTSs. Unlike existing smoothing methods of wave power, the proposed strategy does not require any additional energy storage systems.

- The proposed ICC can achieve the two conflicting objectives simultaneously: wave power smoothing and high wind energy capture efficiency. Simulation results show the standard deviation of wave power is decreased by 10~20 times while the loss of wind power capture is less than 1%.

- Offshore wind farms can smooth the fluctuating wave power generated from any kind of WECs, since the input signal to a wind farm is the total output electrical power of a

wave farm. This makes the proposed wave power smoothing strategy applicable to all kinds of WEC technologies.

1.3.2 Smoothing Wind Power

Based on the background discussed in Section 1.2.2, it is a good proposal to smooth wind power with variations less than tens of seconds by utilizing the kinetic energy stored in WTSs. However, the existing methods cannot achieve the following two objectives simultaneously: well smoothing of wind power and obtaining high wind energy capture efficiency. In this way, a new method to control WTSs rotating inertial energy to smooth wind power is proposed in this thesis. This thesis focuses on the second operation region of a WTS in which the maximum wind capture is implemented. Because in the first region a WTS does not move, and in the third operation region the output wind power is a constant value since the pitch angle control is implemented. In the second operating region, in order to achieve smoothed wind power output, it is of importance for a WTS to have approximate maximum wind power capture (wind power capture is close to that of the MPPT control) under varying wind velocities. To achieve this, the key thing is to design the power reference properly. The designed power reference of the proposed wind power smoothing method includes two parts. The first part is to make a WTS approximately recover (or duplicate) the power trajectory of the MPPT control. This means that the recovered power curve can follow the change of the power trajectory of the MPPT control, although the average of the former is little less than the latter due to the smoothing action. The second part is to smooth the power curve of the first part, which is the difference between the average and the real-time of the first part. Then it can be seen that the average output power of a WTS is equal to the average of the recovered curve, which is little less than that of the MPPT control due to the little loss of wind power capture. In this way, two objectives

of smoothed wind power output and approximate maximum wind power capture are achieved simultaneously.

Compared to existing works, the advantage of the proposed wind power smoothing control is that it can have the following merits at the same time.

- It can smooth wind power output with variations within tens of seconds and still keep a high wind power capture efficiency;
- It can maintain stabilities of WTSs under variable wind velocities;
- It can mitigate the mechanical stress of a wind turbine by giving a smoother torque reference compared with that under the MPPT control, thus expanding the wind turbines lifetime;
- It is easy in practical implementation since no modification to the existing devices and no installation of extra energy storage systems are needed.
- It can reduce wind power capture loss by smoothing the output power from a wind farm and by the proposed coordination control of multiple WTSs. Because there is an inherent smoothing effect in a wind farm and different WTSs have different wind velocities and thus have different kinetic energy storage capabilities.

The difference of the two control methods in Chapter 2 and Chapter 3 should be pointed out here. Although the structure of the proposed power reference for wind power smoothing is the same as that of ICC for wave power smoothing, the deduction procedures and logic, and thus the related coefficient of the control reference, are different. This is because by using WTSs to smooth wave power, the required compensation power ΔP_c can be easily obtained from the measured information of the electrical power from a wave farm, while to smooth wind power

itself the compensation value needs to be estimated. Thus, the deduction logic in Chapter 3 is trying to set a power reference which can recovery the power trajectory of the MPPT control under the smoothing situation and then to smooth the recovered trajectory, while the deduction logic in Chapter 2 is that under the smoothing situation the rotor speed deviates from its optimum and the resulted change of kinetic energy should be all used for smoothing wave power.

1.3.3 Isolating and Suppressing Forced Oscillations

As mentioned in Section 1.1.3, wind energy will account for a great proportion in the future energy scenario [34]. Also, a few works have been published by using variable-speed WTSs as kinetic energy storage to support power grids, such as to support and regulate grid frequency [149-151], to suppress inter-area oscillations [152-156], etc..

Inspired by the above background, this thesis presents a proposed isolation and suppression strategy of forced oscillations based on controlling wind farms to generate compensated power opposite to the forced oscillating power. The proposed method uses the large amount of inertial energy of wind farms without requirement of installing extra energy storage and power electronic devices. Similar to that of smoothing wave power, to isolate and suppress forced oscillations, it is important for a wind farm to generate oscillating power exactly opposite to the forced oscillating power while retaining the capability of high wind power capture under varying wind speeds. In view of this, ICC is adopted.

By adopting ICC, a wind farm can timely release or absorb power opposite to the oscillating power from disturbed area(s), thereby preventing the forced oscillations from propagating to the rest of power grid (isolated). At the same time the oscillating power in the disturbed area(s) is also reduced (suppressed).

The contributions of proposed strategy for forced oscillations isolation and suppression are fourfold:

- The proposed strategy represents the first active use of the large inertia from a wind farm as energy storage to isolate and suppress forced oscillations while obtaining the wind power capture close to that of MPPT control.

- The proposed strategy is easily to implement with only the information of the oscillating power from the disturbed area(s). A priori knowledge of the frequencies of the external perturbations are not required.

- The proposed power compensation control is universal and not restricted to fixed system structures. On the contrary, the existing damping control methods based on state-space equations of a power system have limited applicability since they are subject to fixed control structures and specific power systems [153].

- Although the strategy proposed aims to suppress forced oscillations, it is also helpful to damp inter-area oscillations.

1.4 Outline of Thesis

The research in this thesis is conducted via theoretical derivation and time domain simulations in Real Time Digital Simulator (RTDS). The outline of the thesis is given as follows:

Chapter 2 This Chapter aims to smooth wave power which fluctuates heavily at typical periods of 5~12 s. The wave power smoothing scheme through controlling the large kinetic energy of nearby offshore wind farms is proposed. ICC is developed to achieve the wave power smoothing and high wind energy capture efficiency. Simulations of DFIG-based and PMSG-based WTSs in RTDS are provided to validate the performance of the proposed method.

Chapter 3 This Chapter is to smooth wind power with variations less than tens of seconds. The smoothing is achieved by controlling the kinetic energy of WTSs by adopting the structure of the power reference of ICC proposed in Chapter 2. The smoothing control proposed in Chapter 3 is derived in a logic different from that of ICC due to in the wind power self-smoothing situation. A way to estimate the required wind power compensation is also developed. Finally simulation of DFIG-based and PMSG-based WTSs in RTDS is provided to validate the performance of the proposed method.

Chapter 4 This Chapter is to isolate and suppress forced oscillations. The physical principles and characteristics of forced oscillations are analyzed first. Then utilizing the inherent large kinetic energy of wind farms to isolate and suppress forced oscillations is proposed by adopting ICC. Simulation results of the two-area power system with a DFIG-based wind farm using RTDS are provided to demonstrate that the proposed method can isolate and suppress forced oscillations, and damp inter-area oscillations as well.

Chapter 5 This chapter concludes the thesis and discusses possible future work.

CHAPTER 2 WAVE POWER SMOOTHING

2.1 Introduction

This chapter uses the material in the published paper [157]. It introduces a novel scheme to smooth the output power of a wave farm by utilizing the large inertia of nearby offshore WTSs. ICC is deduced to control the WTSs to generate fluctuating power opposite to the fluctuating components of the wave power. Section 2.2 describes the system configurations of the proposed wave-wind farm. Section 2.3 provides detailed theoretical deduction of the proposed ICC for a single WTS. Then the coordination control for several WTSs within a wind farm is deduced with the purpose of decreasing wind power capture loss caused by the smoothing action. In Section 2.4, a single DFIG-based WTS and PMSG-based WTS are simulated in RTDS to verify the performance of the proposed ICC method. Quantitative analysis of the dynamic performance is also provided to show the relationship between wave power smoothing effect and wind power capture efficiency. Then simulation results of a wind farm with two DFIG-based WTSs are performed to show that the coordination ICC of multiple WTSs can improve the efficiency of wind energy capture. Finally, Section 2.5 summarizes the major results of this chapter.

Symbols

ΔP_c Oscillating component of the total electrical power from a wave farm

$\overline{P_{wave}}$ The average of the total electrical power from a wave farm

$-\Delta P_c$ Oscillating component of the output electrical wind power for smoothing wave power

P_{wind}^0 The output electrical wind power due to power captured from environmental wind

K_{opt} Optimal coefficient for maximum wind power capture

$\omega_{r\_opt}(t)$ Real-time rotor speed of a WTS under the MPPT control

$\omega_{r\_DCC}(t)$ Real-time rotor speed of a WTS under DCC

$\omega_{r\_id}(t)$ Real-time rotor speed of a WTS under expected smoothing situation

$\omega_r(t)$ Real-time rotor speed of a WTS under ICC

ε Loss of wind power capture due to the rotor speed deviating away from its optimum

$T_{ref-MPPT}$ Given torque reference of a WTS under the MPPT control

$T_{ref-DCC}$ Given torque reference of a WTS under DCC

T_{ideal} Expected torque reference for a WTS when the WTS is used to smooth wave power

$T_{ref-ICC}$ Given torque reference of a WTS under ICC

T_{int} Extra torque term in the torque reference in ICC compared with that of DCC

ΔE Kinetic energy change of a WTS when $\omega_r(t)$ decelerates or accelerates from $\omega_{r\_opt}(t)$

J Moment of inertia of a WTS

ξ Wave-wind ratio

c_v Variation coefficient

2.2 Configuration of a Proposed Wave-Wind Farm System

The proposed wave-wind farm system is shown in Figure 2-1. The wind farm can be composed of either DFIG-based WTSs or PMSG-based WTSs. The wave farm is composed of a parallel set of FSIGs. Each FSIG has a 5~12 s periodically fluctuating mechanical input torque. The interactions of the prime mechanical movers with sea waves are ignored, since only the electrical characteristics of WECs need to be considered.

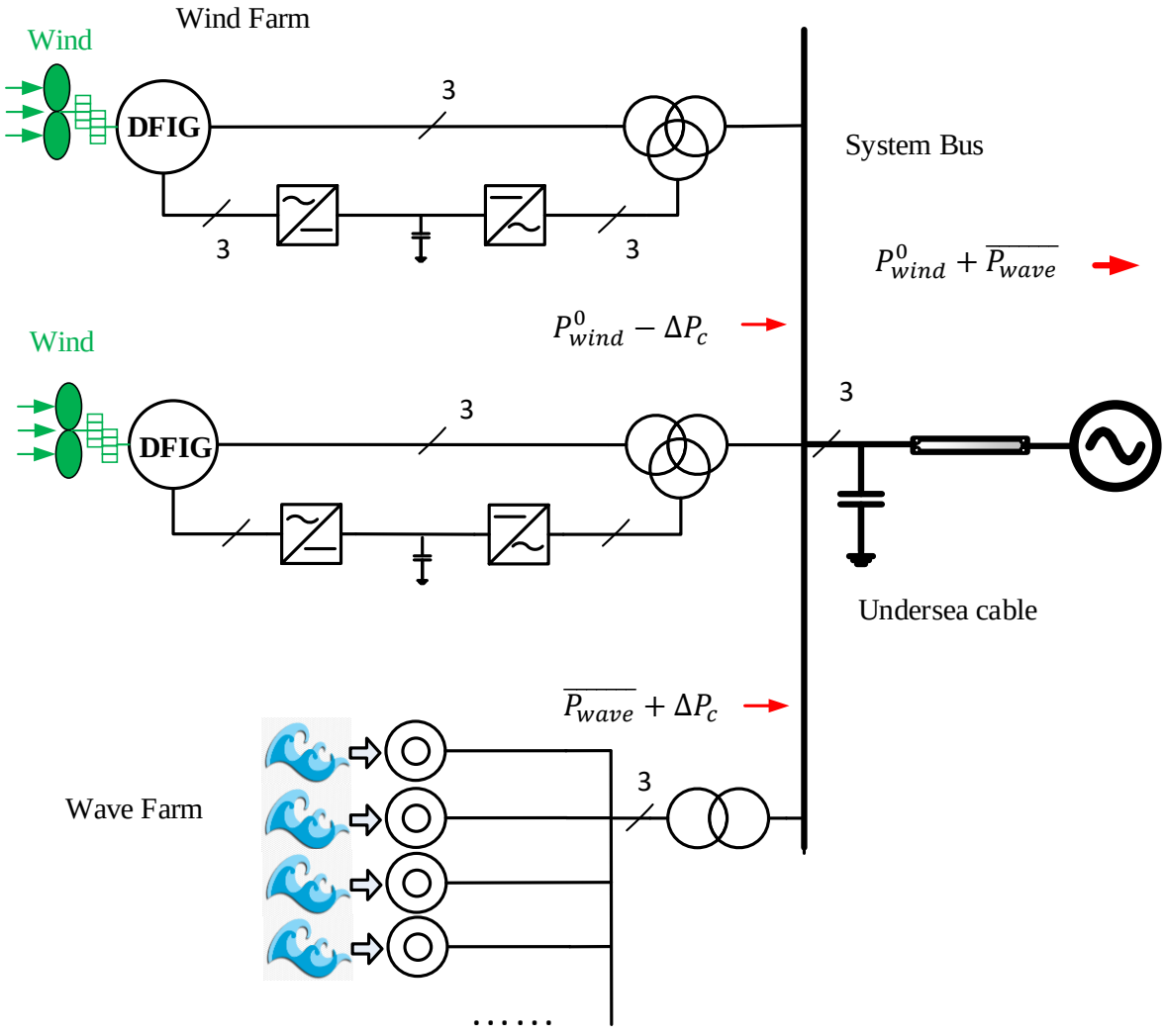

Figure 2-1 The proposed wave-wind farm system.

The use of FSIGs for representing the wave farm is reasonable. This is because from the power grid point of view, it can cover the worst output electrical wave power generated by the WECs

introduced in Chapter 1. Among the existing WECs, overtopping devices and oscillating bodies using hydraulic systems, e.g. Pelamis [20], use FSIGs as the mechanical-electrical conversion devices. As for oscillating bodies using linear generators whose output currents have varying phases, back-to-back converters are usually adopted to convert the current before it is transmitted to a power grid. Thus, the external characteristics of the final output electrical power from this type of WECs is equivalent to that of a synchronous generator. Hence, using a FSIG to represent an oscillating body using linear generators is reasonable. An OWC usually uses a DFIG as an electricity conversion system to mimic WTSs and maximize wave power capture. Thus, using FSIGs to represent OWCs is also reasonable.

A capacitor bank is connected at the PCC of the wave-wind farm system to compensate the reactive power required for the FSIGs. The undersea alternating current (AC) cables are used to connect the farm to the onshore grid.

The wave farm in the proposed wave-wind farm system generates fluctuating electrical power, which is composed of a mean $\overline{P_{wave}}$ and a real-time varying value ΔP_c. The power from the wind farm includes two parts: (1) the output electrical wind power P_{wind}^0 coming from the external wind; (2) $-\Delta P_c$ is converted from the kinetic energy of the WTSs which is used to smooth the wave power and has zero mean in the long run. According to the above analysis, the power of the PCC will be the sum of $\overline{P_{wave}}$ and P_{wind}^0, which means the power on the system bus is smoothed.

2.3 Development of the Proposed ICC Method

Before introducing the proposed ICC method, Direct Compensation Control (DCC) for wave power smoothing via the MPPT control [44, 158] is described. Then to overcome the drawbacks of DCC, ICC is provided. To illustrate the control strategy, the wind farm consisting of only a single WTS is introduced first for the purpose of clarity, and then it is extended to the wind farm consisting of many WTSs.

2.3.1 Direct Compensation Control (DCC)

In the MPPT control [44, 158], the power or toque reference of a WTS is designed as

$$P_{ref-MPPT} = K_{opt}\omega_{r\_opt}^{3}(t) \tag{2.1}$$

$$T_{ref-MPPT} = K_{opt}\omega_{r\_opt}^{2}(t) \tag{2.2}$$

where $\omega_{r\_opt}(t)$ represents the real-time rotor speed of the WTS under the MPPT control. K_{opt} represents the optimal coefficient for the maximum wind power capture and it is given by

$$K_{opt} = 0.5\rho\pi R^{5}C_{\rho max}/\lambda_{opt}^{3} \tag{2.3}$$

where λ_{opt} is the optimal value of the tip speed ratio λ, and $C_{\rho max}$ represents the maximum value of the power coefficient $C_{\rho}(\lambda,\beta)$ with the pitch angle $\beta = 0°$ and $\lambda = \lambda_{opt}$. This study uses the $C_{\rho}(\lambda,\beta)$ curve adopted from [159, 160] with the definition of

$$C_{\rho}(\lambda,\beta) = 0.517\left[\frac{116}{k} - 0.4\beta - 5\right]e^{-\frac{21}{k}} + 0.0068\lambda \tag{2.4}$$

where $\frac{1}{k} = \frac{1}{\lambda+0.08\beta} - \frac{0.035}{\beta^{3}+1}$.

The diagram of the MPPT control is shown in Figure 2-2.

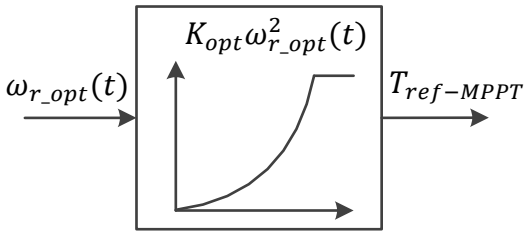

Figure 2-2 Control diagram of the MPPT control in a single WTS.

It is assumed in this chapter that the electrical power of the generator is the same as the given power reference due to the fast dynamic characteristics of VSC.

To smooth the fluctuating power from the wave farm by using the rotating kinetic energy of the WTSs in the combined wave-wind system, the basic principle is as follows: the WTSs are controlled to generate fluctuating power that is exactly opposite to the oscillating components of the wave power. Then the transmission lines of the wave-wind farm is smoothed, which means wave power is smoothed.

Define the oscillating components of the wave power as

$$\Delta P_c = P_{wave} - \overline{P_{wave}} \tag{2.5}$$

where P_{wave} is the total output electrical power from the wave farm, and $\overline{P_{wave}}$ is the average value, obtained through a moving average filter (MAF). It can be seen from (2.5) that in the long run, the average of ΔP_c is zero ($\overline{\Delta P_c} = \overline{P_{wave}} - \overline{P_{wave}} = 0$). According to the smoothing principle, the wind farm should generate the opposite power $-\Delta P_c$ to compensate ΔP_c.

The working principle of a MAF is that in each fixed time-step the input signal is sampled and then the average of the last N input samples is calculated as the output of the MAF. Hence, the MAF window time used in this thesis represents the sum of the N fixed time-step period.

The idea of the DCC method is to add $-\Delta P_c$ directly to (2.1) to generate the power or torque references for the WTS (shown in Figure 2-3), given by

$$P_{ref-DCC} = P_{ref0} - \Delta P_c \neq K_{opt}\omega_{r\_opt}(t) - \Delta P_c \tag{2.6}$$

$$= K_{opt}\omega_{r\_DCC}^3(t) - \Delta P_c \tag{2.7}$$

and

$$T_{ref-DCC} = K_{opt}\omega_{r\_DCC}^2(t) - \Delta P_c/\omega_{r\_DCC}(t) \tag{2.8}$$

where $\omega_{r\_DCC}(t)$ is the real-time rotor speed of the WTS under the DCC control.

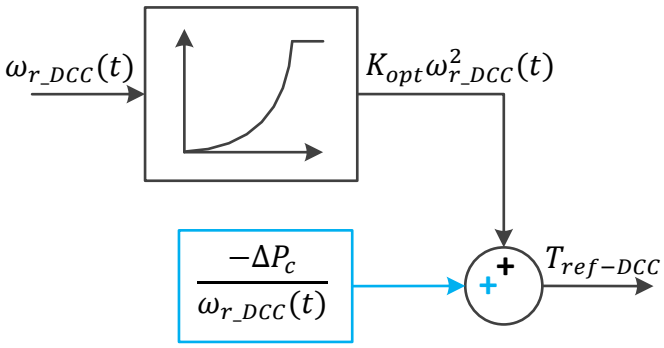

Figure 2-3 Control diagram of the DCC method in a single WTS.

From (2.6) and (2.7) it can be seen that $\omega_{r\_opt}(t) \neq \omega_{r\_DCC}(t)$ which means that when $-\Delta P_c$ is added into the MPPT control, $\omega_{r\_DCC}(t)$ is no longer equal to $\omega_{r\_opt}(t)$. This is because the additional term $-\Delta P_c$ makes the WTS accelerates or decelerates, resulting in the rotor speed $\omega_{r\_DCC}(t)$ deviating away from its optimum value $\omega_{r\_opt}(t)$. Thus, although the term $-\Delta P_c$ in (2.7) or $-\Delta P_c/\omega_{r\_DCC}(t)$ in (2.8) is able to smooth the wave power, the term $K_{opt}\omega_{r\_DCC}^3(t)$ in (2.7) or $K_{opt}\omega_{r\_DCC}^2(t)$ in (2.8) introduces new undesired fluctuations (shown in Figure 2-4) to $-\Delta P_c$, making the fluctuations of the wind power output not exactly opposite to that of wave power. Under such situation, the fluctuations of wave power cannot be completely

compensated. This means that the DCC method with the control reference in the form of (2.6) or (2.7) as shown in Figure 2-3 cannot smooth the wave power well.

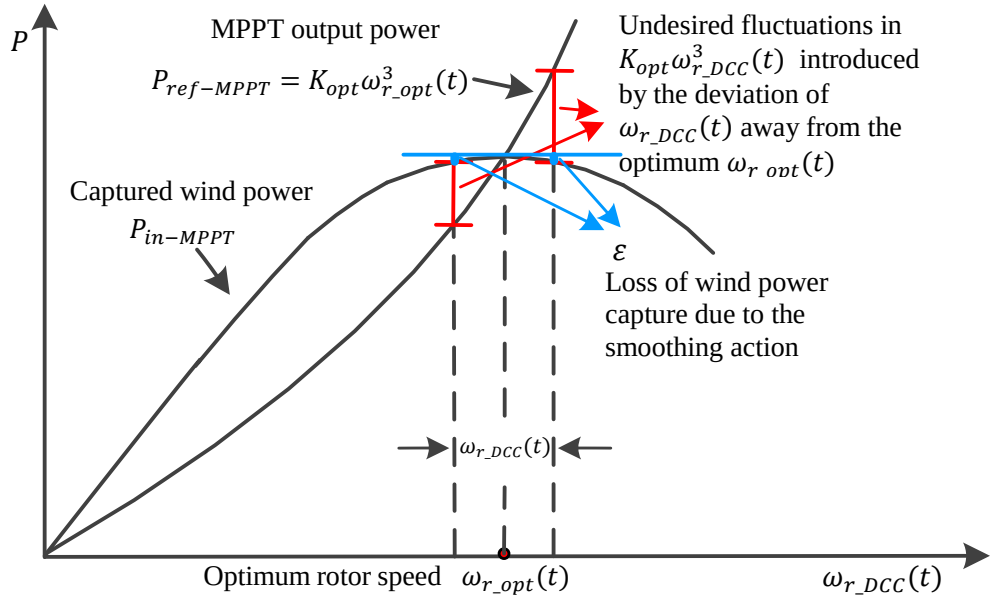

Figure 2-4 The undesired fluctuations in $K_{opt}\omega_{r\_DCC}^3(t)$ introduced by the deviations of $\omega_{r\_DCC}(t)$ from the optimum $\omega_{r\_opt}(t)$ when controlled by the DCC method (2.7).

2.3.2 Integral Compensation Control (ICC)

From the above analysis, the DCC method cannot well smooth the wave power for the reason that in (2.7) the term $K_{opt}\omega_{r\_DCC}^3(t)$ introduces new unwanted fluctuations to $-\Delta P_c$, making the output fluctuations of wind power not exactly opposite to that of the wave power. Therefore, as seen from Figure 2-4, the ideal (or expected) power output of a WTS should include two parts. One part of the wind power is the captured wind power from environmental wind, and the other part of the wind power is $-\Delta P_c$ which is used to compensate the fluctuations of wave power. Thus, considering that the loss of wind power capture will happen all the time during the smoothing operation, the ideal (or expected) power or torque output of the WTS should be in the form of

$$P_{ideal} = K_{opt}\omega_{r\_opt}^3(t) - \Delta P_c - \varepsilon \tag{2.9}$$

$$T_{ideal} = K_{opt}\omega_{r\_opt}^2(t) - \frac{\Delta P_c}{\omega_{r\_id}(t)} - \frac{\varepsilon}{\omega_{r\_id}(t)} \quad (2.10)$$

where $\omega_{r\_id}(t)$ is the real-time rotor speed of the WTS in the ideal (or expected) situation, and ε (also shown in Figure 2-4) is the difference between the maximum captured wind power under the MPPT control and the real captured wind power under the smoothing control due to the deviation of the rotor speed from its optimum. Thus, ε represents the loss of wind power capture caused by the smoothing action, and it is nonnegative all the time since the real-time rotor speed always deviates from the optimum $\omega_{r\_opt}(t)$.

From Figure 2-4, it can be seen that ε is small and it is expected to be small. This means that the smoothing operation should not cause the rotor speed deviating from its optimum too much, resulting in a big loss of wind power capture. Otherwise, the proposed scheme by using the kinetic energy to smooth wave power is not economic and thus not practical.

In (2.9), the first part ($K_{opt}\omega_{r\_opt}^3(t) - \varepsilon$) and second part $-\Delta P_c$ give the expected two objectives of approximate maximum wind power capture and wave power smoothing, respectively, when the kinetic energy of a WTS is used to smooth wave power.

However, applying the power reference (2.9) directly cannot ensure the WTS stable. The reason is that under the smoothing situation, $K_{opt}\omega_{r\_opt}^3(t)$ does not response the energy level of the WTS. This means $K_{opt}\omega_{r\_opt}^3(t)$ cannot automatically balance the input and output energy of the WTS and make the WTS stable under disturbances, such as the sudden drop of input wind speed. This is because now under the ideal smoothing situation the real-time rotor speed is $\omega_{r\_id}(t)$ instead of $\omega_{r\_opt}(t)$. In order to automatically make a WTS stable, the real-time rotor speed which includes the energy information should be used as a feedback signal. This is also the reason why in the classic MPPT control, the real-time rotor speed, instead of other calculated rotor speed, is used as a feedback signal in the given power or torque

references. So now if in (2.9) $K_{opt}\omega_{r\_opt}^3(t)$ is replaced by $K_{opt}\omega_{r\_id}^3(t)$, the WTS can stay stable automatically. However, if in (2.9) $K_{opt}\omega_{r\_opt}^3(t)$ is replaced by $K_{opt}\omega_{r\_id}^3(t)$, (2.9) becomes the DCC control except that it does not have the small value of $-\varepsilon$. Since DCC cannot smooth the wave power well, (2.9) cannot smooth the wave power well as well, thus cannot achieve the expected two objectives of approximately maximum wind power capture and wave power smoothing simultaneously.

In order to obtain these two objectives simultaneously and make the WTS stable, ICC is proposed by adding another term into (2.9) and replacing $K_{opt}\omega_{r\_opt}^3(t)$ with $K_{opt}\omega_r^3(t)$. $\omega_r(t)$ is real-time rotor speed under the ICC control. In other words, ICC is proposed by adding another term plus $-\varepsilon$ into DCC, so that the unwanted fluctuations in DCC are compensated.

Now, how to add the additional term becomes the key point of the proposed ICC method. In the following, the detailed deduction of the proposed ICC method is provided.

Defining the additional term as T_{int}, adding it into (2.10), and at the same time replacing $K_{opt}\omega_{r\_opt}^2(t)$ with $K_{opt}\omega_r^2(t)$, yields

$$T_{ref-ICC} = K_{opt}\omega_r^2(t) - \frac{\Delta P_c}{\omega_r(t)} - \frac{\varepsilon}{\omega_r(t)} + T_{int} \tag{2.11}$$

The $\omega_{r\_id}(t)$ in (2.10) is also replaced by the real-time rotor speed of $\omega_r(t)$ of the ICC control.

It should be noted that the ε in (2.9)-(2.11) (shown in Figure 2-4), has the same meaning, representing the loss of wind power capture caused by the deviation of the real-time rotor speed away from the optimum value. Furthermore, ε is nonnegative all the time.

Figure 2-5 shows the brief control block of the ICC control.

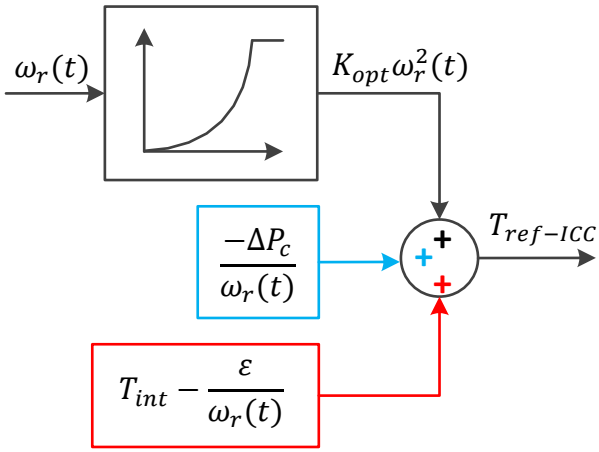

Figure 2-5 Brief control diagram of the proposed ICC in a single WTS.

Since the proposed ICC is trying to achieve the two objectives of approximate maximum wind power capture and wave smoothing simultaneously, by making (2.10) equivalent to (2.11), it follows that

$$K_{opt}\omega_r^2(t) - \frac{\Delta P_c}{\omega_r(t)} + T_{int} - \frac{\varepsilon}{\omega_r(t)} = K_{opt}\omega_{r\_opt}^2(t) - \frac{\Delta P_c}{\omega_{r\_id}(t)} - \frac{\varepsilon}{\omega_{r\_id}(t)} \tag{2.12}$$

Since both $\omega_r(t)$ and $\omega_{r\_id}(t)$ represent the real-time rotor speed, they are equal ($\omega_r(t) = \omega_{r\_id}(t)$). Then from (2.12), it follows that

$$T_{int} = -K_{opt}\left(\omega_r^2(t) - \omega_{r\_opt}^2(t)\right) \tag{2.13}$$

Meanwhile, the stored kinetic energy ΔE in the WTS is changing due to output fluctuating power ΔP_c. Thus ΔE is

$$\Delta E = \int_0^t \Delta P_c \, dt \tag{2.14}$$

On the other hand, when the rotor speed $\omega_r(t)$ decelerates or accelerates from the optimal rotor speed $\omega_{r\_opt}(t)$ due to output fluctuating power ΔP_c, the change of the kinetic energy has

$$\Delta E = \frac{1}{2} \cdot J\left(\omega_r^2(t) - \omega_{r\_opt}^2\right) \tag{2.15}$$

where J represents the moment of inertia of the WTS.

Comparing (2.14) with (2.15) yields

$$\omega_r^2(t) - \omega_{r\_opt}^2(t) = \frac{2}{J}\int_0^t \Delta P_c \, dt \tag{2.16}$$

From (2.16), it can be seen that the change of kinetic energy ($\omega_r(t)$ deviating away from the optimum $\omega_{r\_opt}(t)$) is all used for smoothing ΔP_c. Substituting (2.16) into (2.13) gives

$$T_{int} = \frac{-2K_{opt}}{J}\int_0^t \Delta P_c \, dt \tag{2.17}$$

By combining (2.11) and (2.17), it follows that

$$T_{ref-ICC} = K_{opt}\omega_r^2(t) + \frac{-\Delta P_c}{\omega_r(t)} + \frac{2K_{opt}}{J}\int_0^t (-\Delta P_c)\, dt - \frac{\varepsilon}{\omega_r(t)} \tag{2.18}$$

Now by ignoring $\frac{\varepsilon}{\omega_r(t)}$ in $T_{ref-ICC}$, (2.18) becomes

$$T_{ref-ICC} = K_{opt}\omega_r^2(t) + \frac{-\Delta P_c}{\omega_r(t)} + \frac{2K_{opt}}{J}\int_0^t (-\Delta P_c)\, dt \tag{2.19}$$

Then in the proposed ICC method the torque reference $T_{ref-ICC}$ expressed in (2.19) is applied to the rotor side converter of a WTS.

When comparing the proposed ICC (2.19) with the DCC (2.8), the only difference is the extra term $\frac{2K_{opt}}{J}\int_0^t (-\Delta P_c)\, dt$. The extra term in (2.19) is for compensating the undesired fluctuations in $K_{opt}\omega_{r\_DCC}^3(t)$ shown in Figure 2-4, so that the WTS under ICC can produce extract fluctuating power opposite to the fluctuations of wave power.

The neglecting $\frac{\varepsilon}{\omega_r(t)}$ in (2.18) is necessary and reasonable, considering the following three aspects.

First, neglecting $\frac{\varepsilon}{\omega_r(t)}$ has little effect on the smoothing performance since ε is sufficiently small, which can be seen from Figure 2-4. The simulation results in Section 2.4 will also demonstrate that the loss of wind power capture is sufficiently small.

Second, neglecting $\frac{\varepsilon}{\omega_r(t)}$ does not affect the stability of the WTS. In the given torque reference (2.19) the last two terms have zero average, and the first term uses the rotor speed as the feedback signal. These two factors together make the WTS stable automatically.

Third, neglecting $\frac{\varepsilon}{\omega_r(t)}$ is beneficial for practical engineering operation. In engineering practice, the mechanical power from the captured wind is difficult to measure, which means ε is hard to obtain.

From (2.19), the power reference is

$$P_{ref-ICC} = K_{opt}\omega_r^3(t) + \omega_r(t) \cdot \frac{2K_{opt}}{J} \int_0^t (-\Delta P_c)\, dt - \Delta P_c$$

$$= P_{wind}^0 - \Delta P_c \tag{2.20}$$

where

$$P_{wind}^0 = K_{opt}\omega_r^3(t) + \omega_r(t) \cdot \frac{2K_{opt}}{J} \int_0^t (-\Delta P_c)\, dt \tag{2.21}$$

The P_{wind}^0 is defined in Section 2.2, representing the captured wind power from the environmental wind.

It should be noted that although in this work the torque reference (2.19) is used for a WTS, the power reference (2.20) can also be used. They both result in the same control performance.

Figure 2-6 shows the proposed ICC for a wave-wind farm in which the wind farm has only one WTS. From Figure 2-6, it can be seen that the proposed control scheme (2.19) is easy in implementation since only two additional terms are added compared with the original MPPT control reference (2.2). In addition, the only extra measurement signal is the electrical power from the wave farm, which is conveniently accessible.

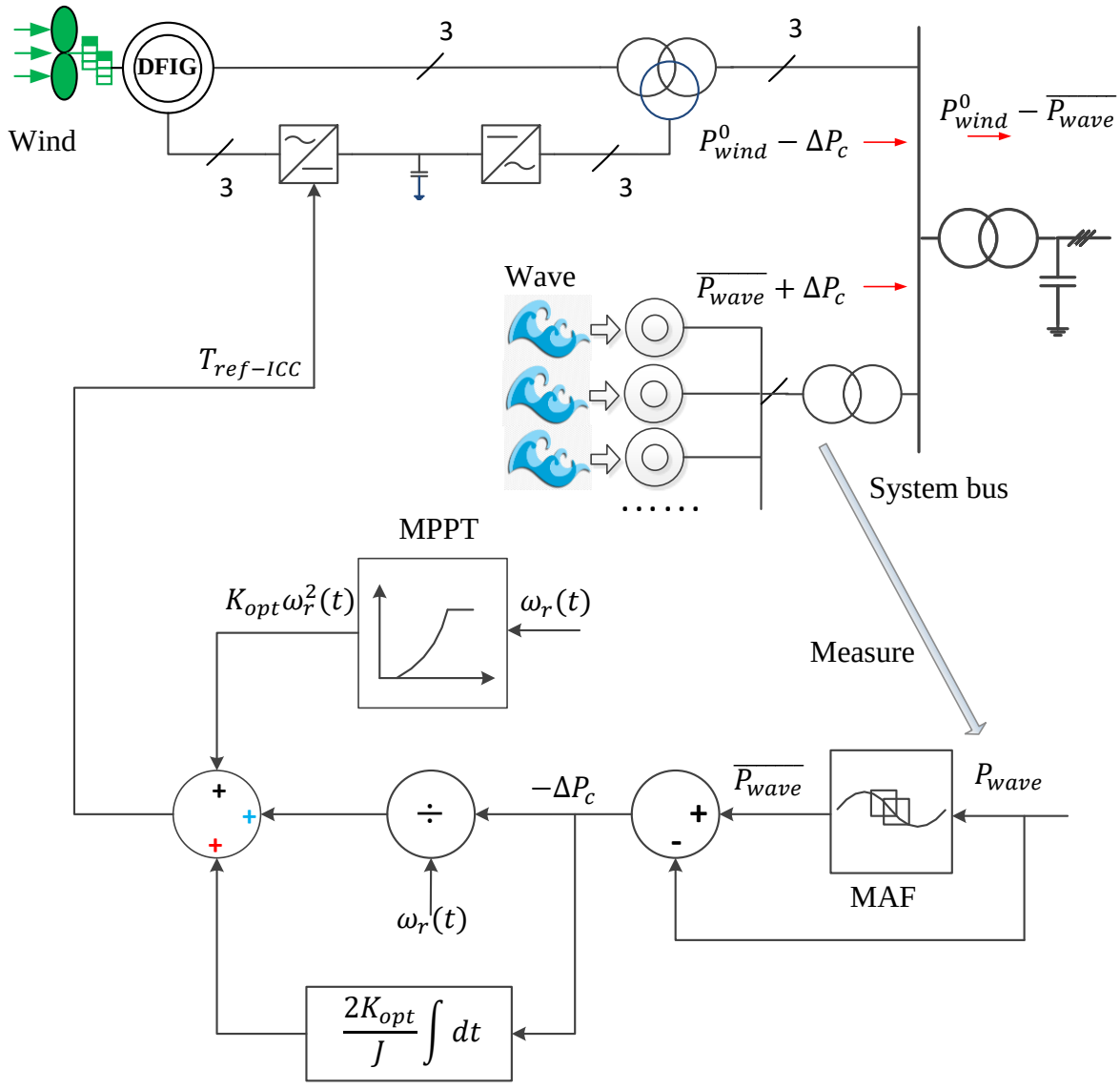

Figure 2-6 The control structure of the proposed ICC for a single WTS.

2.3.3 Coordinative ICC within a Wind Farm

For a wave-wind farm system consisting of M WTSs, the torque reference of each WTS is the same as that in Section 2.3.2, except that $-\Delta P_c$ is replaced by $-\Delta P_{ci}$. This is because the i^{th} WTS is only responsible for compensating part of the total fluctuating wave power ΔP_c. In the wind-farm system, considering that the stored kinetic energy of a WTS is in proportion to the squared rotor speed, $-\Delta P_{ci}$ is defined as

$$-\Delta P_{ci} = \frac{\bar{\omega}_{ri}^2(t)}{\sum_{j=1}^{M} \bar{\omega}_{rj}^2(t)} \cdot (-\Delta P_c) \tag{2.22}$$

where $\bar{\omega}_{ri}(t)$ represents the average rotor speed of the i^{th} WTS, obtained from a MAF. In this way, the total compensated power equals to $-\Delta P_c$ since it always has

$$\sum_{i=1}^{M}(-\Delta P_{ci}) = -\Delta P_c \tag{2.23}$$

The reason for allocating the compensation wave power as (2.22) is that it can reduce the total loss of wind energy capture caused by the smoothing operation. This is due to the fact that in real situations each WTS experiences different wind speeds, and the WTSs with higher wind speeds have higher rotor speeds and can naturally release more kinetic energy. Thus, based on (2.22), WTSs with higher rotor speeds will be automatically allocated more wave power to smooth and WTSs with lower rotor speeds will be automatically allocated less wave power to smooth. This allows the required compensation wave power being dynamically allocated to each WTS based on their kinetic energy storage capability. In this way, the total loss of wind power capture caused by the smoothing operation can be reduced.

2.4 Case Studies

2.4.1 Test System

In order to demonstrate that the proposed ICC can achieve the two objectives of wave power smoothing and high wind energy capture simultaneously, both DFIG-based and PMSG-based WTSs are simulated on RTDS platform under different constant wind speeds as well as varying wind speeds. Two kinds of wave-wind farm test systems are built. One test system is composed of one WTS and three FSIGs (named as "one-WTS system"), and the other system is composed of two WTSs and six FSIGs (named as "two-WTS system") used to demonstrate the benefits of the coordinative ICC within a wind farm.

The simulations parameters for the DFIGs, PMSGs and wave FSIGs are listed in Table A-1, Table A-2 and Table A-3 in Appendix A, respectively. In a DFIG-based WTS, only two masses are modelled, the turbine itself and the DFIG. The cut-in wind speed is 6 m/s and the rated wind speed is 12.5 m/s. The maximum rotor speed of the DFIG is 1.25 $p.u.$. In a PMSG-based WTS, the cut-in wind speed is also 6 m/s but the rated wind speed is 12 m/s. The maximum rotor speed of the PMSG is 1.0 $p.u.$.

The mechanical input torques of the FSIGs in the wave farm are simulated by random sinusoidal waves. Each sinusoidal wave is the sum of a random constant and a sinusoid whose amplitude is the same as the constant, making the output power of each FSIG fluctuating from zero to twice its average. These sinusoidal waves have random frequencies, but all within a typical time period of 5~12 s In the following case studies, the MAF window time is chosen to be 100 s.

The following sections describe six case studies about DFIG-based and PMSG-based WTSs in RTDS under constant and variable wind speed situations, to validate the effectiveness of the proposed ICC method.

2.4.2 Wave Power Smoothing under Constant Wind Speeds

The following three cases are to illustrate the performance of the proposed method under constant wind speed both in DFIG-based and PMSG-based one-WTS system.

Case 1: In this case, the DFIG-based one-WTS system is simulated under the constant wind speed of 9.5m/s. The simulation results of the proposed ICC and DCC methods are compared.

Case 2: In this case, the PMSG-based one-WTS system is simulated under 10m/s constant wind speed. Comparative simulation results under the proposed ICC and DCC methods are provided.

Case 3: This case is to show the relationship between the wave power smoothing effect and wind power capture efficiency under different constant wind speeds in DFIG-based one-WTS system.

The simulation results for Case 1 are shown in Figure 2-7. Figure 2-7(a) shows that the power of the system bus is smoothed well by using the proposed ICC. Figure 2-7(b) and Figure 2-7(c) show that the fluctuation range of the DFIG rotor speed and the captured wind power are almost the same under the both control methods. This is because the same ΔP_c is introduced in both methods, making the change of the kinetic energy in the WTS almost in the same range. Although the rotor speed and the loss of wind power capture are almost in the same range, the smoothing effect by ICC is better than that of DCC. This is because under DCC the WTS cannot generate the fluctuating power exactly opposite to the fluctuations of the output power of the wave farm, due to the undesired fluctuations in $K_{opt}\omega_{r\_DCC}^3(t)$ introduced by the

deviations of $\omega_{r\_DCC}(t)$ from the optimum $\omega_{r\_opt}(t)$ in the DCC method (2.6) (The details are described in Section 2.3.1); While, as shown in Figure 2-7(d), the WTS under ICC can generate the fluctuating power exactly opposite to the fluctuating parts of the wave power since the additional integral term T_{int} is introduced into DCC to compensate the undesired fluctuations.

Figure 2-7(c) shows that the captured wind power under ICC is slightly smaller than the maximum under the MPPT control, which validates that the WTSs can obtain the high wind energy capture efficiency, although the DFIG-based WTS releases or absorbs fluctuating power around 1.0 time of its average output power, as seen from Figure 2-7(d). Figure 2-7(b) shows that the DFIG always swings around the optimum rotor speed under the MPPT control, which demonstrates that the WTS is controlled well as a kinetic energy storage unit. This shows the potential of using the large inertia of WTSs to smooth the wave power which fluctuates heavily at short-term periods. This also verifies that ε in (2.18) is sufficiently small and can be ignored.

According to the fact that the loss of wind energy capture mainly results from the deviation of the rotor speed from its optimum, as illustrated in Figure 2-4, a larger rotor inertia of a WTS can lead to less rotor speed deviation and thus less loss of wind energy capture.

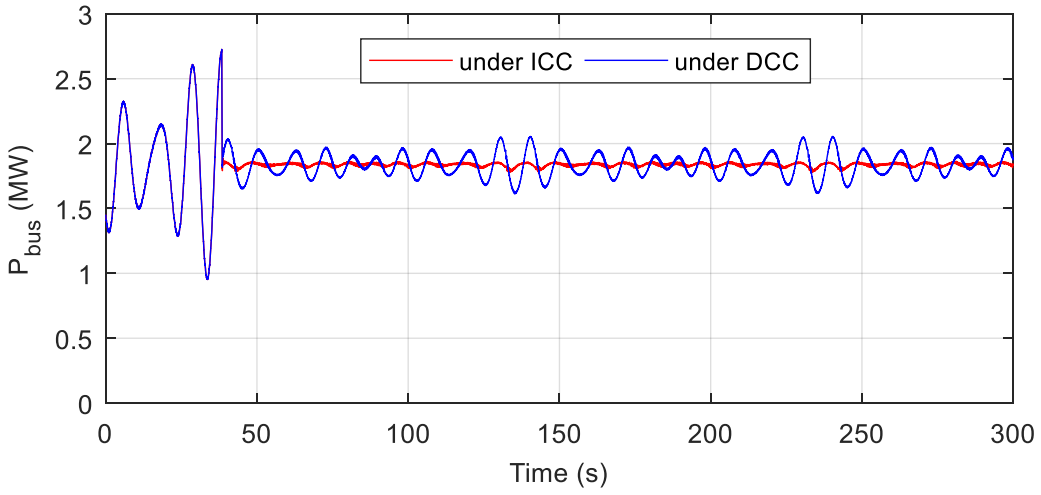

(a) The total power that is injected into the system bus under the ICC and DCC control.

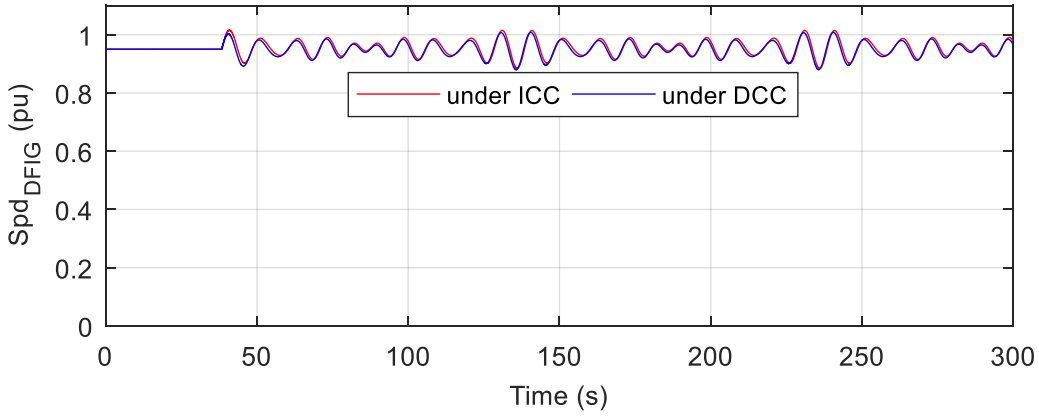

(b) Profile of the DFIG rotor speed under the ICC and DCC control.

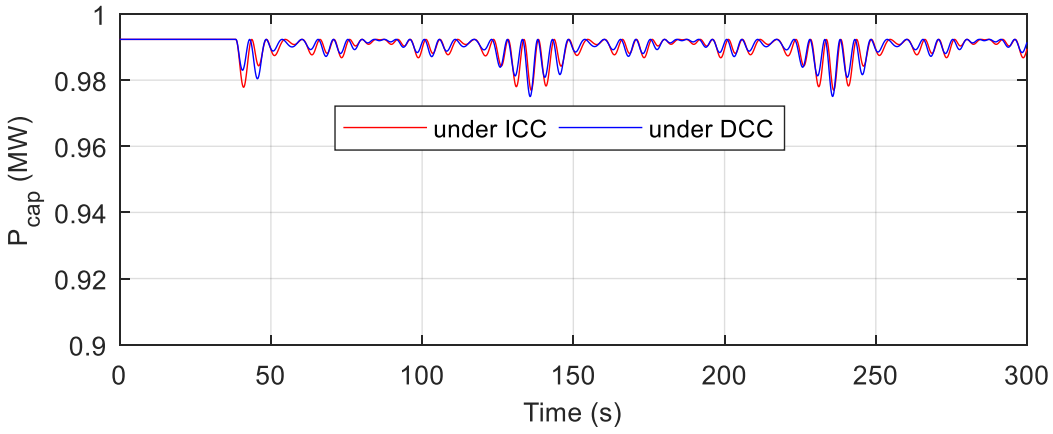

(c) Profile of the wind power capture of the DFIG-based WTS under the ICC and DCC control.

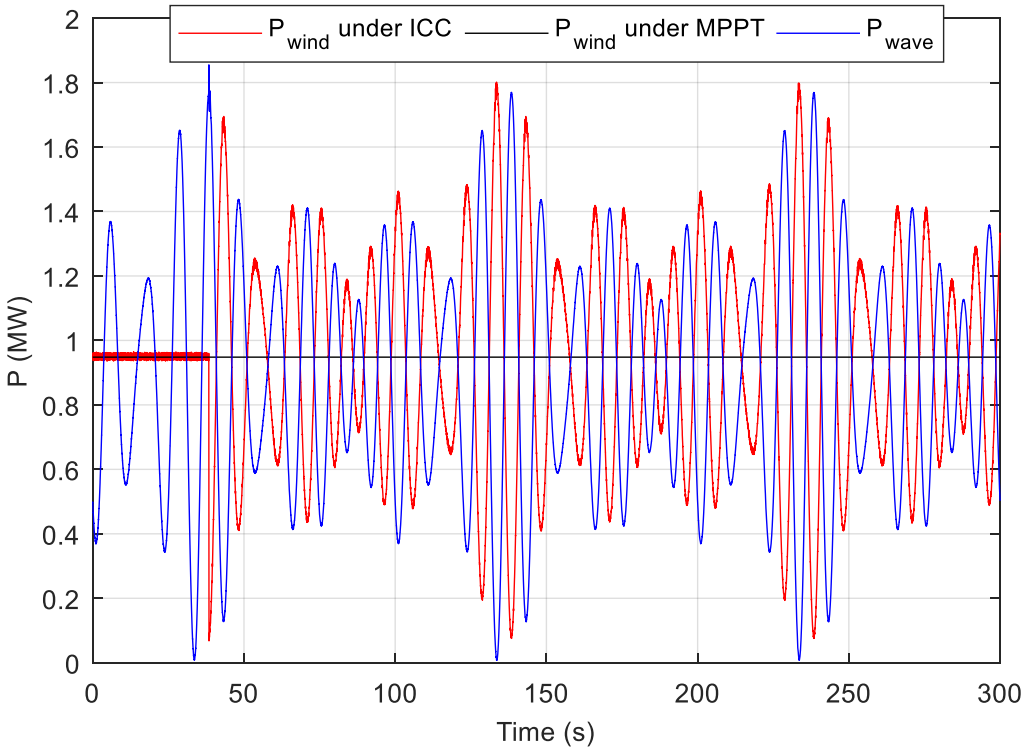

(d) The output power of the wave farm and the DFIG-based WTS under the ICC and MPPT control.

Figure 2-7 Comparative simulation results under DCC, the proposed ICC and MPPT control under Case 1. DCC and ICC are activated at 40 s.

The simulation results for Case 2 are shown in Figure 2-8. It can be seen that the simulation results of the PMSG-based one-WTS system are similar to those in Case 1, which verifies the effectiveness of the proposed ICC used in PMSG-based WTSs.

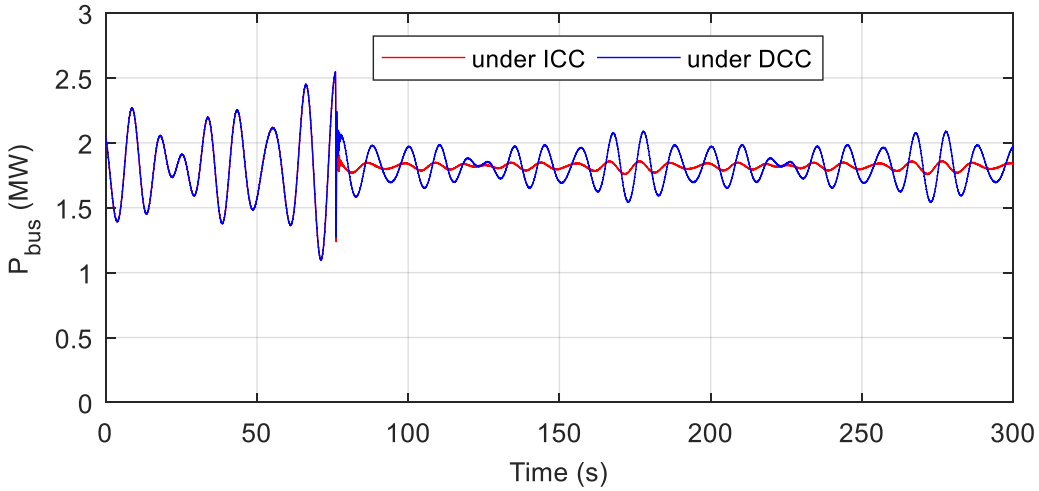

(a) The total power that is injected into the system bus under the ICC and DCC control.

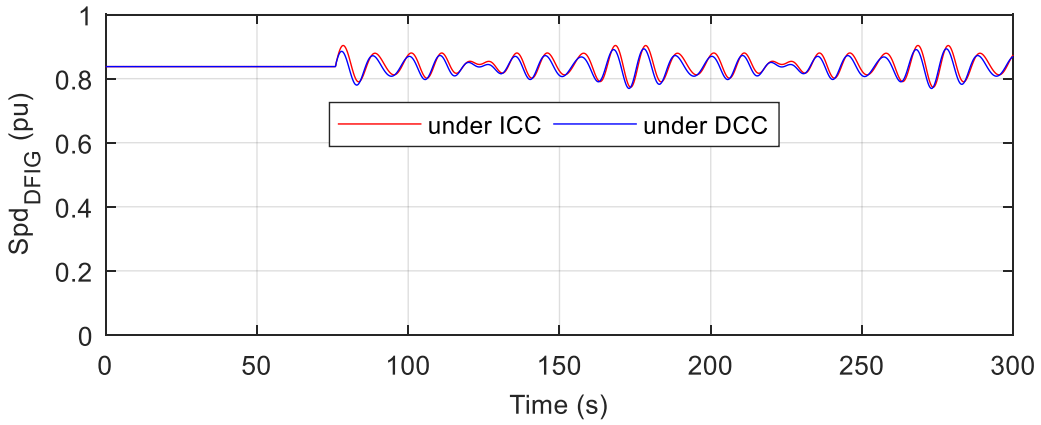

(b) Profile of the PMSG rotor speed under the ICC and DCC control.

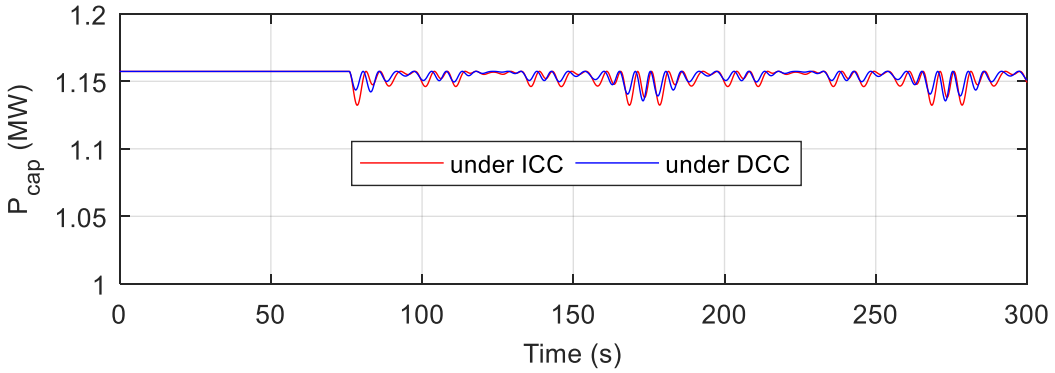

(c) The wind power capture of the PMSG-based WTS under the ICC and DCC control.

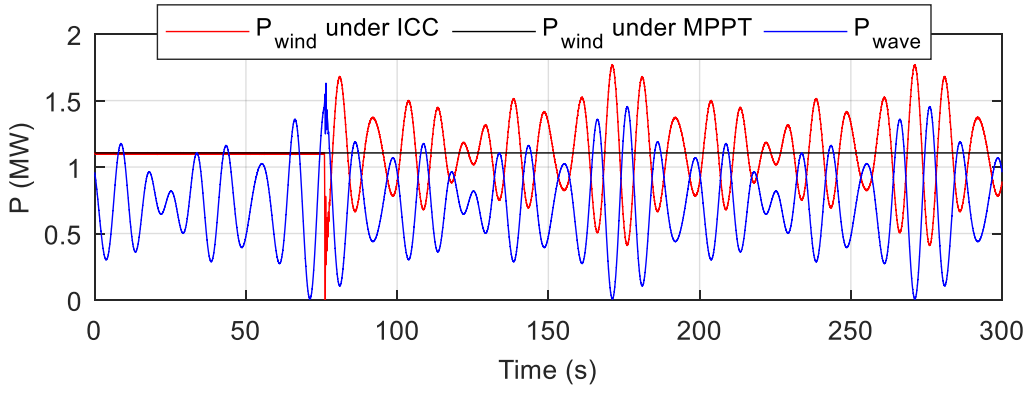

(d) The output power of the wave farm and the WTS under the ICC and MPPT control.

Figure 2-8 Comparative simulation results under DCC, the proposed ICC and MPPT control under Case 2. DCC and ICC are activated at 75 s.

The results of Case 3 are provided in Figure 2-9. In Figure 2-9 the variable ξ is defined as the wave-wind ratio, which has no unit and is calculated by

$$\xi = \overline{P_{wind}}/\sigma_{P_{wave}} \tag{2.22}$$

where $\overline{P_{wind}}$ represents the average value of P_{wind}, which is the total output power of a wind farm when controlled by MPPT, and $\sigma_{P_{wave}}$ represents the standard deviation of P_{wave}, which is the output electrical power of a wave farm. This index indicates that to realize a required smoothing effect, the required number of WTSs is related to the fluctuating degree of wave power.

In order to assess the smoothing performance, two quantitative indexes are used. The first one is called the standard deviation of the active power flowing on the system bus $\sigma_{P_{bus}}$, representing the smoothness of the wave power on the system bus. The second index is the efficiency of wind power capture $\eta_{P_{cap}}$. It is the ratio of the average captured wind power of the wind farm under ICC and the MPPT control. Thus, $1-\eta_{P_{cap}}$ denotes the percentage of the wind power capture loss due to the wave power smoothing action.

Figure 2-9(a) and Figure 2-9(b) show the values of $\sigma_{P_{bus}}$ and $\eta_{P_{cap}}$ for different ξ (defined in (2.22)), respectively. It is seen that by using the proposed ICC, $\sigma_{P_{bus}}$ is reduced significantly by 10~20 times and only 1% of $\eta_{P_{cap}}$ is lost when ξ is bigger than 2. When ξ is bigger than 2.6, the percentage of the wind power capture loss $(1-\eta_{P_{cap}})$ is smaller than 0.5%. This implies that with the loss of wind energy capture less than 5%, a WTS, which outputs 2.6 MW average power under the MPPT control, can smooth fluctuating wave power with 1 MW standard deviation. These two figures also indicate that a larger ξ leads to less loss of wind power capture.

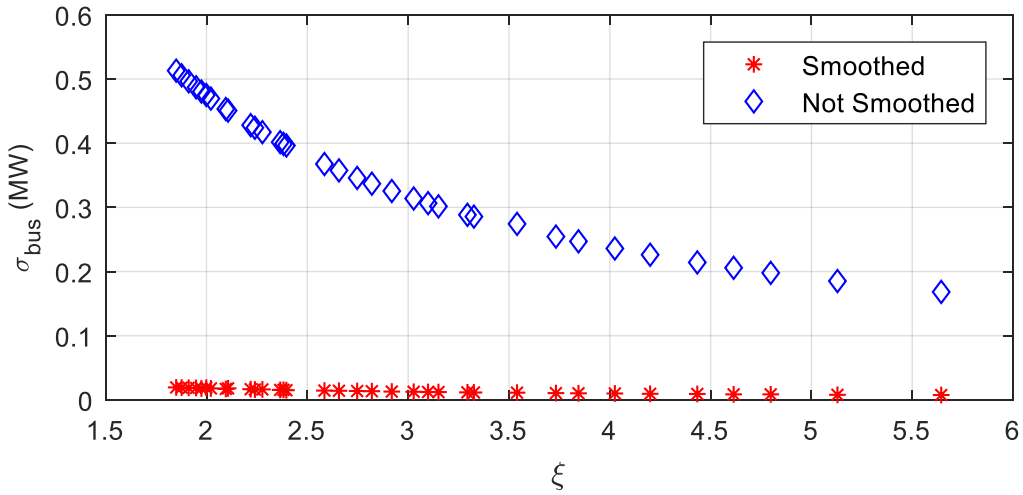

(a) Power standard deviations of the system bus ($\sigma_{P_{bus}}$).

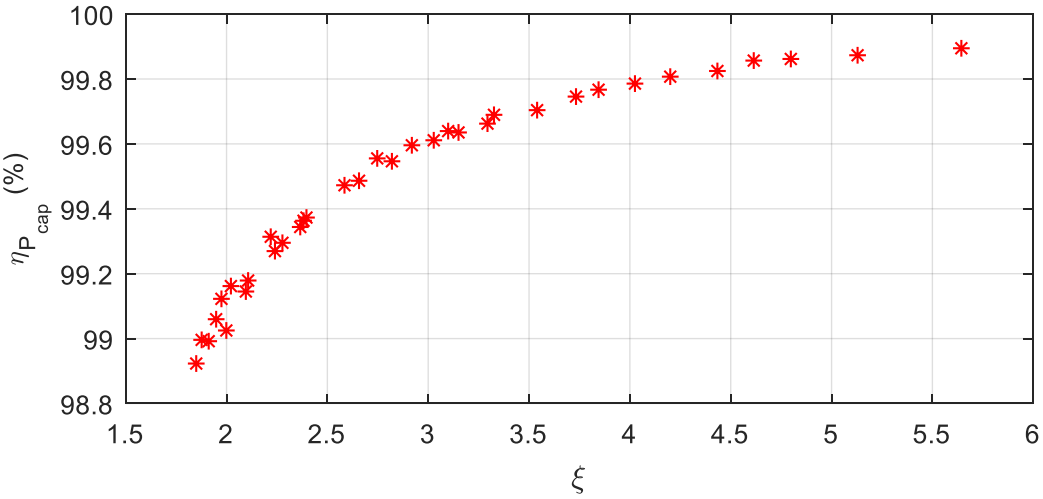

(b) Efficiency ($\eta_{P_{cap}}$) of wind power capture for different ξ.

Figure 2-9 Simulation results under Case 3.

2.4.3 Wave Power Smoothing under Variable Wind Speeds

The following two cases are used to show the performance of the proposed ICC under variable wind speeds in a DFIG-based one-WTS system and a PMSG-based one-WTS system.

Case 4: In this case, the DFIG-based one-WTS system is simulated under variable wind speeds to illustrate that the DFIG-based WTS under the proposed ICC can smooth the wave power and meanwhile automatically follow the change of wind speeds and achieve high wind energy capture efficiency.

Case 5: In this case, the PMSG-based one-WTS system is simulated under varying wind speeds to illustrate that the PMSG-based WTS under the proposed ICC can smooth the wave power and achieve high wind power capture efficiency in this circumstance.

The simulation results of Case 4 are presented in Figure 2-10. The profile of the real-time wind speed borrowed from [161] is shown in Figure 2-10(a). It should be noted that in the real implementation of the proposed ICC, the wind speed is not needed to be known.

Figure 2-10(b) shows that when the smoothing action is activated at $t = 218s$, the DFIG-based WTS immediately generate fluctuating power which is opposite to the fluctuations of wave power, making the wave power smoothed. Meanwhile, it can be seen that from 218 s to 450 s the average value of the output wind power always follows the output wind power under the MPPT control, indicating that the DFIG-based WTS with ICC can achieve high wind power capture under variable wind speeds, which can also be seen from Figure 2-10(d).

Figure 2-10(c) shows that the WTS always operates around the optimum rotor speeds under varying wind speeds, which makes the wind power capture close to its maximum as seen from Figure 2-10(d). Thus, both the results in Figure 2-10(c) and Figure 2-10(d) verify that the WTS can follow the wind speeds automatically and achieve high wind energy capture efficiency. From Figure 2-10(d) it also can be seen that the loss of wind power capture is in the same range of that in Figure 2-7(c) where the wind speed is constant. By comparing the black curve of P_{wind} under MPPT in Figure 2-10(b) with the black curve of P_{cap} under MPPT in Figure 2-

10(d), it can be seen that the output power P_{wind} is smoother than the captured wind power P_{cap}. This is due to the inherent inertial effect existing in the WTS.

For *Case* 4, ξ equals to 2.6 and the efficiency of the captured wind power $\eta_{P_{cap}}$ is 99.6%. $\eta_{P_{cap}}$ and ξ in this case are calculated during time interval [218, 450] s. This result of $\xi \sim \eta_{P_{cap}}$ is consistent with that in Figure 2-9(b). Finally, Figure 2-10(e) shows that after 218 s, the wave power flowing on the system bus is well smoothed by ICC and the fluctuations left only come from the fluctuations of the capture wind power, which can be verified by comparing the almost same dynamic characteristics of P_{wind} under MPTT (black line) in Figure 2-10(b) with that in Figure 2-10(e) after 218 s.

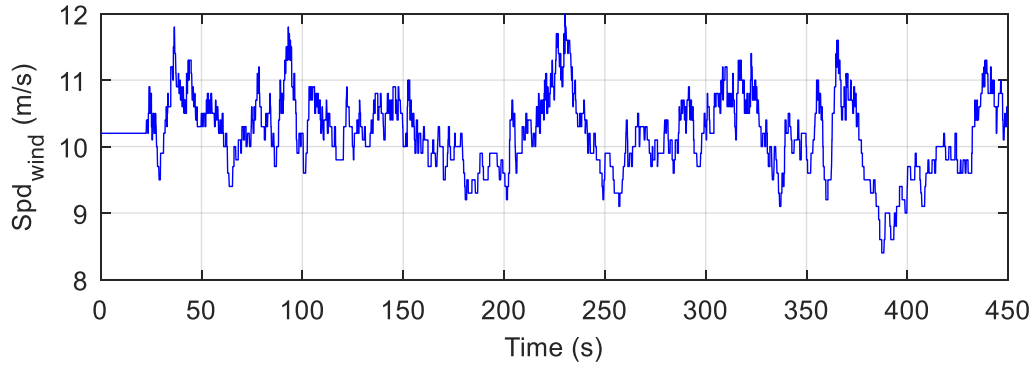

(a) Profile of the wind speeds simulated.

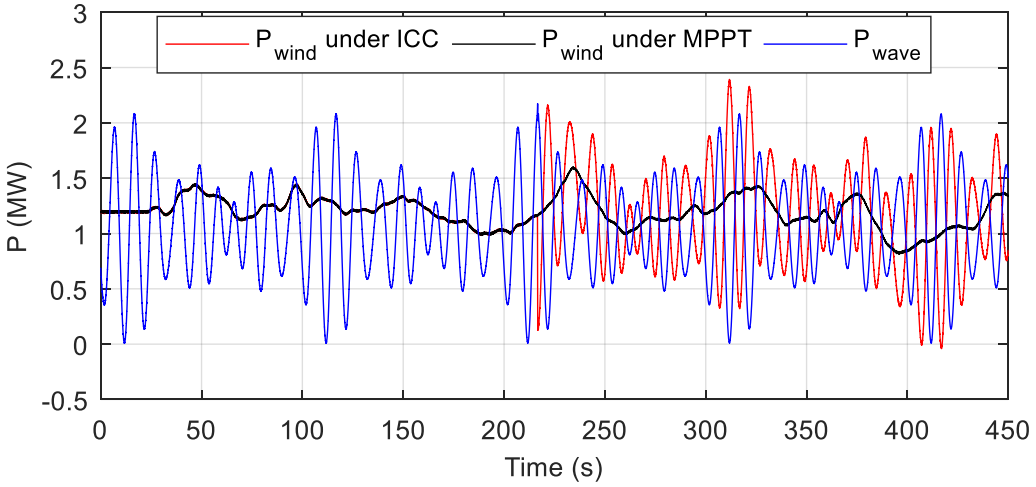

(b) The output power of the wave farm and the DFIG-based WTS under the ICC and MPPT control.

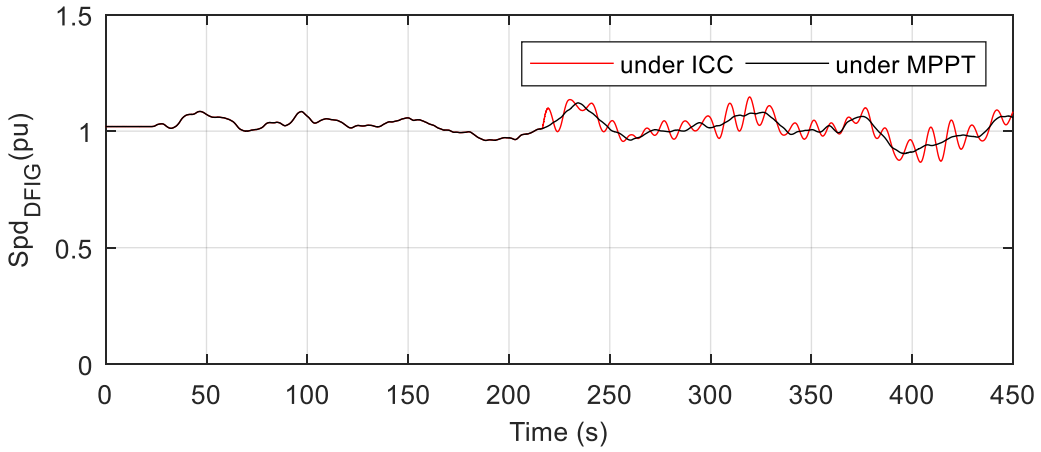

(c) Profile of the DFIG rotor speed under the ICC and MPPT control.

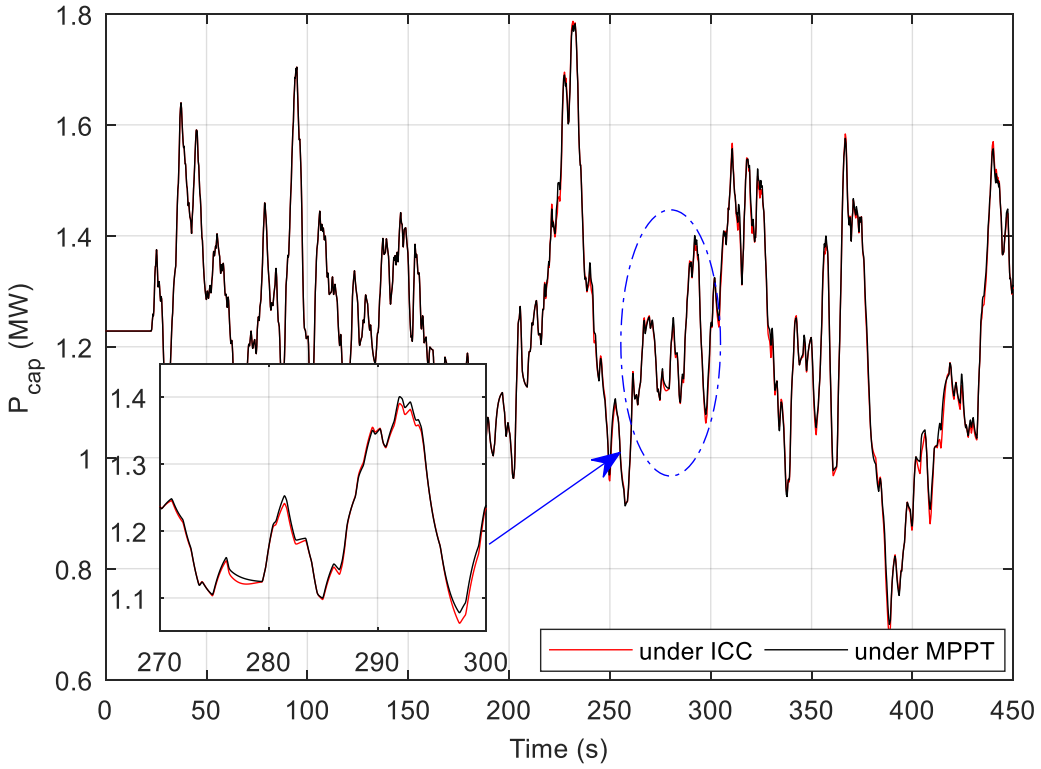

(d) Profile of the captured wind power under the ICC and MPPT control.

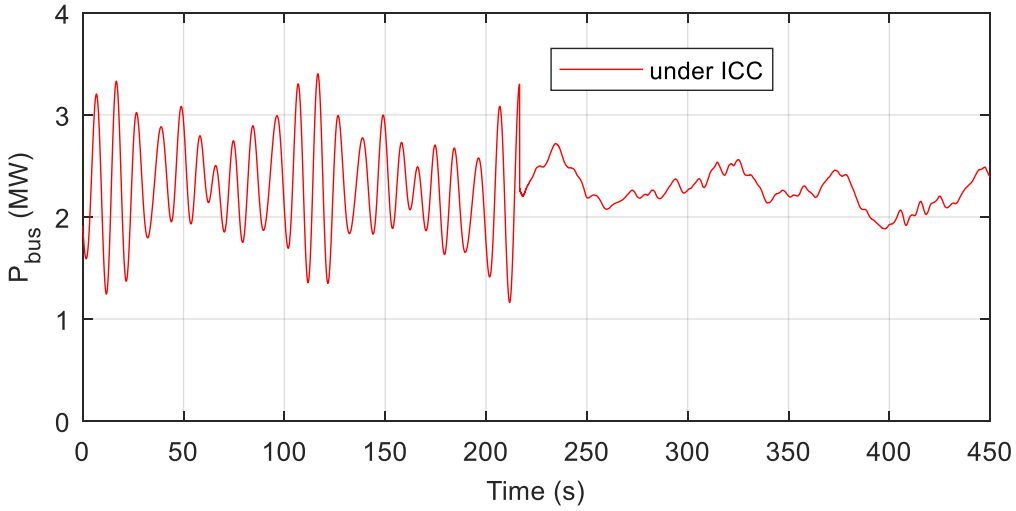

(e) The total power that is injected into the system bus under ICC.

Figure 2-10 Comparative simulation results of the proposed ICC and MPPT control under Case 4 with ICC activated at 218 s.

The results of Case 5 are given in Figure 2-11. Figure 2-11 shows that the results of the PMSG-based WTS in this case are similar to those in Case 4, demonstrating that the proposed ICC under variable wind speeds is also effective for PMSG-based WTSs.

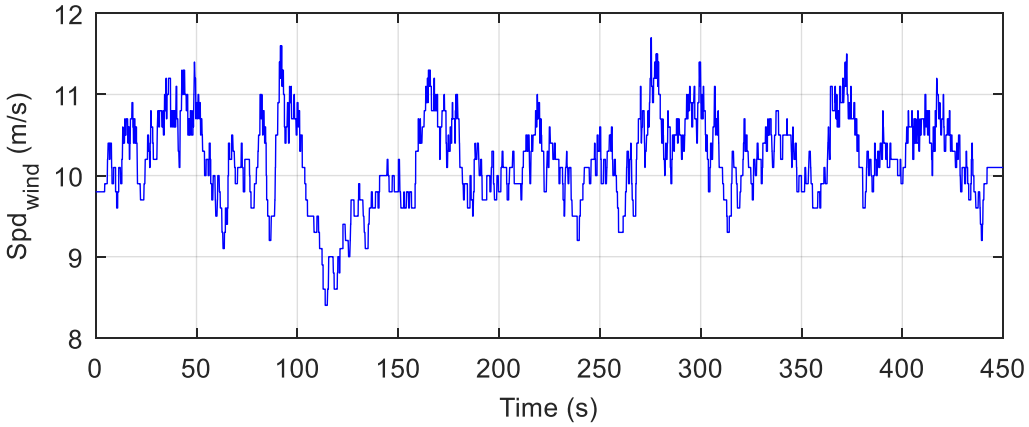

(a) Profile of the wind speeds simulated.

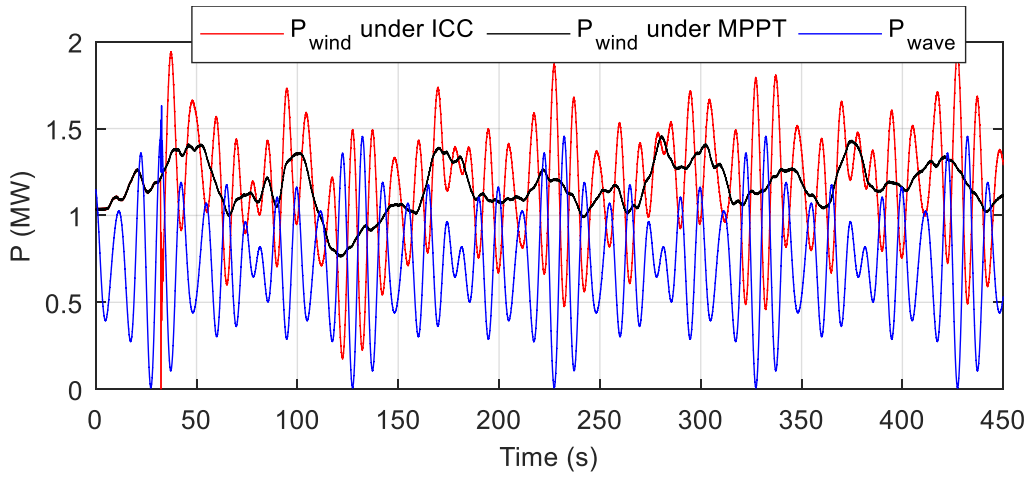

(b) The output power of the wave farm and the PMSG-based WTS under the ICC and MPPT control.

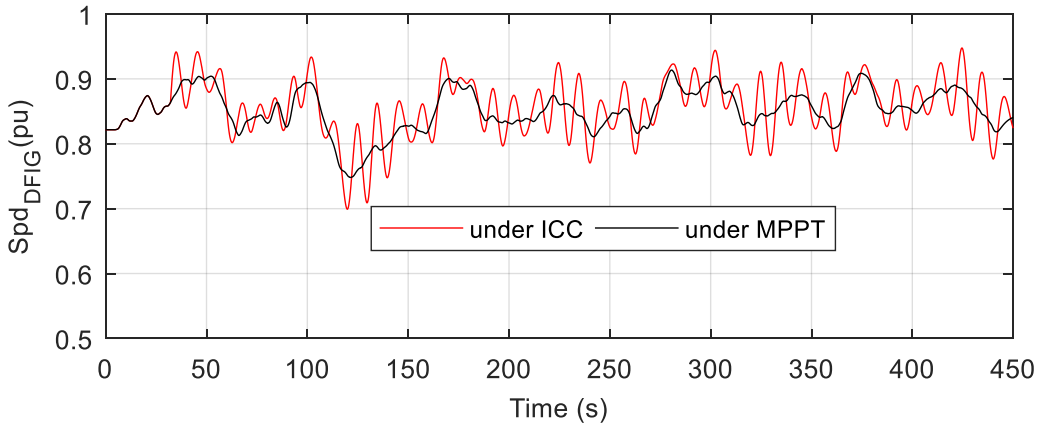

(c) Profile of the PMSG rotor speed under the ICC and MPPT control.

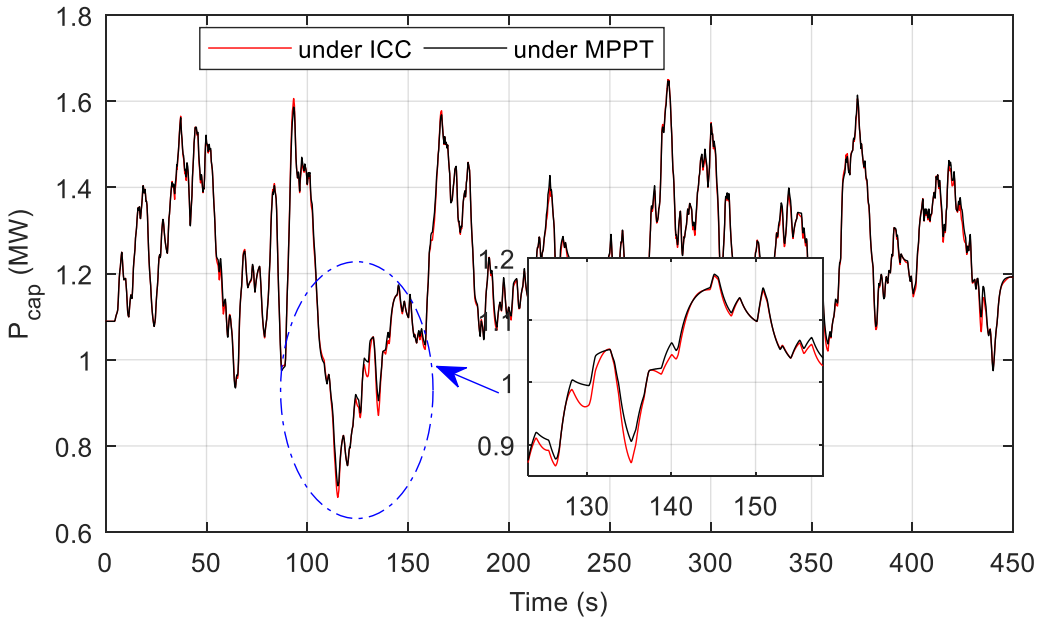

(d) Profile of the captured wind power under the ICC and MPPT control.

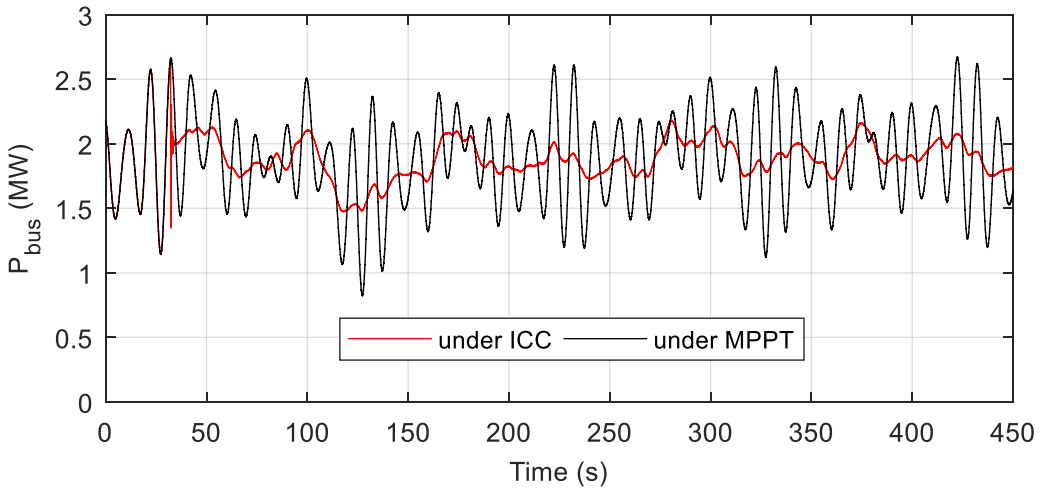

(e) The total power that is injected into the system bus under the ICC and MPPT control.

Figure 2-11 Comparative simulation results of the proposed ICC and MPPT control under Case 5. ICC is activated at 30 s.

2.4.4 Coordinative ICC within a Wind Farm

Case 6: In this case, two DFIG-based WTSs are simulated in a two-WTS system to demonstrate that the coordination algorithm of (2.22) has the ability in reducing the loss of wind power capture.

The simulation results for Case 6 are shown in Figure 2-12. Figure 2-12(a) shows the two varying wind speed profiles for the two WTSs (referred as WTS1 and WTS2). It is shown in Figure 2-12(b) that after the smoothing operation is activated at $t = 130s$, the fluctuating wave power flowing on the system bus is instantly smoothed, similar to that in other cases.

With higher wind speeds input, WTS2 has higher rotor speed than WTS1, as seen from Figure 2-12(c). Then, according to the coordination algorithm (2.20), WTS2 is automatically allocated more wave power to smooth, making its output power fluctuate more violently than that of WTS1, as seen from Figure 2-12(d). Although the fluctuation range of their output power is

different, the fluctuation amplitudes of the two WTSs rotor speeds are almost in the same range, as seen from Figure 2-12(c). This is important since it can reduce the loss of wind power capture and maintain the stability of WTSs. Otherwise, if the required compensation power is evenly distributed among the WTSs, the rotor speeds of those WTSs with smaller wind speeds will fluctuate more dramatically, leading to more wind power capture loss.

Finally, Figure 2-12(c) also shows that each WTS can always operate around the optimum rotor speed and follow the change of wind speed, similar to that illustrated in Cases 1-4.

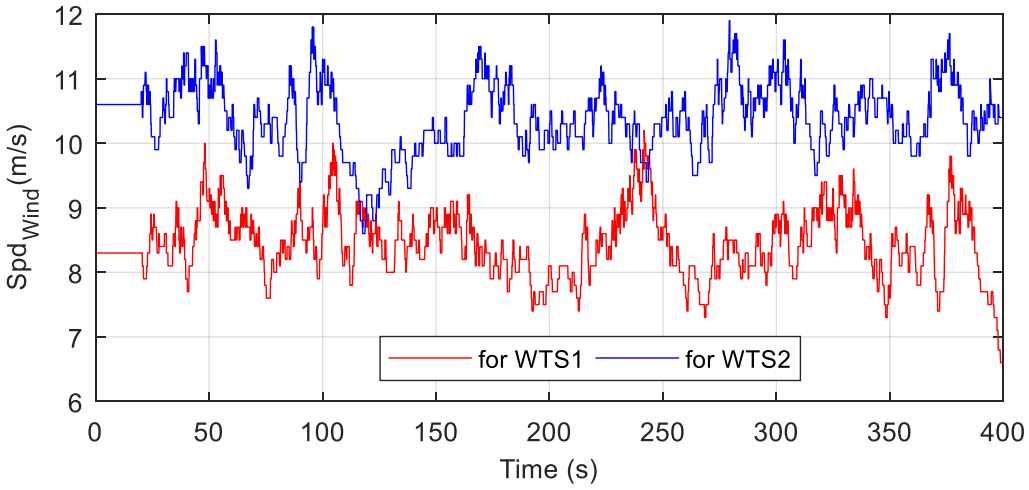

(a) The simulated wind speeds for the two DFIG-based WTSs.

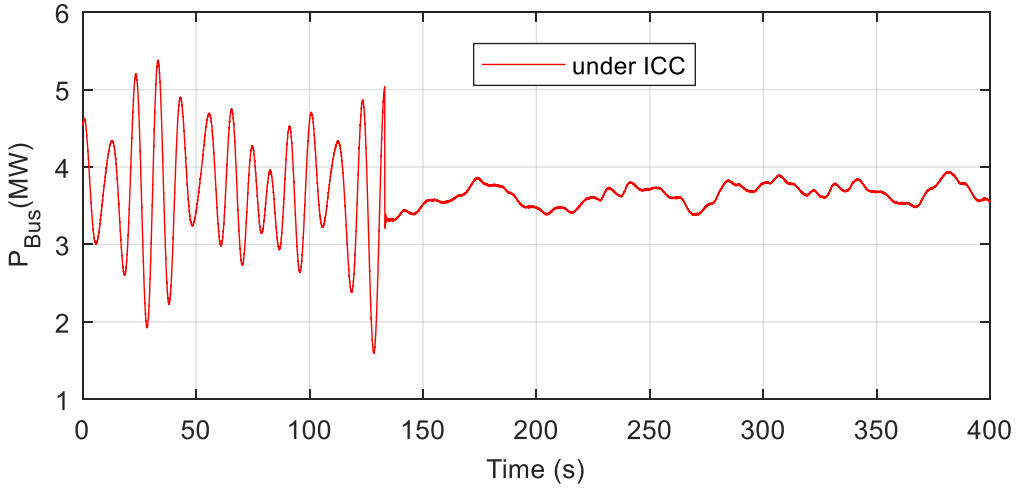

(b) The total power that is injected into the system bus under ICC.

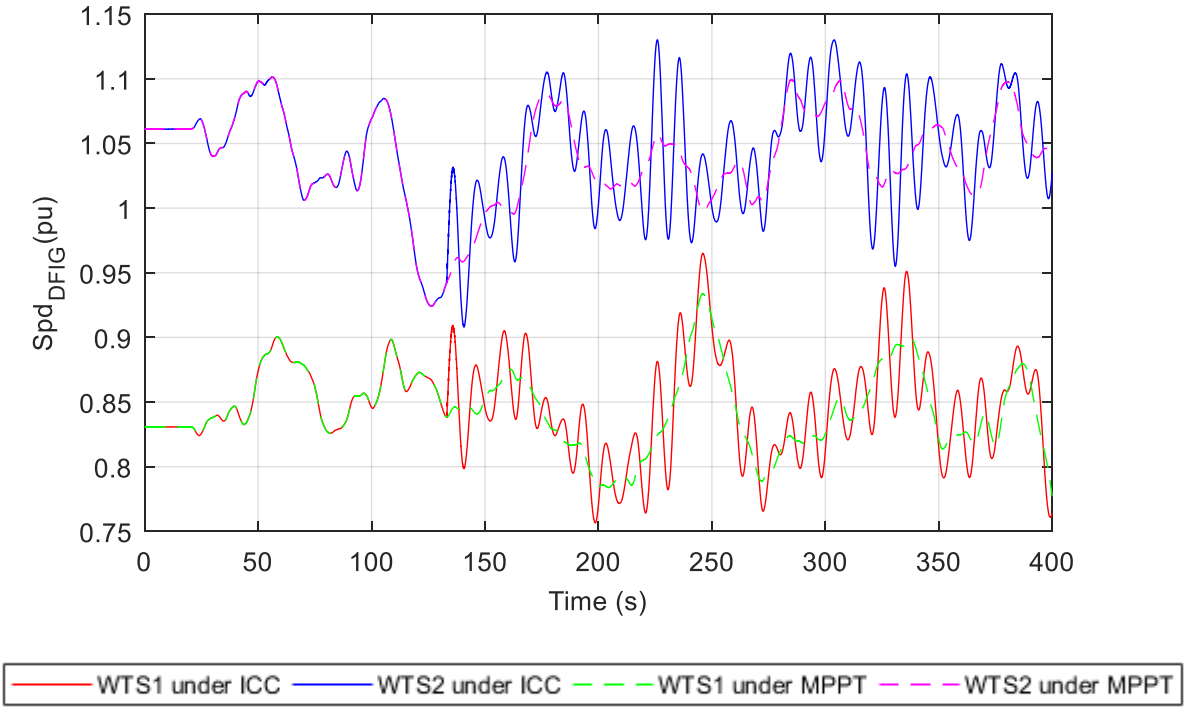

(c) The two DFIGs rotor speed under the ICC and MPPT control.

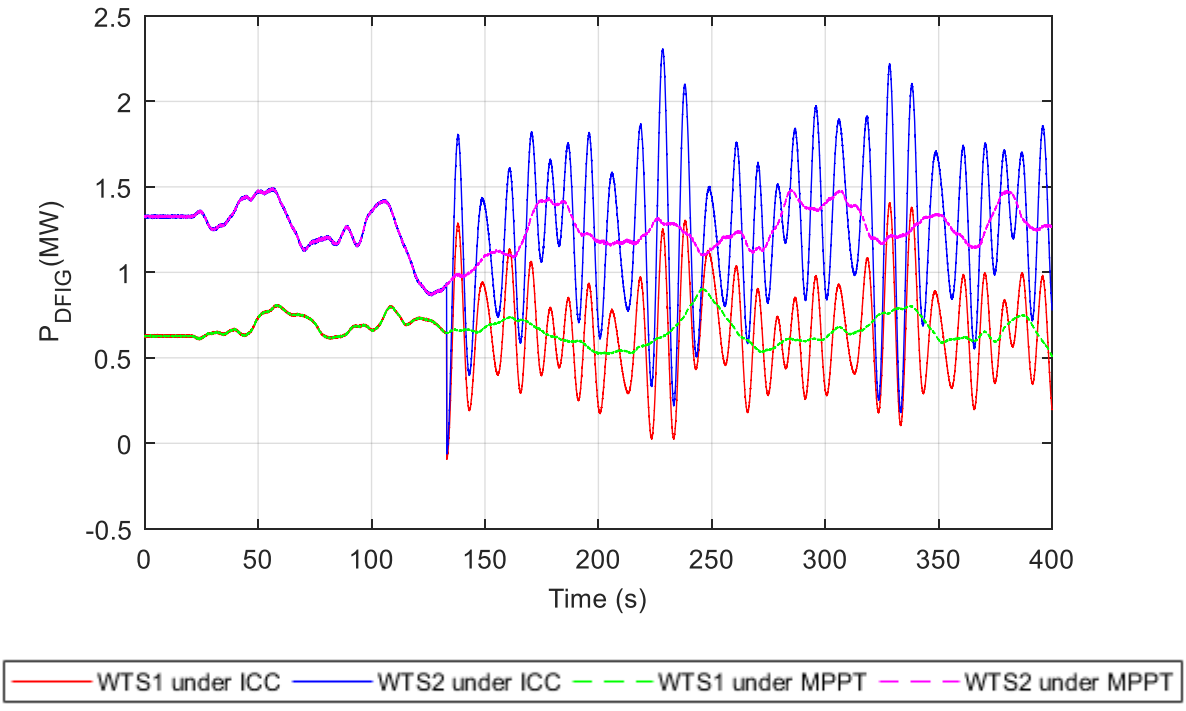

(d) Profile of the output power of the two DFIGs under the ICC and MPPT control.

Figure 2-12 Comparative simulation results of the proposed ICC and MPPT control under Case 6 with ICC activated at 130 s.

2.5 Summary

The output wave power from most of the existing WECs fluctuates heavily with variations from zero to several times of the average. Although the amplitudes of the fluctuations are big, the periods are typically within 5~12 s. This motivates the idea introduced in this chapter by controlling the large inertia of WTSs as short-term kinetic energy storage device to smooth the power output of a wave farm. Standing on the many benefits and the increasing trend of the combined generation of wind and wave energy, the proposed design has the advantages of smoothing the electrical wave power output without installing additional energy storage and power electronic devices.

To achieve the objectives of smoothing wave power whilst obtaining high wind energy capture efficiency, a big challenge is to control the WTSs rotors as kinetic energy units and at the same time make the WTSs follow the change of wind speed to achieve wind power capture close to the maximum. In this Chapter, this challenge is solved by the proposed ICC. By using ICC, WTSs can output power with fluctuations exactly opposite to that of the wave power so that the wave power is smoothed. Meanwhile, the WTSs can follow the varying wind speed automatically, resulting in the wind power capture close to its maximum. When there are many WTSs within a wind farm experiencing different wind speeds, a coordination algorithm is proposed to allocate the compensating wave power among them according to their rotor speeds. Thus, the loss of wind power capture can be reduced. ICC can be used both in the DFIG-based WTSs and PMSG-based WTSs to smooth the output power from all kinds of WECs.

Finally, simulations for both DFIG-based and PMSG-based wind farms under constant and variable wind speeds were carried out in RTDS. The simulation results validated the performance of the proposed ICC and the quantitative analysis based on the simulation results gave the relationship between wave power smoothing effect and wind power capture

efficiency. The quantitative analysis results showed that the standard deviation of the power flowing on the system bus can be decreased by 10~20 times by using the proposed ICC, while the wind power capture loss is less than 1%.

CHAPTER 3 WIND POWER SMOOTHING

3.1 Introduction

This chapter uses the material in the published paper [162]. It proposes a novel strategy to achieve wind power self-smoothing and approximate maximum wind power capture (wind power capture close to the maximum), by controlling the wind turbines inertial energy. Section 3.2 describes the proposed wind power smoothing control design, with details of the deduction procedure, first for a single WTS and then for multiple WTSs in a wind farm. In Section 3.3, a single DFIG-based and PMSG-based WTSs are simulated in RTDS and the simulation results validate the performance of the proposed control. Quantitative analysis of the dynamic performance is also provided. Then simulations of a wind farm with two WTSs are performed to show that the coordination of multiple WTSs can improve the efficiency of wind power capture. Finally, Section 3.4 summarizes the main results of this chapter.

Symbols

$P_{ref-MPPT}$ Power reference of a WTS under the MPPT control

$\omega_{r0}(t)$ Real-time rotor speed under the MPPT control

K_{opt} Optimal coefficient for maximum wind power capture

P_{ref-SM} Power reference of a WTS under the wind power smoothing control

$\omega_r(t)$ Real-time rotor speed under the wind power smoothing control

ΔP_c Fluctuating component of the output wind power required to be smoothed

K A coefficient of the power reference of the proposed wind power smoothing control

$\varepsilon(t)$ Loss of wind power capture due to the smoothing operation

$P_{in-MPPT}(t)$ Real-time captured wind power under the MPPT control

$P_{in-SM}(t)$ Real-time captured wind power under the proposed wind smoothing control

ω_0 The rotor speed when the smoothing action begins at the time t_0

J Moment of inertia of a WTS

P_{opt} Approximation of the power reference of the MPPT control

$\overline{P_{opt}}$ Average of P_{opt} obtained through a MAF

H A constant used for approximation of $\varepsilon(t)$

T_{ref-SM} Torque reference of the proposed wind power smoothing control

$\omega_{r0est}(t)$ Estimation of $\omega_{r0}(t)$ under the wind power smoothing situation

c_v Relative standard deviation used for indicating smoothness degree of a fluctuating variable

η Wind power capture efficiency

3.2 Development of the Proposed Wind Power Smoothing Control

3.2.1 Smoothing Control for a Single WTS

In Section 2.3.2 in Chapter 2 the power or torque reference of a WTS for smoothing wave power under ICC is designed as

$$P_{ref-ICC} = K_{opt}\omega_r^3(t) + K\int_{t_0}^{t}(-\Delta P)_c\,dt \cdot \omega_r(t) - \Delta P_c \tag{3.1}$$

$$T_{ref-ICC} = K_{opt}\omega_r^2(t) + K\int_{t_0}^{t}(-\Delta P_c)\,dt - \frac{\Delta P_c}{\omega_r(t)} \tag{3.2}$$

where $K = \frac{K_{opt}}{J}$, K_{opt}, J and $\omega_r(t)$ are defined in Chapter 2, and ΔP_c is the fluctuating component of the wave power.

In this chapter, in order to realize wind power self-smoothing, the idea of controlling WTSs inertia as kinetic energy storage devices is still applicable here. This means that the structure of the power or torque reference (3.1) or (3.2) is still applicable. However, the control algorithm will be designed in a different way and the parameter K is re-designed, due to in the specific wind power self-smoothing situation: In Chapter 2 the fluctuating component of the wave power ΔP_c can be measured directly, but in Chapter 3 ΔP_c is the fluctuating component of the output wind power which cannot be measured under the smoothing situation. Thus, the deduction logic in Chapter 3 is trying to set a power reference which can recovery the power trajectory of the MPPT control under the smoothing situation and then to smooth the recovered trajectory, while the deduction logic in Chapter 2 is that under the smoothing situation the rotor speed deviates from its optimum and the resulted change of kinetic energy should be all used for smoothing wave power. Therefore in this chapter the parameters of K and ΔP_c need to be re-designed.

In what follows, the way of designing the parameter K is given in detail.

Under the MPPT control, a WTS is usually controlled by applying the following power or torque reference [44, 123]

$$P_{ref-MPPT} = K_{opt}\omega_{r0}^3(t) \tag{3.3}$$

$$T_{ref-MPPT} = K_{opt}\omega_{r0}^2(t) \tag{3.4}$$

where $\omega_{r0}(t)$ is the real-time rotor speed of the WTS under the MPPT control. In order to smooth the output power under the MPPT control, the power reference under the smoothing situation should be given in the form of

$$P_{ref-SM} = P_{ref-MPPT} - \Delta P_c - \varepsilon(t) \tag{3.5}$$

Substituting (3.3) into (3.5) gives,

$$P_{ref-SM} = K_{opt}\omega_{r0}^3(t) - \Delta P_c - \varepsilon(t) \tag{3.6}$$

where $\varepsilon(t)$ is defined in (2.12), which is the difference between the maximum captured wind power under the MPPT control and the real captured wind power under the smoothing control. ΔP_c is equal to the oscillating components of $P_{ref-MPPT}$, and $-\Delta P_c$ is used to compensate and smooth the fluctuations of $P_{ref-MPPT}$ and has zero mean in the long run.

It is worth noting that the power reference (3.6) cannot be used as the real power reference for a WTS due to the following two facts:

- $\omega_{r0}(t)$ in (3.6) is unknown under the smoothing condition since $\omega_{r0}(t)$ is the real-time rotor speed of the MPPT control.

- To keep the WTS stable and automatically maximize wind power capture under variable wind speeds, the cubic of the real-time rotor speed needs to be used in the WTS power reference, as described in Section 2.3.2.

Therefore, the structure (3.1) of the power reference of ICC is used and re-called here as

$$P_{ref-SM} = K_{opt}\omega_r^3(t) + K\int_{t_0}^{t}(-\Delta P_c)\,dt \cdot \omega_r(t) - \Delta P_c \tag{3.7}$$

The parameter K in (3.7) will be obtained through making the power reference (3.6) equal to (3.7), and using the law of conservation of energy.

On one hand, with the MPPT control (3.3) the change of the kinetic energy from time t_0 to t under variable wind speed is

$$\int_{t_0}^{t}[P_{in-MPPT}(t) - P_{ref-MPPT}(t)]\,dt = \frac{J}{2}[\omega_{r0}^2(t) - \omega_0^2] \tag{3.8}$$

where $P_{in-MPPT}(t)$ is the real-time captured power from wind under the MPPT control. ω_0 is the rotor speed when the smoothing action begins at the time t_0. It is assumed here that the electrical power of the generator is the same as the given power reference due to the fast dynamic characteristics of VSC.

On the other hand, under the proposed smoothing control (3.7), the kinetic energy change from time t_0 to t under the same variable wind speed is

$$\int_{t_0}^{t}[P_{in-SM}(t) - P_{ref-SM}(t)]\,dt = \frac{J}{2}[\omega_r^2(t) - \omega_0^2] \tag{3.9}$$

where $P_{in-SM}(t)$ is the real-time captured power under the smoothing control.

The relationship between $P_{in-MPPT}(t)$ under the MPPT control and $P_{in-SM}(t)$ under the proposed smoothing control, as mentioned in (3.5) and (3.6), is

$$P_{in-SM}(t) = P_{in-MPPT}(t) - \varepsilon(t) \tag{3.10}$$

Subtracting (3.9) from (3.8) yields

$$\int_{t_0}^{t} [P_{in-SM}(t) - P_{in-MPPT}(t)] - [P_{ref-SM}(t) - P_{ref-MPPT}(t)]\, dt$$

$$= \frac{J}{2}[\omega_r^2(t) - \omega_{r0}^2(t)] \tag{3.11}$$

Re-write (3.5) and (3.10) as

$$P_{ref-SM} - P_{ref-MPPT} = -\Delta P_c - \varepsilon(t) \tag{3.12}$$

$$P_{in-SM}(t) - P_{in-MPPT}(t) = -\varepsilon(t) \tag{3.13}$$

Substituting (3.12) and (3.13) into (3.11) gives

$$\int_{t_0}^{t} \Delta P_c\, dt = \frac{J}{2}[\omega_r^2(t) - \omega_{r0}^2(t)] \tag{3.14}$$

Therefore, (3.14) gives the relationship between ΔP_c and the rotor speeds $\omega_r(t)$ and $\omega_{r0}(t)$.

Since (3.6) and (3.7) are equivalent, it holds that

$$K = \frac{K_{opt}[\omega_{r0}^3(t) - \omega_r^3(t)] - \varepsilon(t)}{\int_{t_0}^{t}(-\Delta P_c)dt \cdot \omega_r(t)} \tag{3.15}$$

By substituting (3.16) into (3.17), the unknown parameter K is deduced as

$$K = \frac{2}{J}\frac{K_{opt}[\omega_{r0}^3(t) - \omega_r^3(t)] - \varepsilon(t)}{\omega_r(t)[\omega_{r0}^2(t) - \omega_r^2(t)]} \tag{3.16}$$

Now the assumption of using a small constant H to replace $\varepsilon(t)$ should be made here. In the simulation case studies presented in Section 3.3, the value of H is obtained through trial and error. This assumption is reasonable due to the following three aspects:

- In engineering practice, $\varepsilon(t)$ is hard to obtain since the mechanical power from captured wind is difficult to measure.

- The variations in $\varepsilon(t)$ are very small.

- The WTS can still be stable even a small error occurs in K, since the real-time rotor speed is used as a feedback signal in the power reference (3.7), and both $\int_{t_0}^{t}(-\Delta P_c)\,dt$ and $-\Delta P_c$ in (3.7) have zero mean in the long run. Since the real-time rotor speed indicates the energy level of the WTS, using it as a feedback signal in the power reference can automatically maintain the stability of the WTS.

Therefore, the parameter K can be calculated by

$$K \approx \frac{2}{J}\frac{K_{opt}[\omega_{r0}^3(t)-\omega_r^3(t)]-\mathrm{H}}{\omega_r(t)[\omega_{r0}^2(t)-\omega_r^2(t)]} \tag{3.17}$$

In (3.17) the real-time rotor speed $\omega_r(t)$ can be easily measured. Now the real-time rotor speed $\omega_{r0}(t)$ of the WTS under the MPPT control is the only parameter remaining to be obtained. It cannot be measured like $\omega_r(t)$, since now the WTS is under the smoothing control, and not under the MPPT control. In Section 3.2.2 a method to estimate $\omega_{r0}(t)$ from the measured real-time wind speed is proposed.

The given power reference (3.7) of the proposed smoothing control has two variables K and ΔP_c to be determined. Since the parameter K can be calculated using (3.17), what remains is how to obtain ΔP_c. A way of determining ΔP_c will be given in the rest of this section.

Define P_{opt} in (3.18) as the approximation of the maximum wind power capture,

$$P_{opt} = K_{opt}\omega_r^3(t) + K\int_{t_0}^{t}(-\Delta P_c)\,dt \cdot \omega_r(t) \tag{3.18}$$

Due to the equivalence of (3.6) and (3.7), it holds that

$$P_{opt} = K_{opt}\omega_r^3(t) + K\int_{t_0}^{t}(-\Delta P_c)\,dt \cdot \omega_r(t) = K_{opt}\omega_{r0}^3(t) - \varepsilon(t) \approx K_{opt}\omega_{r0}^3(t) - \mathrm{H} \quad (3.19)$$

From (3.19) it can be seen that P_{opt} is very close to the output power $K_{opt}\omega_{r0}^3(t)$ of the MPPT control. This approximation will be verified by the simulation results in Section 3.3.

Then the proposed power reference (3.7) can be rewritten as

$$P_{ref-SM} = P_{opt} - \Delta P_c \quad (3.20)$$

Hence, ΔP_c can be calculated by

$$\Delta P_c = P_{opt} - \overline{P_{opt}} \quad (3.21)$$

where $\overline{P_{opt}}$ is the average of P_{opt} obtained through a MAF.

Now since both parameters K and ΔP_c are known in the power reference (3.7), the torque reference is calculated by

$$T_{ref-SM} = \frac{P_{ref-SM}}{\omega_r(t)} \quad (3.22)$$

It is worth noting that either the power reference (3.7) or (3.20) or torque reference (3.22) can be applied to the rotor-side converter of a WTS.

Figure 3-1 shows the proposed control diagram for a single DFIG-based or PMSG-based WTS to smooth their output power. It should be noted that under the constant wind speed, the output wind power is constant, so in theory there is no need to smooth it. This explains the results under the proposed control shown in Figure 3-1. From Figure 3-1, it can be seen that under a constant wind speed, ΔP_c is zero, so its integral will keep constant. Thus, P_{opt} will be constant

and so as the given power reference $\overline{P_{opt}}$. Therefore, under constant wind speed, no smoothing operation is executed.

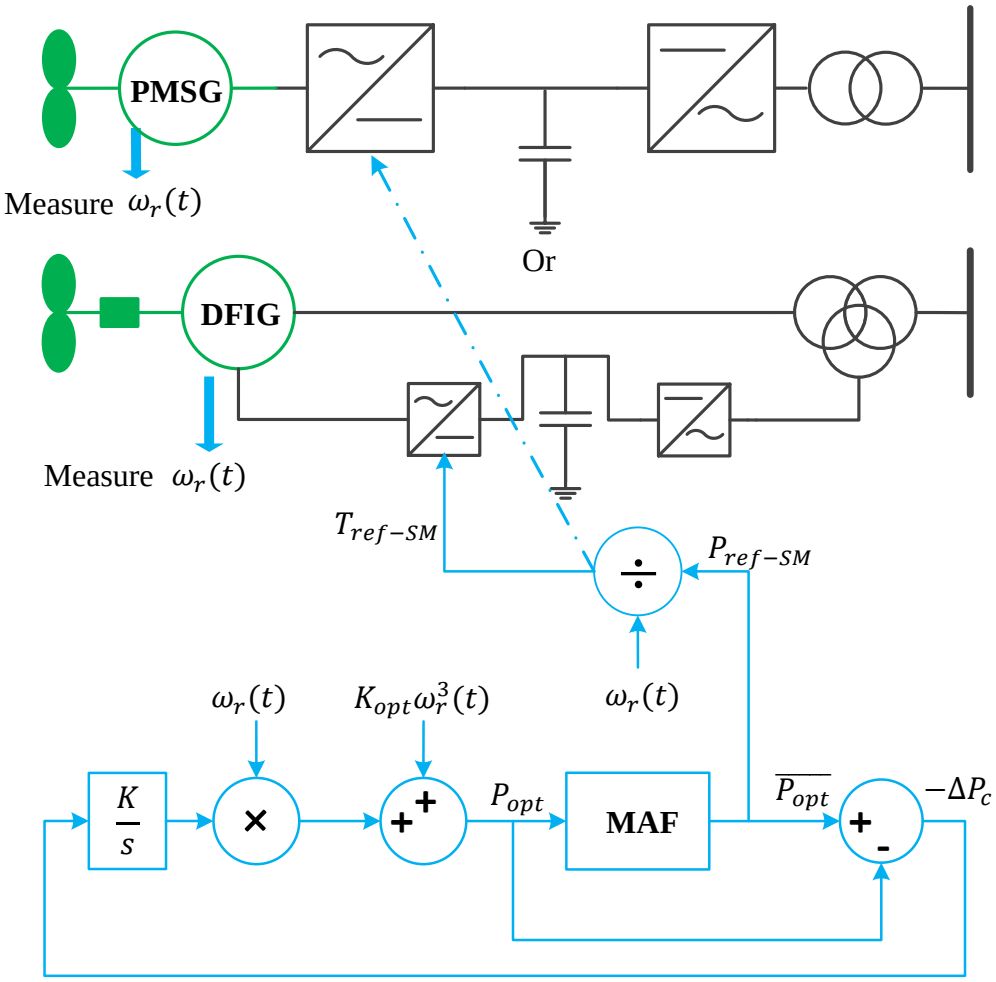

Figure 3-1 The proposed control diagram for a single DFIG-based or PMSG-based WTS to smooth their output electrical power.

To sum up, the basic idea behind the proposed smoothing control described in (3.7) or (3.20) are as follows: The first part $P_{opt} = K_{opt}\omega_r^3(t) + K\int_{t_0}^{t}(-\Delta P_c)\,dt \cdot \omega_r(t)$ is to recover the WTS output power trajectory when it is controlled by MPPT, which is theoretically verified in (3.19). The second part ΔP_c defined in (3.21) is to compensate the fluctuations of the former P_{opt} and realize the smoothed wind power output. The basic idea also implies that the output power of a WTS by using the proposed smoothing control can always approximately follow the average output power of the MPPT control.

3.2.2 Estimation of the Optimal Rotor Speed under Smoothing Condition

It is known that under each fixed wind speed v_w the related optimum rotor speed ω_{opt} of a WTS can be calculated by [44]

$$\omega_{opt} = \frac{\lambda_{opt} v_w}{R} \tag{3.23}$$

where λ_{opt} is the optimal tip speed ratio and R is the rotor radius of the wind turbine.

However, under real-time variable wind speed $v_w(t)$, due to the inherent inertial effect, the real-time rotor speed $\omega_{r0}(t)$ under the MPPT control is not equal to the optimum values $\omega_{opt}(t)$. The relationship between $\omega_{r0}(t)$ and $\omega_{opt}(t)$ in s-domain can be expressed as

$$\omega_{r0}(s) \approx \frac{\omega_{opt}(s)}{Ts+1} = \frac{\lambda_{opt} v_w(s)/R}{Ts+1} \tag{3.24}$$

where T is related to the inertial effect in a WTS, and so it can be set as the inertial constant of the WTS. Then, the estimation value of $\omega_{r0}(t)$ can be obtained by

$$\omega_{r0est}(s) = \frac{\lambda_{opt} v_w(s)/R}{Ts+1} \tag{3.25}$$

The simulation results shown in Figure 3-2 show that when the T in (3.25) is set as the inertia constant of the WTS, the estimated rotor speed $\omega_{r0est}(t)$ can well follow the actual $\omega_{r0}(t)$ under the MPPT control. This implies that (3.25) is reasonable for calculating the value of the real-time rotor speed $\omega_{r0}(t)$ under the MPPT control. With the estimation $\omega_{r0est}(t)$ for $\omega_{r0}(t)$, the parameter K can be finally calculated from (3.17).

Summarizing, from Figure 3-1, it can be seen that the proposed wind power self-smoothing scheme is easy to implement with only two extra terms compared with MPPT (3.3). In addition, since the wind speed is already known in a WTS, there is no extra measurement signal.

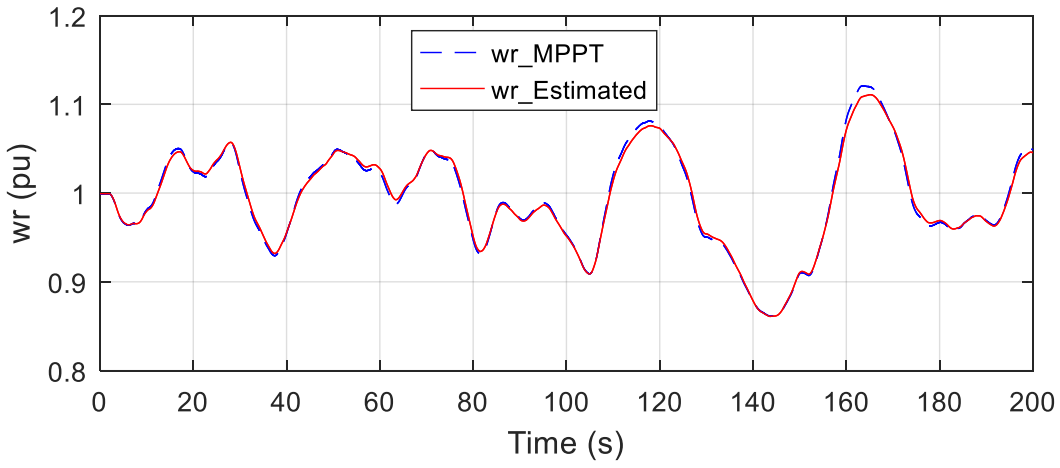

Figure 3-2 Comparison of the estimated value $\omega_{r0est}(t)$ by (3.25) and the real-time rotor speed $\omega_{r0}(t)$ of the MPPT control.

3.2.3 Coordination Control within a Wind Farm

Smoothing the output wind power of a wind farm can be different from that of a single WTS. This is because: (1) Less smoothing effort is needed when the smoothing is based on the total output power of a wind farm instead of each individual WTS since there is a natural smoothing effect in a wind farm. (2) The coordination among WTSs can be utilized since those WTSs are experiencing different wind speeds and thus have different kinetic energy storage capabilities. Therefore, coordination of multiple WTSs can reduce the total loss of wind power capture caused by the smoothing operation and enhance the WTSs stability [93, 94]. Similar to the coordination control method in Chapter 2, here each WTS is allocated a part of the total required compensation power according to the square of its rotor speed. The deduction procedure of the coordination is the same as that in Section 3.2.1 and Section 3.2.2, so the details are omitted. The obtained controller for each WTS is summarized as follows:

$$\Delta P_{c\_total} = P_{opt\_tot} - \overline{P_{opt\_tot}},\ P_{opt\_tot} = \sum_{i=1}^{M} P_{opt,i} \tag{3.26}$$

$$P_{opt,i} = [K_{opt}\omega_{r,i}^2(t) + K_i \int_0^t (-\Delta P_{c,i})\, dt] \cdot \omega_{r,i}(t) \tag{3.27}$$

$$\Delta P_{c,i} = \frac{\omega_{r,i}^2(t)}{\sum_{i=1}^{M} \omega_{r,i}^2(t)} \cdot \Delta P_{c\_total} \tag{3.28}$$

$$P_{ref,i} = P_{opt,i} - \Delta P_{c,i} \tag{3.29}$$

$$T_{ref,i} = \frac{P_{ref,i}}{\omega_{r,i}(t)} \tag{3.30}$$

$$K_i = \frac{2}{J_i} \frac{K_{opt}[\omega_{r0,i}^3(t) - \omega_{r,i}^3(t)] - \mathrm{H}}{\omega_{r,i}(t)[\omega_{r0,i}^2(t) - \omega_{r,i}^2(t)]} \tag{3.31}$$

where $-\Delta P_{c\_total}$ is the total compensation wind power and M is the total number of WTSs. For the i^{th} WTS, the terms $P_{opt,i}$, $\omega_{r,i}(t)$, $\Delta P_{c,i}$, $P_{ref,i}$, $T_{ref,i}$ and K_i are defined the same as those in the single WTS case. The proposed coordination control for a wind farm is shown in Figure 3-3.

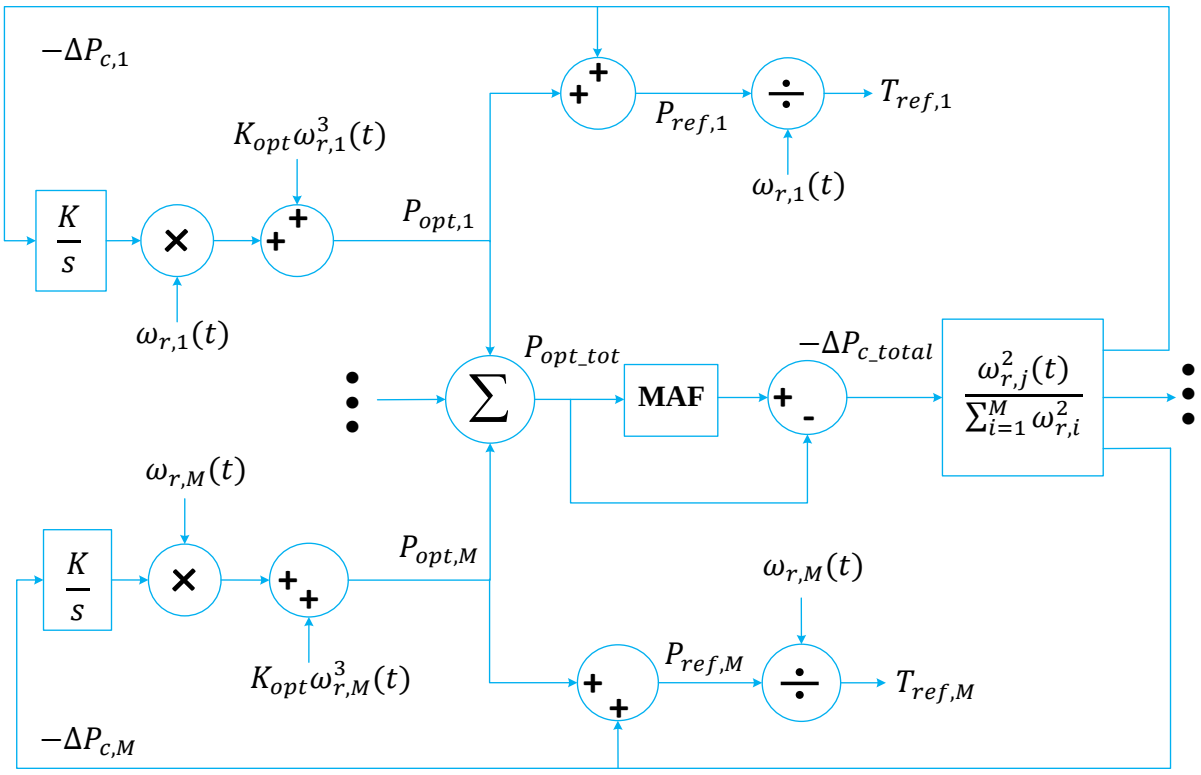

Figure 3-3 The proposed coordination control for a wind farm.

3.3 Case Studies

In order to validate the proposed wind power smoothing control, both DFIG-based and PMSG-based WTSs are simulated, first for a single WTS, then within a wind farm consisting of two WTSs to demonstrate the advantages of the coordination control. Quantitative analysis of wind power capture and smoothing effect of a single WTS under different MAF window time is also provided.

The simulated parameters of the DFIG-based and PMSG-based WTSs are the same as those in Chapter 2, as listed in Table A-1 and Table A-2 in Appendix A, respectively. The real-time wind speed shown in Figure 3-4 and Figure 3-5 are borrowed from [161] and used for the simulations. The mean values in the following simulations are obtained from a MAF with different window time.

In order to describe wind power smoothness, the relative standard deviation c_v, defined here as variation coefficient, is used. The expression of c_v is given by

$$c_v = \frac{\sigma}{\mu} \tag{3.32}$$

where σ is the standard deviation, and μ is the mean.

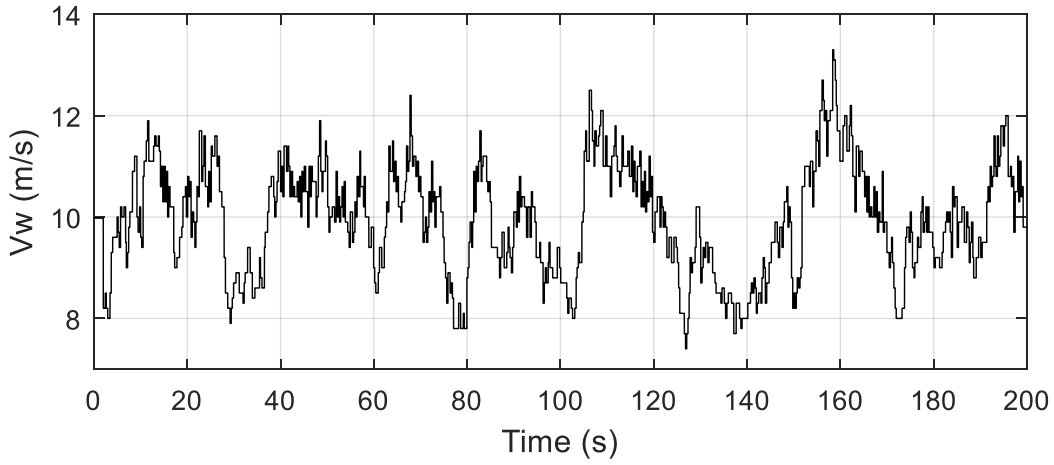

Figure 3-4 The real-time wind velocities utilized under Cases 1-3 and for WTS1 under Case 4.

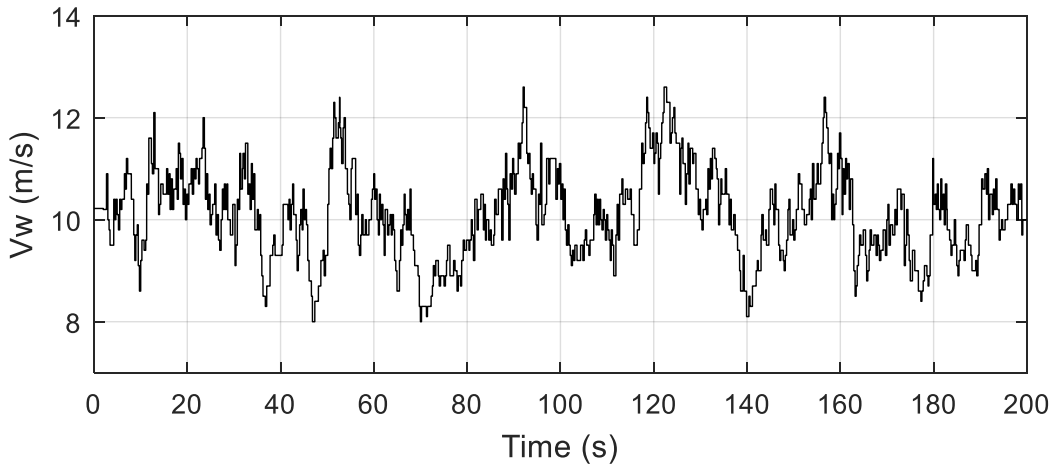

Figure 3-5 The real-time wind velocities utilized for WTS2 under Case 4.

3.3.1 Wind Power Smoothing for a Single WTS

The following two cases are used to illustrate the performance of the proposed smoothing control within a single WTS.

Case 1: Simulations are carried out for a single DFIG-based WTS under the proposed smoothing control and the MPPT control, respectively. The control performance under both $10s$ and $20s$ MAF window time are studied.

Case 2: Simulations are performed for a single direct-driven PMSG-based WTS under the proposed smoothing control and the MPPT control, respectively. The control performance under $10s$ MAF window time are studied.

The comparative simulation results under $10s$ and $20s$ MAF window time of Case 1 are shown in Figure 3-6 and Figure 3-7, respectively.

Figure 3-6(a) and Figure 3-7(a) show that the variation coefficient (c_v) of the output power by using the proposed control is smaller than that with the MPPT control. Figure 3-6(b) and Figure 3-7(b) show that the wind power capture with the proposed control always follows that with

the MPPT control. This is because the rotor speed always operates around the optimum speed under the MPPT control, as shown in Figure 3-6(c) and Figure 3-7(c).

The simulation results in Figure 3-6(b) and Figure 3-7(b) show that the loss of wind power capture mainly happens during the time period of 140 s - 160 s and during this time period the rotor speed deviates from the optimum values most, as seen from Figure 3-6(c) and Figure 3-7(c), although the input wind speed (shown in Figure 3-4) during this time period does not drop a lot. This is because the wind speed shown in Figure 3-4 is high during 105 s – 120 s, then it becomes low for a long time period from 120 s to 155 s. This results indicate that the MAF should not be set too big.

It can also be seen that during this time period of 140 s - 160 s, the rotor speed becomes slow, especially in Figure 3-7 under 20 s MAF window time situation, indicating that the WTS does not have sufficient kinetic energy to implement the smoothing function. Then, at $t = 142s$ the rotor speed reaches its limit, leading to a sudden drop of the output power, as seen from Figure 3-7(a). The sudden drop of power directly leads to sudden drop of the torque which causes fatigue to the WTS mechanical shaft. This sudden-drop phenomenon should be avoided in real implementation. One possible solution is to decrease the MAF window time smoothly before the rotor speed becomes slow and thus the loss of wind power capture can also be reduced.

From the comparative simulation results, it can be seen that if the MAF window time is too short, the calculated ΔP_c in (3.21) will be very small and then the wind power will be smoothed little. If the MAF window time is too long, the calculated ΔP_c in (3.21) will be very large. Then the wind turbine should have big enough kinetic energy storage to smooth the large ΔP_c. However, since the stored kinetic energy is limited, it means that the WTS does not have enough ability to smooth the large ΔP_c. Hence, the rotor speed will often drop to the minimum limit, causing the sudden drop phenomenon all the time.

Figure 3-6(d) and Figure 3-7(d) show that in the proposed control reference (3.7) the first part P_{opt} defined in (3.18) can well track $P_{ref-MPPT}$ of the MPPT control. This validates that P_{opt} can approximate the power reference of the MPPT control, and thus the proposed smoothing control can approximately recover (or duplicate) the power trajectory of the MPPT control.

Figure 3-6(e) and Figure 3-7(e) show that under the proposed smoothing control c_v of the torsional angles between the two shafts of the DFIG is reduced and less than that under the MPPT control. From [26, 148] it is known that the mechanical stress is related to the variations of shaft torsional angle. Therefore, with the proposed smoothing control the mechanical stress of the DFIG is also alleviated.

The simulation results in Figure 3-6 and Figure 3-7 demonstrate that the proposed smoothing scheme can smooth wind power output and achieve approximate maximum wind power capture. They also verify that the assumption of using a small constant H to replace $\varepsilon(t)$ to calculate K in (3.17), as mentioned in Section 3.2.1, is reasonable.

Comparing with the simulation results with $10s$ MAF window time in Figure 3-6, Figure 3-7 shows that with 20 s MAF window time the output power is smoother but the loss of wind power capture is bigger. This illustrates that the smoothing performance is conflicted with the wind power capture. Hence, choosing a proper MAF window time should be related to the two performance indexes: wind power smoothing and wind energy capture efficiency.

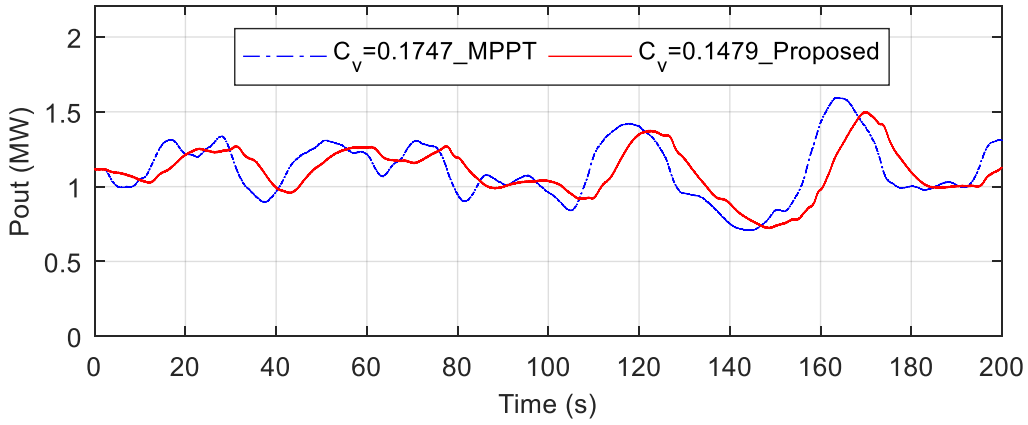

(a) The output power of the DFIG-based WTS.

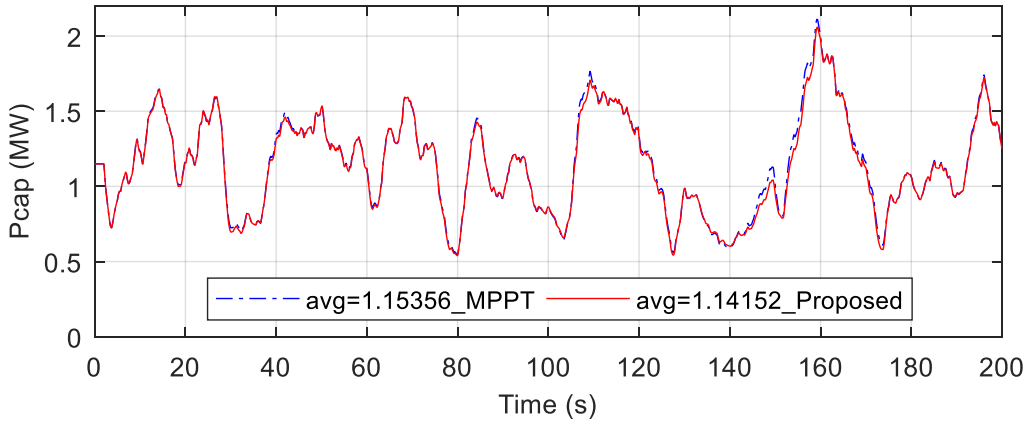

(b) The captured wind power of the DFIG-based WTS.

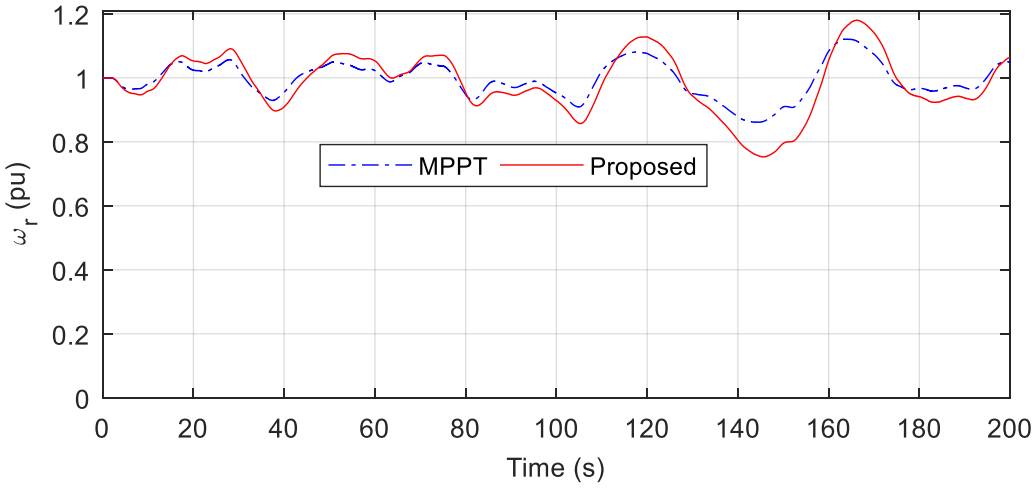

(c) The DFIG rotor speed.

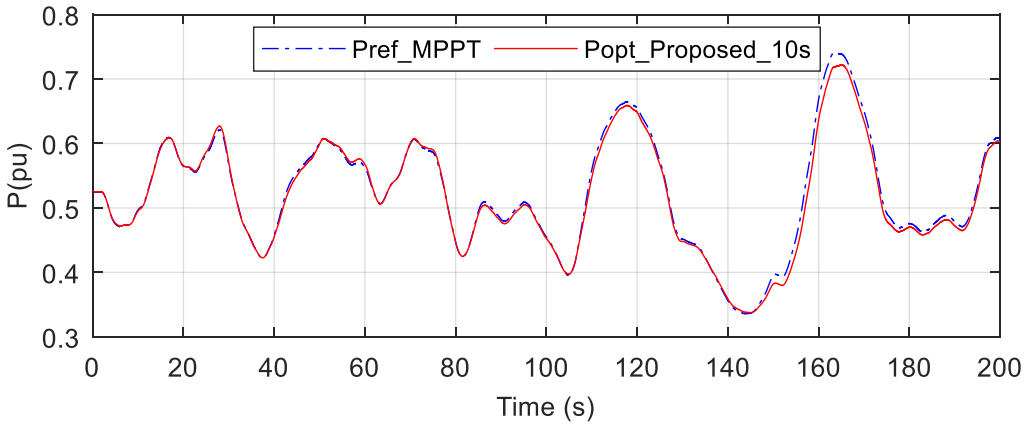

(d) Comparison of P_{opt} under the proposed smoothing condition and $P_{ref-MPPT}$ under the MPPT control.

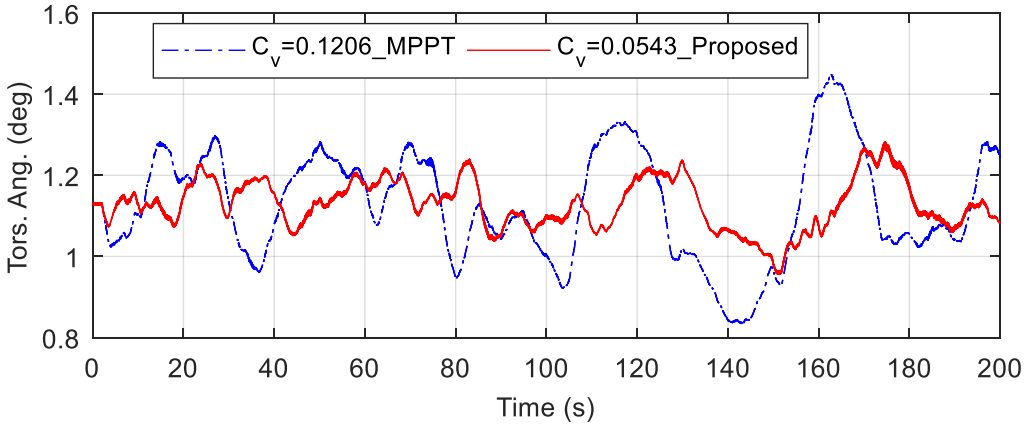

(e) The torsional angle of the DFIG.

Figure 3-6 Simulation results for 10 s MAF window time under Case 1.

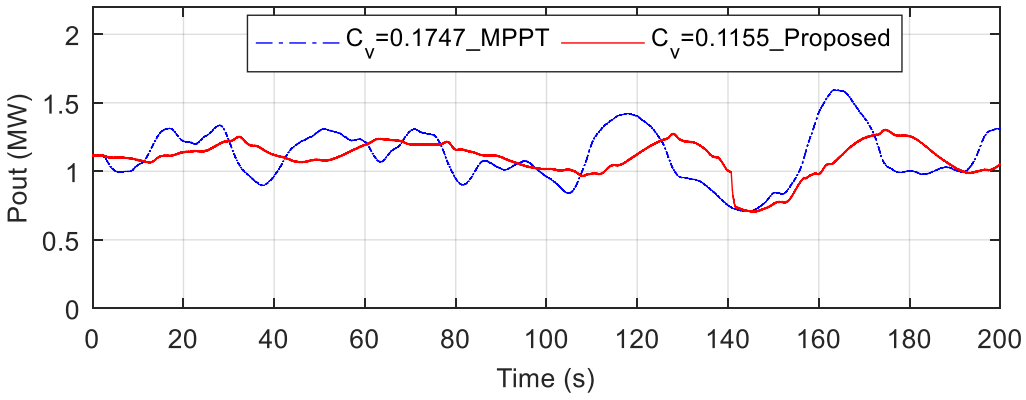

(a) The output power of the DFIG-based WTS.

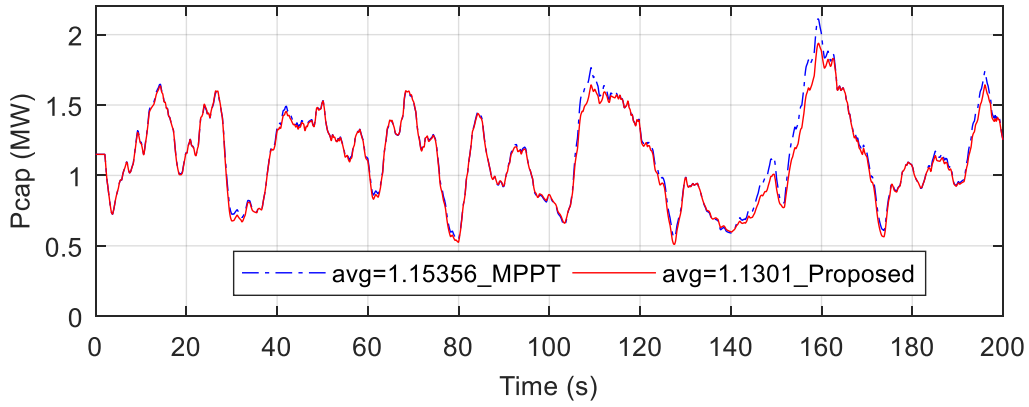

(b) The captured wind power of the DFIG-based WTS.

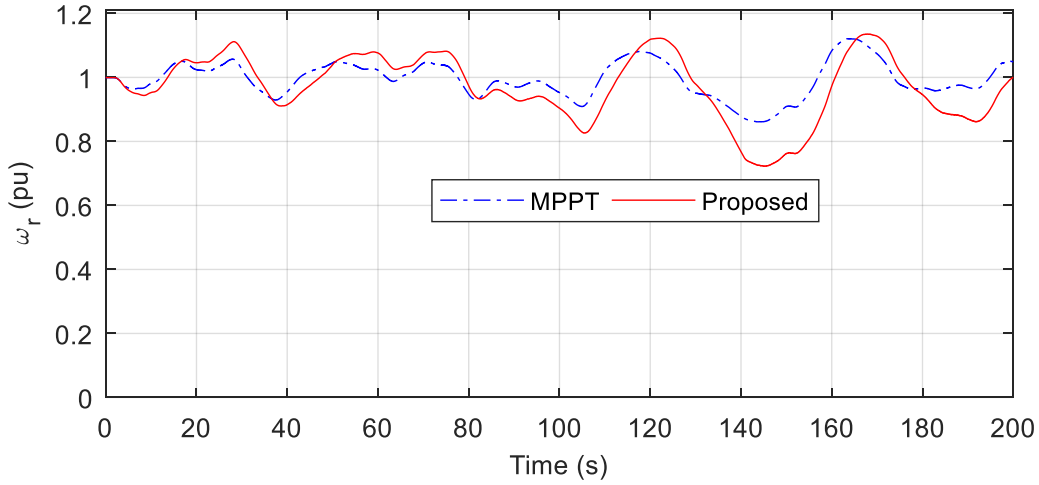

(c) The DFIG rotor speed.

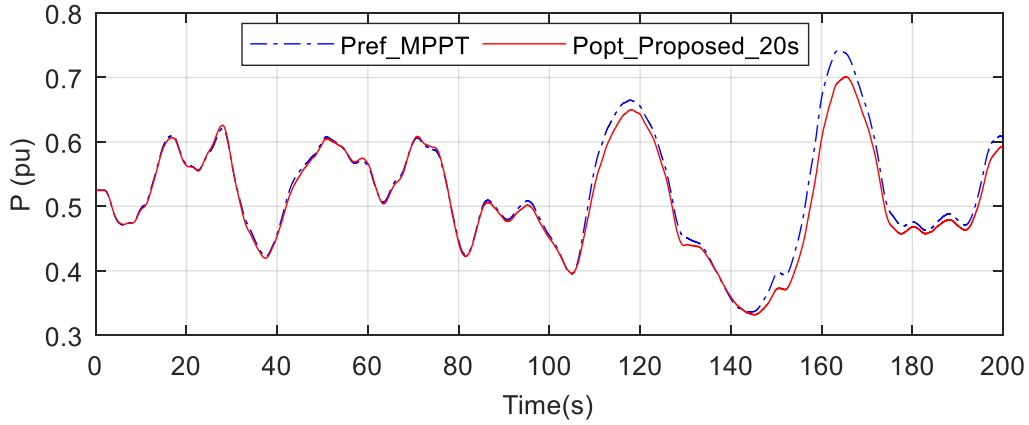

(d) Comparison of P_{opt} under the proposed smoothing condition and $P_{ref-MPPT}$ under the MPPT control.

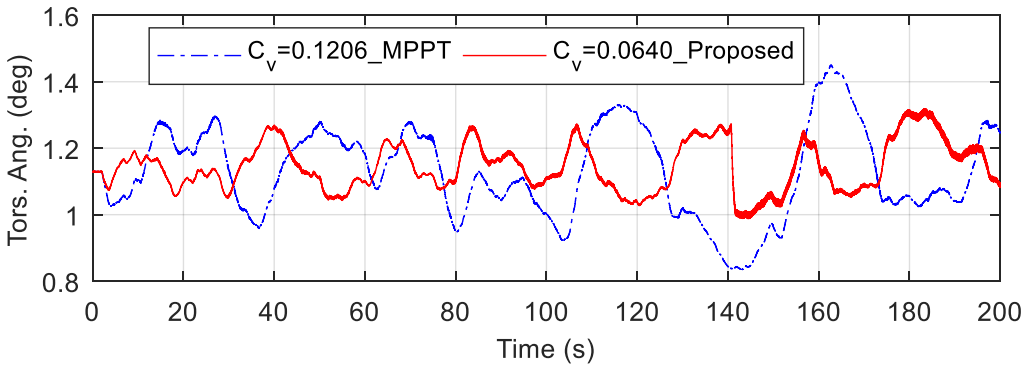

(e) The torsional angle of the DFIG.

Figure 3-7 Simulation results for 20 s MAF window time under Case 1.

The simulation results for Case 2 are shown in Figure 3-8. The simulation results from Figure 3-8(a) to Figure 3-8(d) for a PMSG-based WTS are similar to those for a DFIG-based WTS with 10 s MAF window time in Case 1. This demonstrates that the proposed smoothing control is also effective in direct-drive PMSG-based WTSs.

Figure 3-8(e) show that with the proposed smoothing control, c_v of the PMSG electrical torque is decreased and less than that with the MPPT control, which means that the PMSG mechanical stress is mitigated. This further demonstrates that the proposed smoothing control can not only smooth the output wind power but also mitigate the fatigue of the mechanical stress for both DFIG-based and PMSG-based WTSs. The reason why the electrical torque of the PMSG under the smoothing condition is smoother than that under the MPPT control is that according to $P_e = T_e * \omega_r$, since P_e is smoother (see Figure 3-8(a)) and ω_r is close to ω_{r_opt} (see Figure 3-8(c)), T_e is smoother.

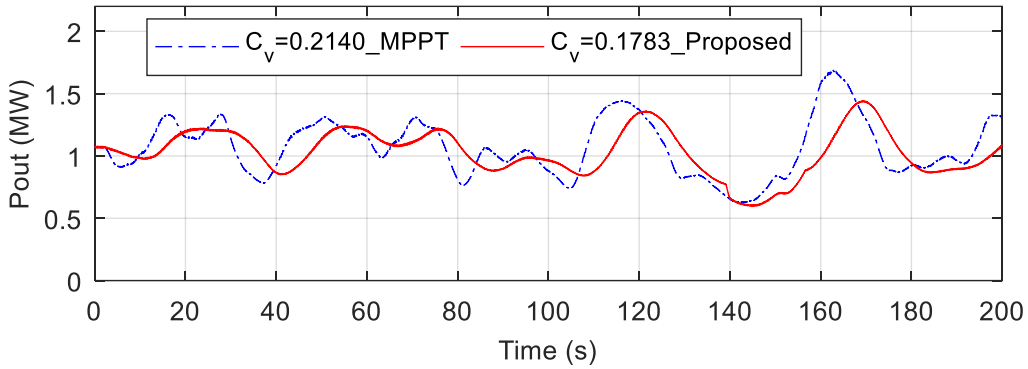

(a) The output power of the PMSG-based WTS.

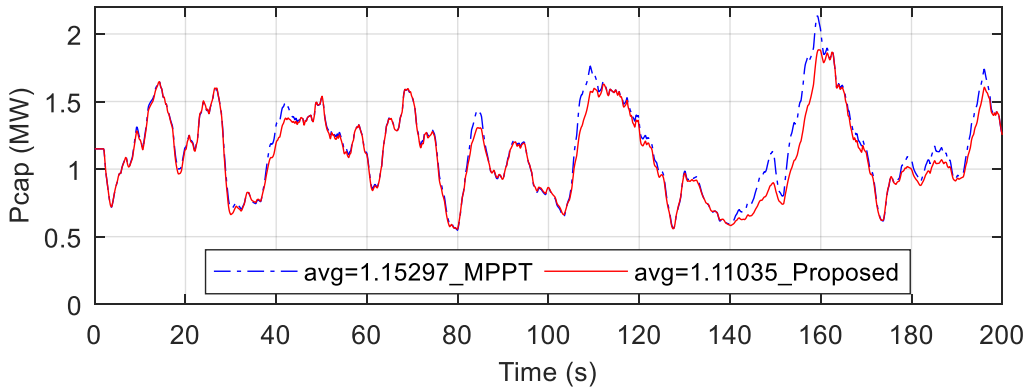

(b) The captured wind power of the PMSG-based WTS.

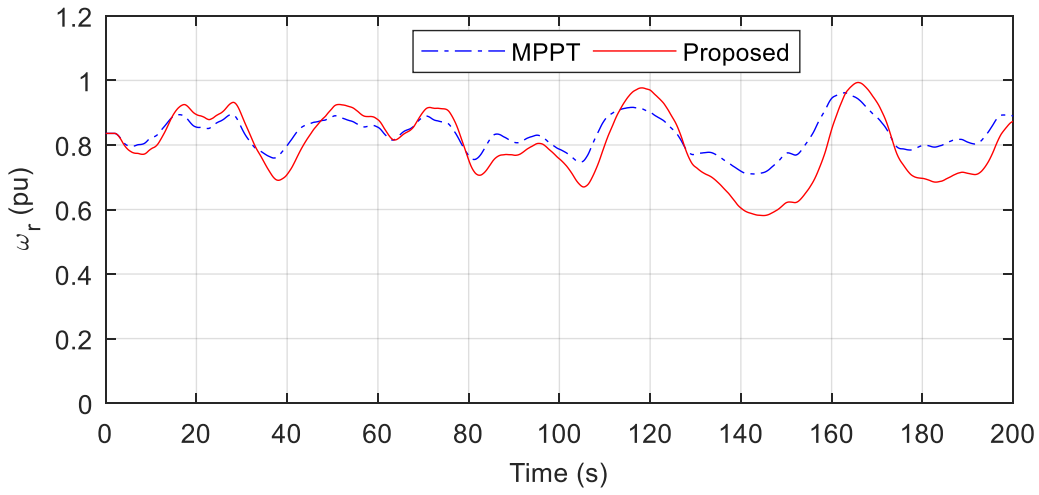

(c) The PMSG rotor speed.

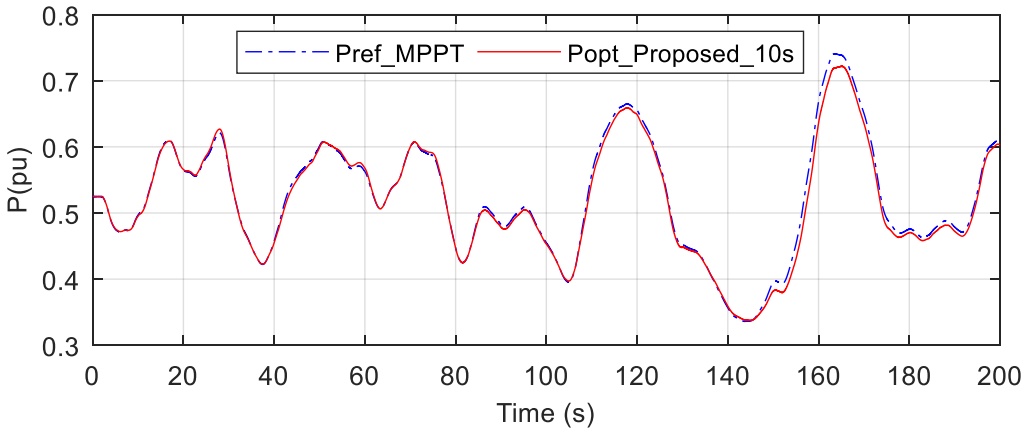

(d) Comparison of P_{opt} under the proposed smoothing condition and $P_{ref-MPPT}$ under the MPPT control.

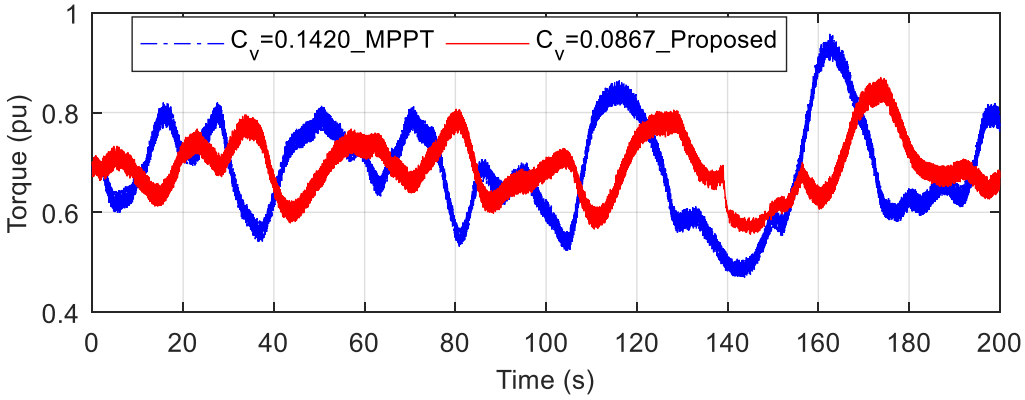

(e) The electrical torque of the PMSG.

Figure 3-8 Simulation results under Case 2.

3.3.2 Quantitative Analysis under Different MAF Window Time

Case 3: Simulations are carried out for a DFIG-based WTS under the same wind speeds shown in Figure 3-4 but with different MAF window time. This is to quantitatively analyse the relationship between the wind power smoothing effect and wind power capture efficiency.

The simulation results of Case 3 are shown in Figure 3-9. The efficiency η shown in Figure 3-9 is defined as

$$\eta = \frac{P_{out-SM}}{P_{out-MPPT}} \tag{3.33}$$

where P_{out-SM} and $P_{out-MPPT}$ are the output power of the WTS with the proposed smoothing control and the MPPT control, respectively.

By using the proposed smoothing control c_v of the output power is significantly reduced as shown in Figure 3-9(a), while the loss of wind power capture is within 2%, as shown in Figure 3-9(b). It can be seen that for a bigger MAF window time, the reduction of c_v of the output power is larger. However, with a larger MAF window time, more sudden drops of the output power would happen. Nevertheless, the sudden-drop phenomenon can be avoided by the aforementioned solution described in Case 1.

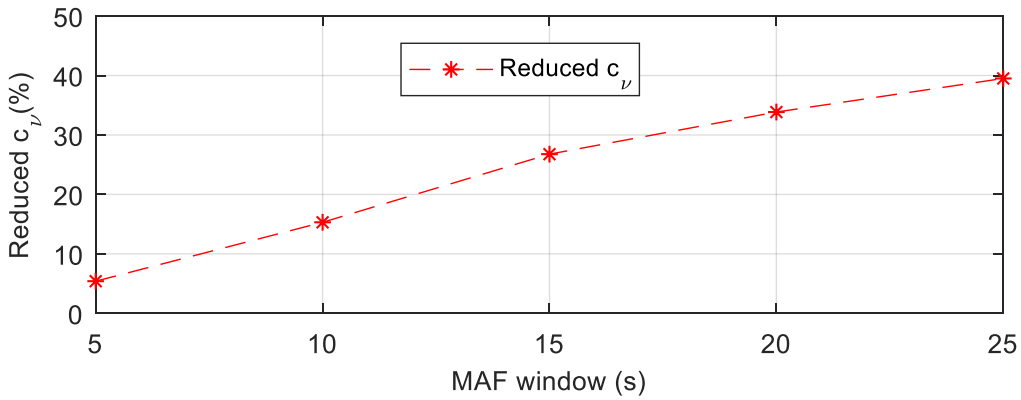

(a) The reduction of the variation coefficient (c_v) of the WTS output power.

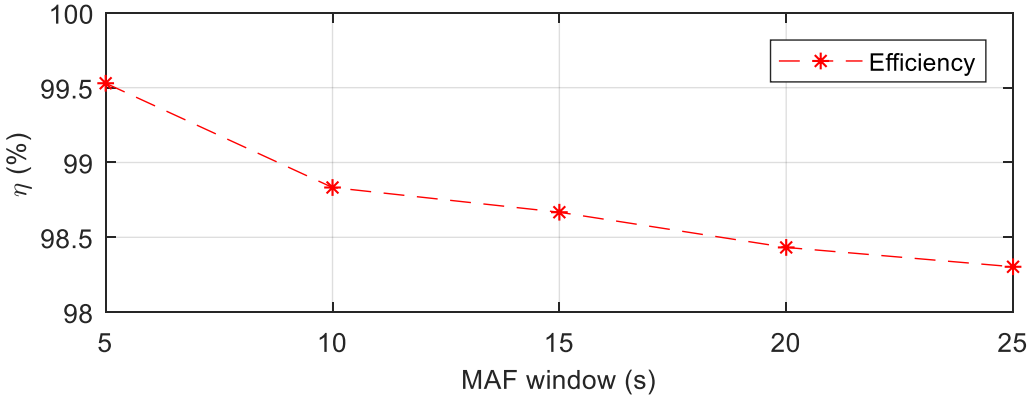

(b) The efficiency of the wind power capture.

Figure 3-9 Simulation results for Case 3.

3.3.3 Wind Power Smoothing within a Wind Farm

Case 4: Simulations are carried out for a wind farm consisting of two DFIG-based WTSs to illustrate the advantages of the coordination control described in Section 3.2.3. The wind speeds used for these two WTSs are shown in Figure 3-4 and Figure 3-5.

The simulation results of Case 4 are shown in Figure 3-10. It is shown in Figure 3-10(a) c_v of the output power of the wind farm with the proposed smoothing control is 0.076, which is 36.11% less than that with the MPPT control. Moreover, as seen from Figure 3-10(b) and Figure 3-10(c), the average of the total wind power capture under the proposed control is only 0.85% less than that under the MPPT control.

In this case, no sudden-drop phenomenon happens in WTS1 although it is still controlled under the same 20 s MAF window time and wind speed input as in Case 1 where the sudden-drop phenomenon happens (shown in Figure 3-7(a)). The reason for this is that with the coordination control of the two WTSs, WTS1 is automatically allocated with smaller compensation power when the WTS1 has small rotor speed at the time around 140 s, while the bigger part is allocated to WTS2 since the rotor speed of WTS2 is higher, as shown in Figure 3-10(d) and Figure 3-10(e). Hence, the rotor speed of WTS1 does not decrease too much, to hit the limitation and trigger the protection action leading to the sudden-drop phenomenon. This is considered to be one of the benefits of using the coordination control. Another benefit of using the coordination control is that the loss of the wind power capture is smaller than that for a single WTS, by comparing Figure 3-10(b) and Figure 3-7(b). The third benefit, as stated in Section 3.2.3, is that less power is required to be smoothed under the coordination control, since there is a natural smoothing effect within a wind farm.

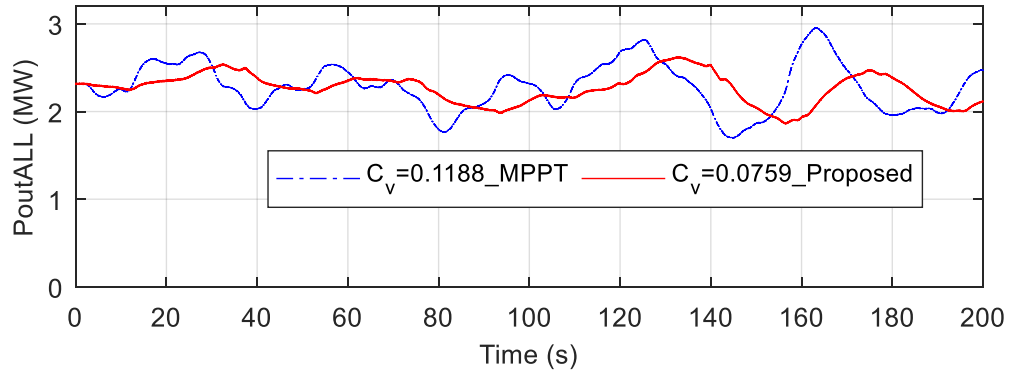

(a) The total output power of the wind farm transmitted to the system bus.

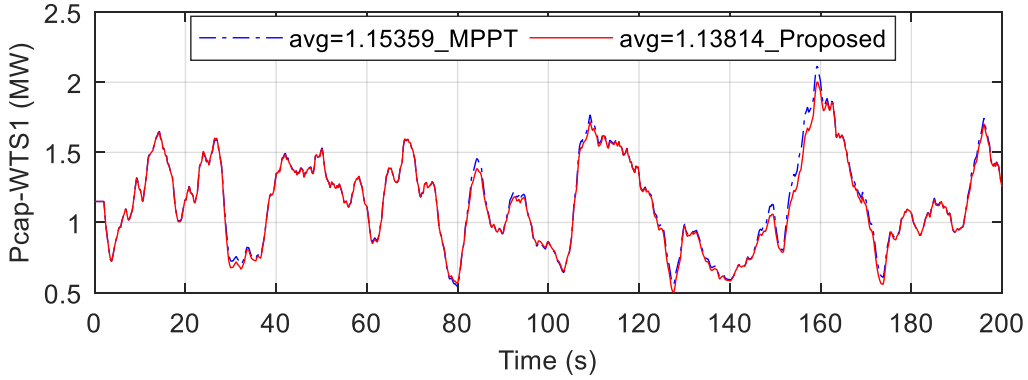

(b) The captured wind power of WTS1.

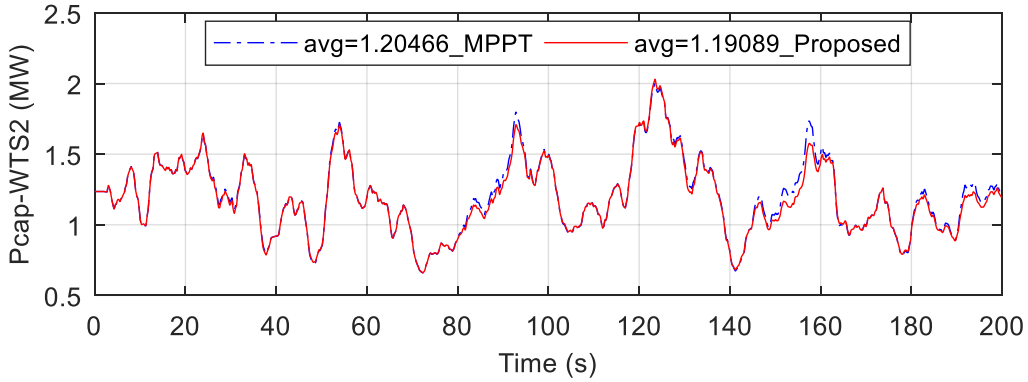

(c) The captured wind power of WTS2.

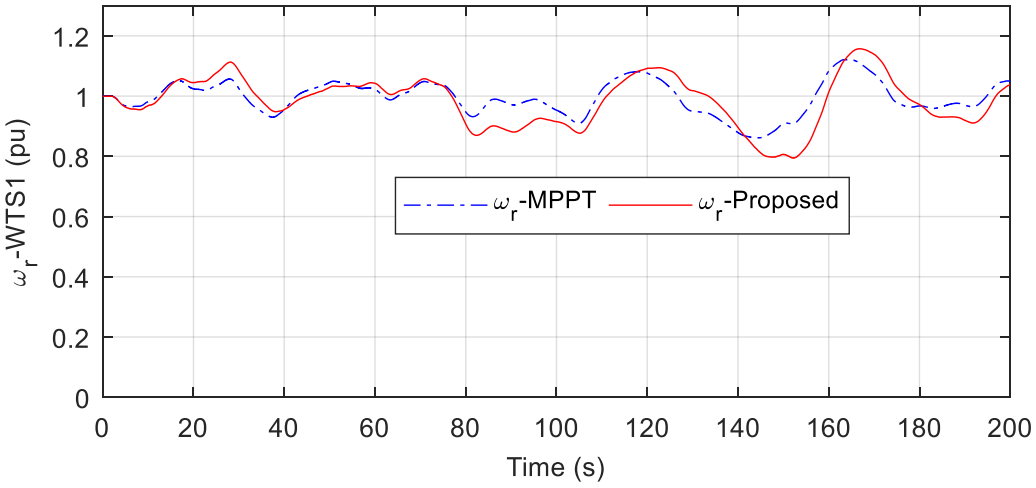

(d) The rotor speed of WTS1.

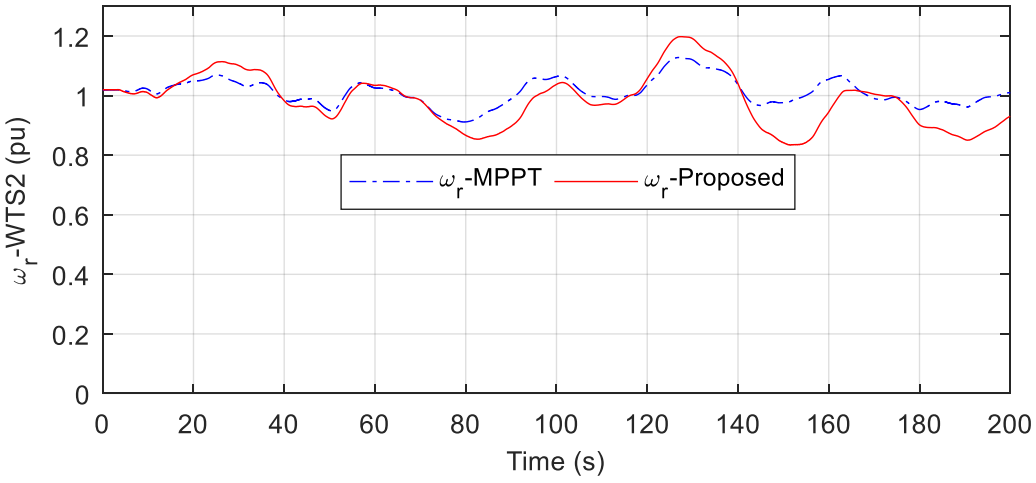

(e) The rotor speed of WTS2.

Figure 3-10 Simulation results under Case 4.

3.4 Summary

This Chapter proposed a new wind power self-smoothing method by controlling the kinetic energy stored in WTSs to smooth the wind power variations less than tens of seconds. Unlike the existing inertial energy smoothing methods, the proposed method can duplicate the trajectory of the MPPT control and in the meantime smooth the output power based on this trajectory. Thus, it makes the rotor speed always run around the optimum operating points, leading to little loss of wind power capture. Considering the natural smoothing effect of a wind farm itself and the WTSs having different wind speeds, a coordination algorithm has been proposed to achieve less loss of the wind power capture. The proposed smoothing scheme can be applied to both DFIG-based and direct-driven PMSG-based WTSs. The quantitative analysis of the smoothing effect and the efficiency of wind power capture was provided for a single WTS. It provides guidance to choose the MAF filtering time constant in order to balance the smoothing effect and wind power capture efficiency.

A single DFIG-based WTS, a single PMSG-based WTS and a wind farm consisting of two DFIG-based WTSs were simulated in the RTDS platform under real wind speed profiles. The simulation results for a single WTS showed that by using the proposed smoothing control, c_v of the output wind power was reduced by 5% - 40%, with less than 2% loss of wind power capture. Moreover, with the coordination control of multiple WTSs within a wind farm the smoothing effect is further improved and the loss of wind power capture is less. The simulation results showed that c_v of the output wind power of the wind farm was reduced by 36.11%, with less than 1% of wind power capture.

CHAPTER 4 FORCED OSCILLATIONS ISOLATION AND SUPPRESSION

4.1 Introduction

This chapter describes a novel scheme to isolate and suppress forced oscillations. This is achieved by controlling the large amount of inertial energy of wind farms to timely release or absorb power which is opposite to the oscillating power from the perturbation areas. Thus, the forced oscillations in the perturbation areas can be prevented from propagating to the rest of the power grid, and meanwhile the oscillating power in the disturbed areas is also reduced and suppressed. Section 4.2 summarizes the classical resonance theory. Section 4.3 illustrates the principles of the proposed method. In Section 4.4, the performance of the proposed method is verified by real-time simulations in a modified two-area power system in RTDS. In addition, simulation studies are also carried out to show the performance of the proposed strategy in damping natural oscillations, i.e. inter-area oscillations. Finally, Section 4.5 concludes the main results of this chapter.

Symbols

P_{ij} Total power on transmission lines between bus i to bus j

$\overline{P_{ij}}$ Average of P_{ij} through a MAF

ΔP_{ij} Oscillating components of P_{ij}

4.2 Resonance Theory from Physics

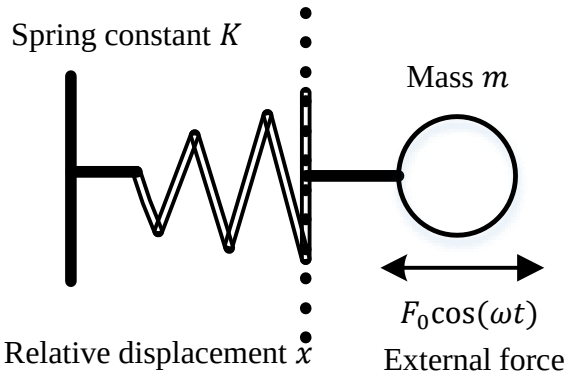

Figure 4-1 Mass-spring system with a sustained external force.

In this section, the theory of the physics resonance is reviewed [141]. Considering a mass-spring system shown in Figure 4-1 with an external force of $F_0\cos(\omega t)$. Based on Newton's law, the following is obtained:

$$m\ddot{x} + b\dot{x} + Kx = F_0\cos(\omega t) \tag{4.1}$$

The natural frequency ω_0, damping γ and damping ratio ζ of the system are defined as

$$\omega_0^2 = \frac{K}{m}, \gamma = \frac{b}{m}, \zeta = \frac{\gamma}{2\omega_0} \tag{4.2}$$

Rewriting (4.1) in the complex plane and using (4.2), the following holds:

$$\ddot{Z} + \gamma\dot{Z} + \omega_0^2 Z = \frac{F_0}{m}e^{j\omega t} \tag{4.3}$$

The solution of equation (4.3) is

$$Z = Ae^{j(\omega t-\delta)} \tag{4.4}$$

where

$$\begin{cases} A = \dfrac{\frac{F_0}{m}}{\sqrt{\left(\omega_0^2-\omega^2\right)^2+(\omega\gamma)^2}} \\ tan\delta = \dfrac{\omega\gamma}{\omega_0^2-\omega^2} \end{cases} \tag{4.5}$$

It can be seen that the forced resonance occurs when the frequency of the external force ω is equal to the natural frequency ω_0. As a results, forced oscillations occur when a power system is disturbed by periodic external perturbations at frequencies close or equal to the natural frequencies of the system. From (4.5), it can also be seen that if the system has no damping ($\gamma = 0$) at $\omega = \omega_0$, the amplitude A of the oscillations becomes infinity. By increasing the damping γ A can be reduced; however, the oscillations cannot be eliminated.

The paper [141] studied the resonance phenomenon (or forced oscillations) between inter-area system modes and the external perturbations. It indicated that the following three conditions play a key role in the strength of the forced oscillation:

- (C1) The proximity between the frequency of the external perturbation force and that of the system mode. As seen from (4.5), resonance would occur only when the frequency of the external periodic perturbations is close enough to the system mode. Moreover, the closer the frequency difference between them is, the bigger the amplitude of the forced oscillation is.

- (C2) The damping level of the system. The lower the damping is, the bigger the strength of the forced oscillation is.

- (C3) The strength of the local grid where the external perturbation locates. The weaker the strength is, the bigger the amplitude of the forced oscillation is.

C1 is a necessary condition for forced oscillations while all of the three conditions C1, C2, and C3 together determine the strength of forced oscillations of the system.

4.3 Forced Oscillations Isolation and Suppression by Wind Farms

4.3.1 Principle of the Proposed Strategy

In this section, the proposed control strategy is described. To illustrate the control strategy, a two-machine system with a wind farm is considered, as shown in Figure 4-2, where SG1 and SG2 are synchronous generators. The wind farm can be composed of DFIG-based or PMSG-based WTSs. SG1 is the disturbed generator, causing the forced oscillation occurred in the system. The power flow on the transmission line between bus 2 and bus 3 is P_{23}, and that between bus 3 and bus 4 is P_{34}. The output power of the wind farm is P_{63}. $\overline{P_{23}}$ is obtained by applying a MAF to P_{23}. P_{MPPT} is the maximum power output of the wind farm under the MPPT control without using the proposed control method. With the proposed control, the wind farm output power is $P_{MPPT} - \varepsilon - \Delta P_{23}$ in which ε is a small value as defined in (2.9).

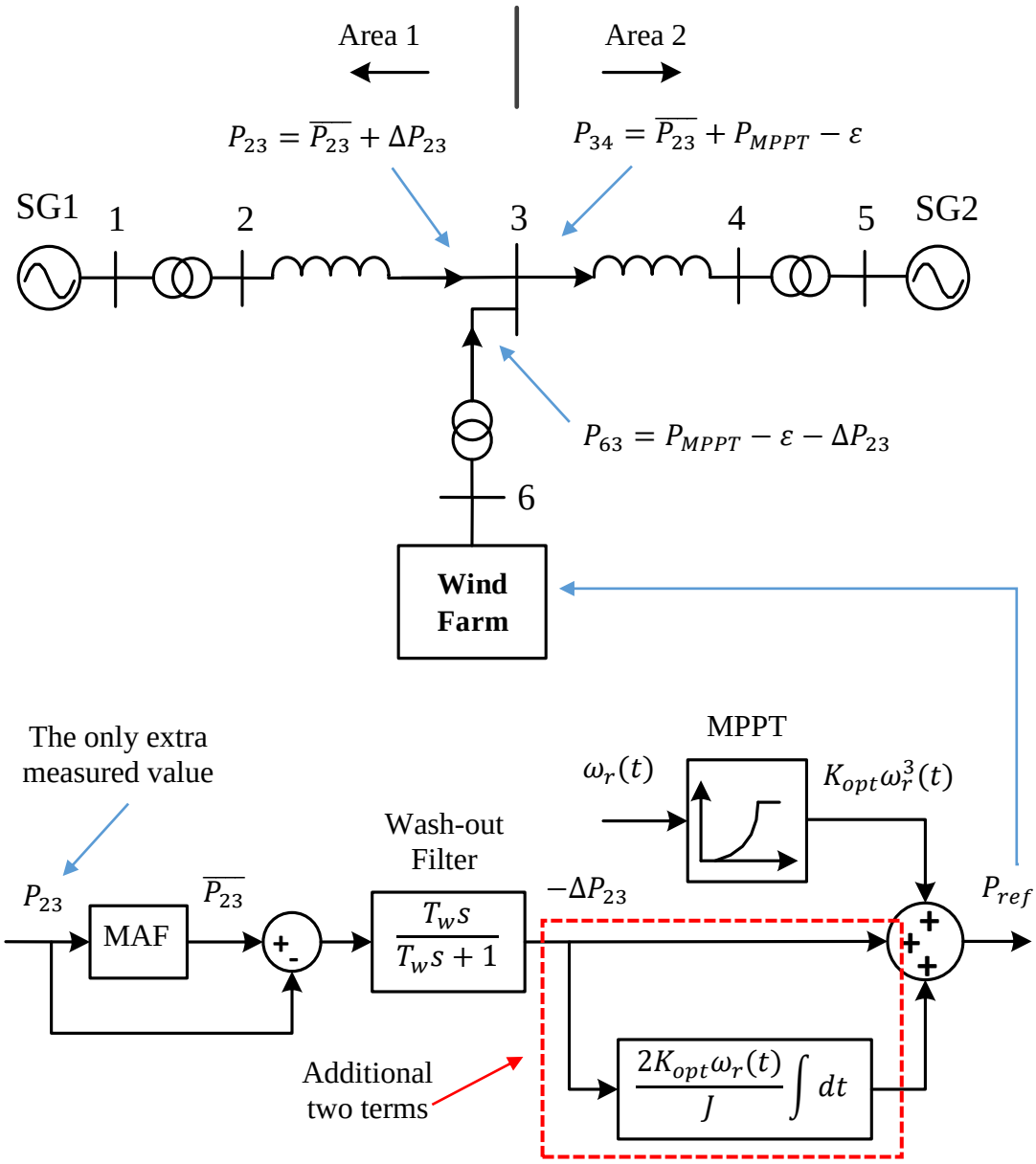

Figure 4-2 A two-machine system with a wind farm to illustrate the proposed forced oscillations isolation and suppression strategy.

Note that forced oscillations are mainly associated with active power and usually a zero-reactive power exchange with the main grid is implemented in a single DFIG-based WTS. Hence, this thesis only considers the oscillating active power and the wind farm is controlled with zero reactive power exchange with the main grid.

The objective of isolating forced oscillation and preventing it from spreading to Area 2 is to smooth P_{34}. A straightforward approach is to control the wind farm to generate oscillating active power $-\Delta P_{23}$ which is opposite to ΔP_{23}. The resulting P_{34} then becomes

$$P_{34} = P_{23} + P_{63} = \overline{P_{23}} + P_{MPPT} - \varepsilon \tag{4.6}$$

In this way, the active power P_{34} that is being injected into Area 2 does not contain an oscillating component; and therefore, the forced oscillation is isolated and contained within Area 1. At the same time, the magnitude of the oscillation (ΔP_{23}) in Area 1 is also reduced (or suppressed), because the active power output of the SG1 is affected by the injected active power of the wind farm. Moreover, as will be demonstrated in Section 4.4, if the wind farm is the closer to SG1, the oscillation in Area 1 (ΔP_{23}) is smaller. This is because that the change in active power output from SG1 is also affected by the location of the wind farm. The associated theories can be found in [71]. Figure 4-2 also shows the way that the signal $-\Delta P_{23}$ is generated from the measurement of P_{23}, in which the wash-out filter is used to block the direct component of $-\Delta P_{23}$. T_w is the time constant of the wash-out filter, and it should be chosen bigger than the oscillating periods of the forced oscillations.

4.3.2 Derivation of the Proposed Control Methodology

For convenience, it is assumed in the following description that a single WTS represents the whole wind farm. To achieve the isolation and suppression of forced oscillation in the system, one necessary condition is that the wind farm can output the active power that is exactly opposite to ΔP_{23}. However, to achieve the wind power capture close to its maximum under the MPPT control, the power reference in a WTS should be related to its real-time rotor speed $\omega_r(t)$, as already described in Chapter 2, which is given by

$$P_{ref0} = K_{opt}\omega_r^3(t) \tag{4.7}$$

where K_{opt} is a constant defined in (2.3).

It has been illustrated in Section 2.3.2 in Chapter 2 that power reference of a WTS given in the form of (4.8) cannot simultaneously achieve high wind energy capture efficiency and function as a flywheel energy storage unit to produce the exact active power of $-\Delta P_{23}$.

$$P_{ref1} = K_{opt}\omega_r^3(t) + (-\Delta P_{23}) \tag{4.8}$$

Hence, in order to control the WTS to generate the additional active power of $-\Delta P_{23}$, the ICC methodology proposed in Chapter 2 is adopted here and given by

$$P_{ref} = K_{opt}\omega_r^3(t) - \Delta P_{23} + \frac{2K_{opt}}{J}\int_0^t(-\Delta P_{23})\,dt * \omega_r(t) \tag{4.9}$$

where J is the moment of inertia of the WTS. The power reference P_{ref} shown in Figure 4-2 is then applied to the rotor-side converter of the WTS.

The proposed control scheme in (4.9) is easy to implement because only two more terms are added into the original MPPT control reference (4.7). In addition, as shown in (4.9), only the power of nearby transmission lines P_{23} is required while the frequency of the forced oscillation is not required to be known. Moreover, as also illustrated in (4.6), in principle, the proposed scheme can always smooth the oscillating power of the transmission line between bus 3 and bus 4, even when both areas are excited with forced oscillations. This idea will be further demonstrated in Section 4.4.2.

4.4 Case Studies

4.4.1 Test System

The two-area power system [75] shown in Figure 4-3, is used to investigate the performances of the proposed method. The system consists of four synchronous generators (G1-G4), static loads with constant active and reactive power consumption, and one aggregated DFIG-based wind farm. The system parameters are obtained from [75], with all the synchronous generators being equipped with a PSS whose gain is 20, to ensure a good damping performance.

The wind farm which consists of 27 DFIG-based WTSs with input wind speed 10 m/s (between cut-in wind speed of 6 m/s and rated wind speed of 12.5 m/s), whose output power is 30 MW under the MPPT control, is simulated in all of the following cases, except Case 4. Case 4 is considered to verify that the proposed control scheme (4.9) still functions well under varying wind speeds. The parameters of the DFIG-based WTS are provided in Table A-1 in Appendix A.

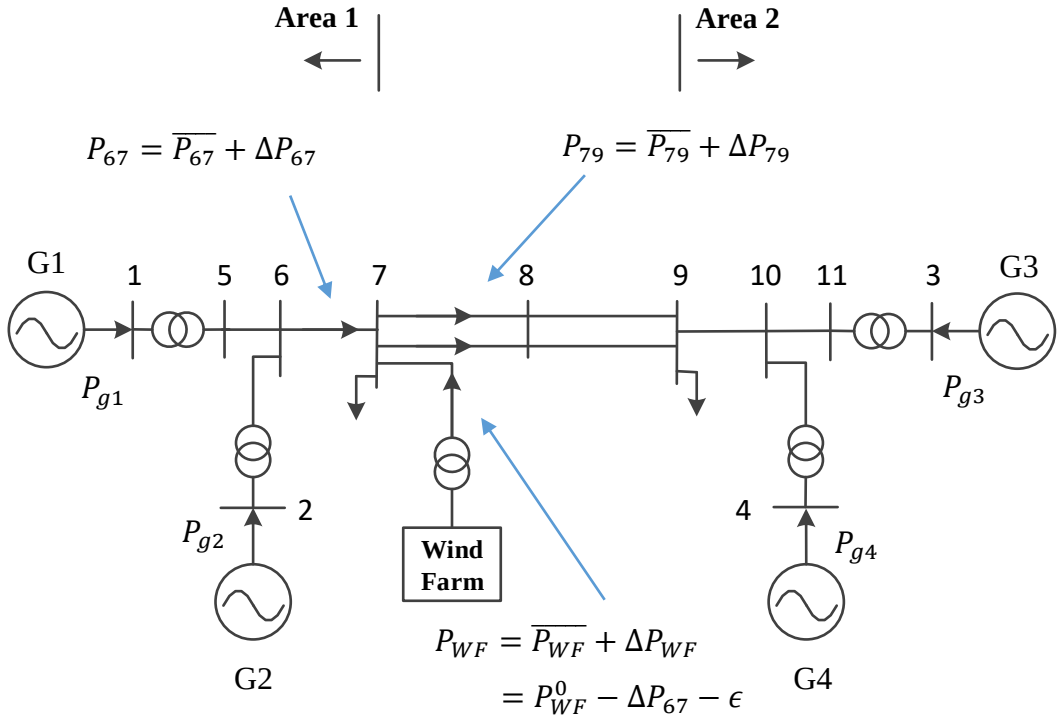

Figure 4-3 The structure of a four-machine two-area system [75] with a wind farm connected at bus 7.

In Figure 4-3, P_{ij} indicates the total power on the transmission line(s) between bus i and bus j. For example, P_{79} indicates the total power of the two transmission lines between bus 7 and bus 9. $\overline{P_{ij}}$ is the average of P_{ij}, and ΔP_{ij} is calculated as $P_{ij} - \overline{P_{ij}}$. The output power of G1 ~ G4 are $P_{g1} \sim P_{g4}$. Under the proposed control, the output power from wind farm is $P_{WF} = P_{WF}^{0} - \Delta P_{67} - \epsilon$, in which P_{WF}^{0} is the total output power of the wind farm under the MPPT control without using the proposed method, and ϵ is a small variable defined the same as ε in Section 4.3.1.

In the following case studies, the MAF window time and the time constant of the wash-out filter, as mentioned in Section 4.3.1, are chosen to be 40 s and 25 s, respectively.

In the following sections, six case studies are carried out using RTDS under different conditions to demonstrate the effectiveness of the proposed method.

4.4.2 Isolation and Suppression of Forced Oscillations

The following four cases are considered to illustrate the performance of the proposed method in the isolation and suppression of forced oscillations. The wind farm is installed at bus 7.

Case 1: In this case, an external sinusoidal perturbation $0.04\sin(0.6 * 2\pi * t)\, p.u.$ (0.04 $p.u.$is equal to 36 MW since the rated power of these synchronous generators is 900 MW) is added to the mechanical torque of G1 from 3.5 s to 28.5 s to excite a forced oscillation. With the proposed method, the wind farm will compensate the oscillating power ΔP_{67}, making P_{79} smoothed so that the forced oscillation will be kept within Area 1 and not spread into Area 2.

Case 2: The settings of Case 2 are the same as those of Case 1, except that the level of loading in each area is different from that in Case 1, causing the average active power flow P_{79} changes

from 397 MW (Case 1) to -400 MW (Case 2). This case is used to demonstrate the effectiveness of the proposed method at different operating conditions.

Case 3: In this case, the sinusoidal fluctuations $0.04\sin(0.6 * 2\pi * t)p.u.$ and $0.04\sin(0.6 * 2\pi * t + \pi)p.u.$ are added to the mechanical torque output of G1 and G3, respectively, from 3.5 s to 28.5 s. Thus the both areas are experiencing external perturbations and the excited forced oscillations in the system are doubled. It is used to demonstrate that the wind farm at bus 7 can always smooth the oscillating power of the tie-lines and makes the tie-lines act as a wall of isolation for the forced oscillations from both areas.

Case 4: The settings in Case 4 is the same as those in Case 1 except that now the WTS is under real-time variable wind speeds. The wind speed data are borrowed from [161]. The purpose of this case is to demonstrate the effectiveness of the proposed method under variable wind speeds.

The simulation results of Case 1 are shown in Figure 4-4 – Figure 4-7. Figure 4-4(a) shows that, without the proposed control scheme, the amplitude of the excited forced oscillation of P_{79} on the tie-lines is 100 MW, which is 2.8 times that of the original perturbation (100/36=2.8), even when the system has good damping performance. The phenomenon coincides with the conclusion made in [71] that the method of increasing damping to suppress forced oscillations is not effective. In contrast, with the proposed method, the oscillations of P_{79} are reduced to a value near zero, because the wind farm generates oscillating active power ΔP_{WF} which is opposite to ΔP_{67}, as seen from Figure 4-4(b). Thus, the forced oscillation is isolated within Area 1 and not spreading into Area 2. At the same time the forced oscillation in Area 1 is also suppressed (Figure 4-4(c)), which is only half of that without the proposed control. This suppression leads to half of the compensated active power needed from the wind

farm because, as explained in Section 4.3.1, the active power output of the synchronous generators in area 1 is affected by the injected active power of the wind farm.

Figure 4-5 further demonstrates that the oscillations of P_{g1} and P_{g2} are greatly reduced (suppressed) and the oscillations of P_{g3} and P_{g4} are almost eliminated (isolated) because the oscillation in P_{79} is well smoothed, thereby eliminating the impact from the perturbation source in Area 1. Although the wind farm releases or absorbs 1.7 times of its total output power under the MPPT control (50/30=1.7), as can be seen from Figure 4-4(b), the loss of wind power capture is minimal, as demonstrated in Figure 4-6.

Figure 4-7 shows the RMS values of the stator and rotor current of a single DFIG-based WTS. It can be seen that the change of the rotor side current is only 20% of the change of the stator side current, indicating that most of the compensated power are flowing through the stator instead of the rotor-side converters. In other words, compared with the method of installing extra E-STATCOM, which needs full-rated converters [71], the extra capacity of the converters in a DFIG-based WTS under the proposed strategy is significantly reduced.

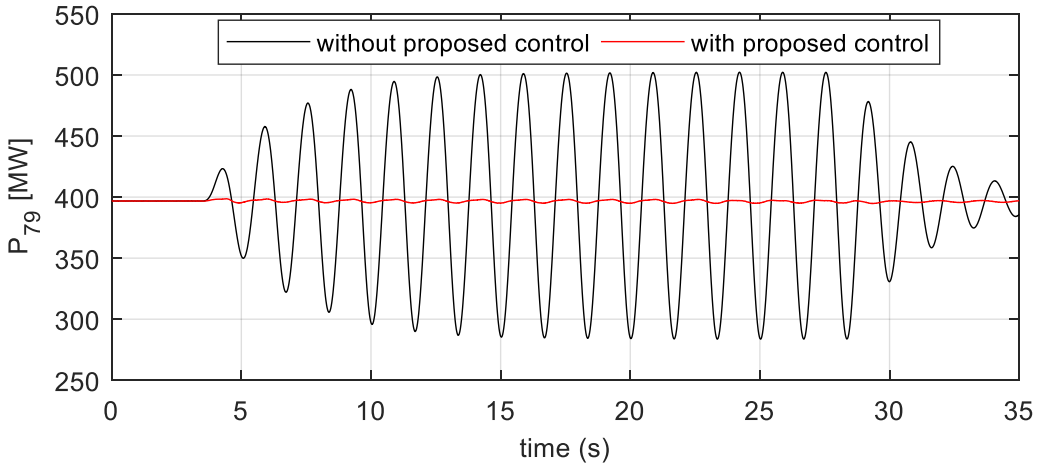

(a) P_{79} with and without the proposed control.

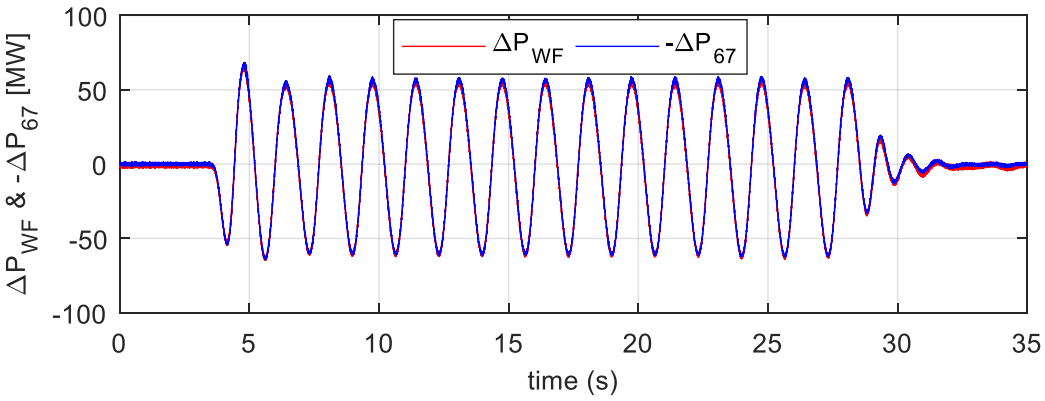

(b) ΔP_{WF} and $-\Delta P_{67}$ under the proposed control.

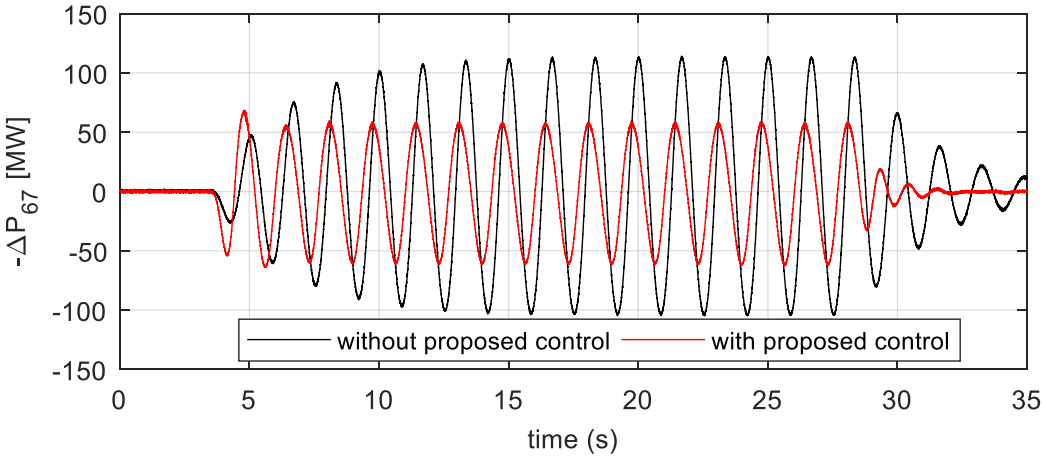

(c) $-\Delta P_{67}$ with and without the proposed control.

Figure 4-4 Simulation results under Case 1.

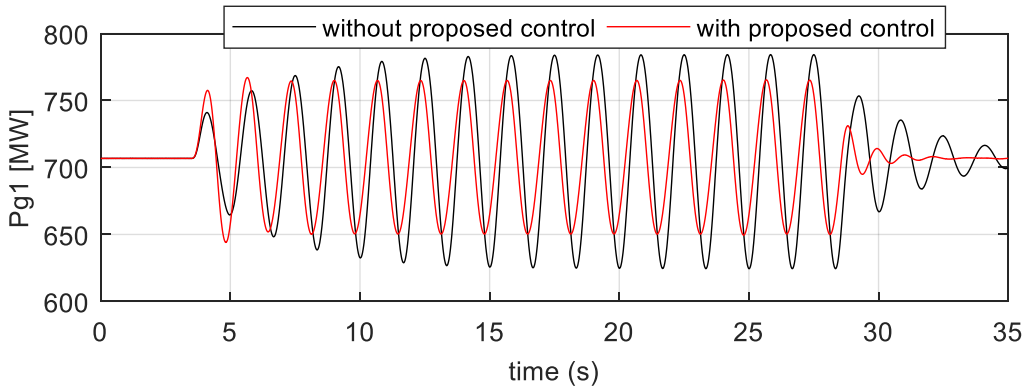

(a) The active power output of G1.

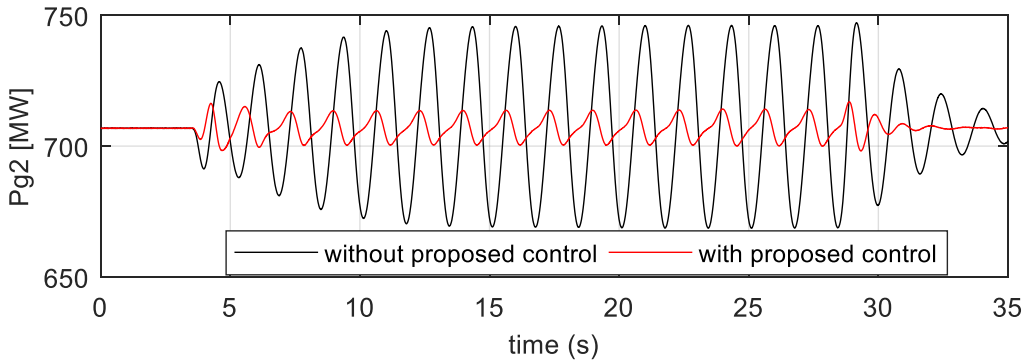

(b) The active power output of G2.

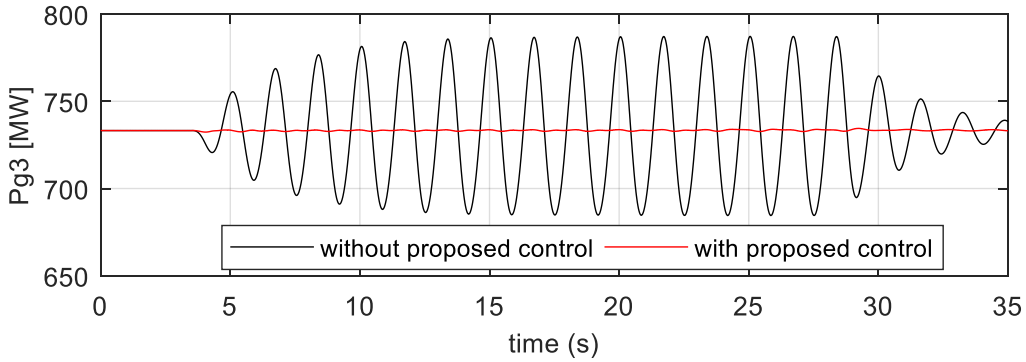

(c) The active power output of G3.

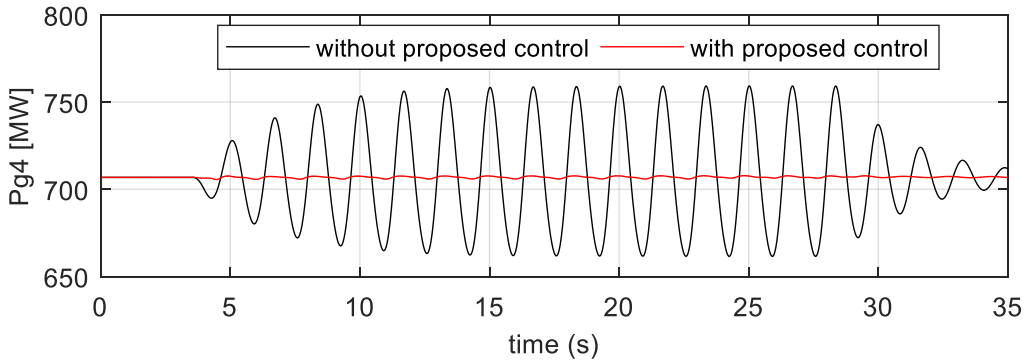

(d) The active power output of G4.

Figure 4-5 The active power output of G1, G2, G3 and G4 under Case 1 with and without the proposed control.

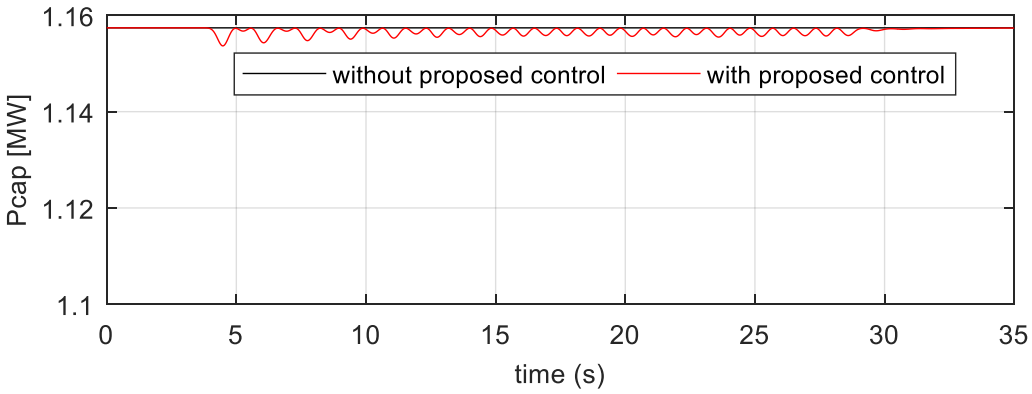

Figure 4-6 The captured wind power of a single WTS with and without the proposed control under Case 1.

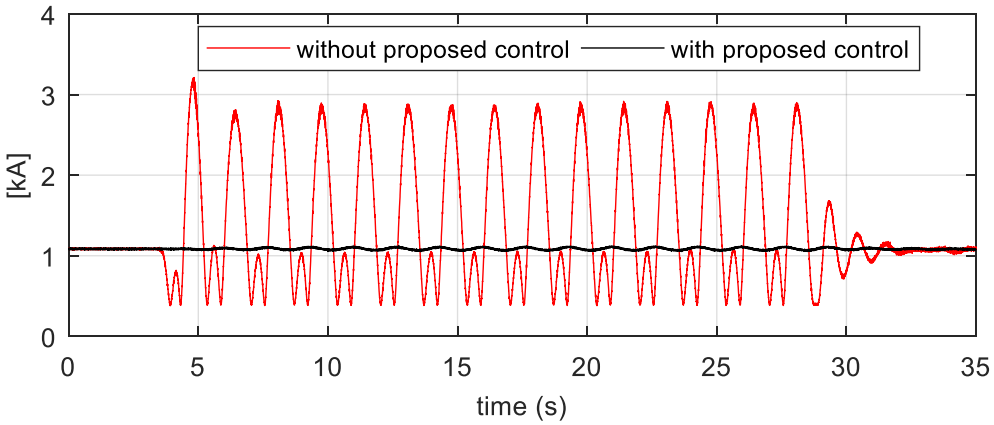

(a) RMS of stator current of a single DFIG under the proposed control.

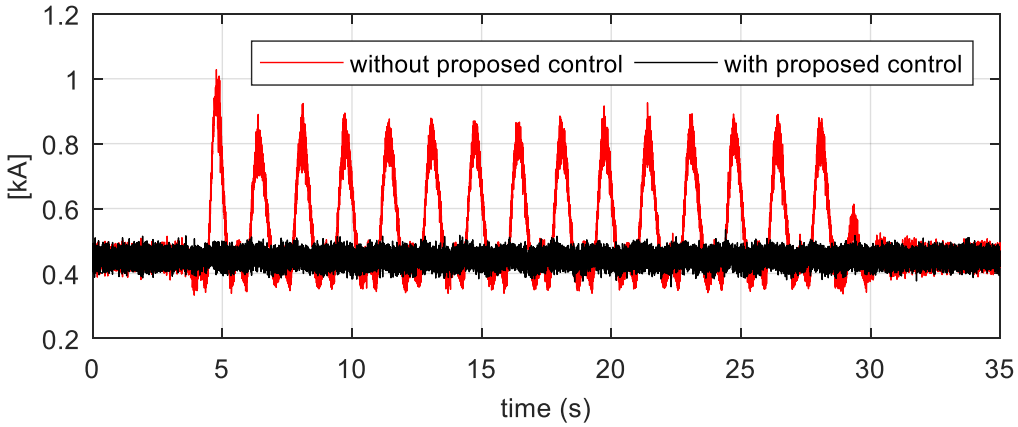

(b) RMS of rotor current of a single DFIG under the proposed control.

Figure 4-7 The rotor and stator current RMS of a single DFIG-based WTS under Case 1.

The simulation results of Case 2 are shown in Figure 4-8. Figure 4-8 shows that although the operating condition is different from that in Case 1, P_{79} is still well smoothed with the proposed control scheme (Figure 4-8(a)), since the wind farm generates oscillating power exactly opposite to ΔP_{67} (Figure 4-8(b)). Moreover, ΔP_{67} is also suppressed (Figure 4-8(c)).

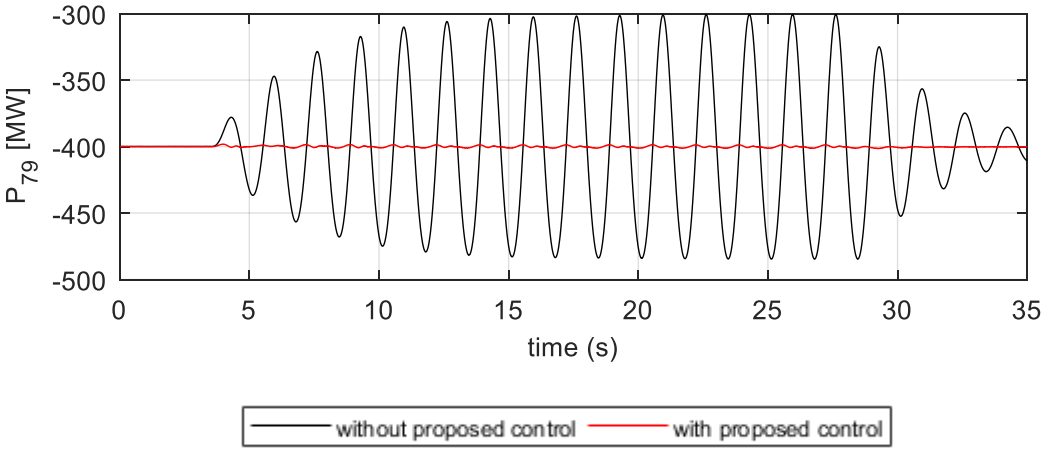

(a) P_{79} with and without the proposed control.

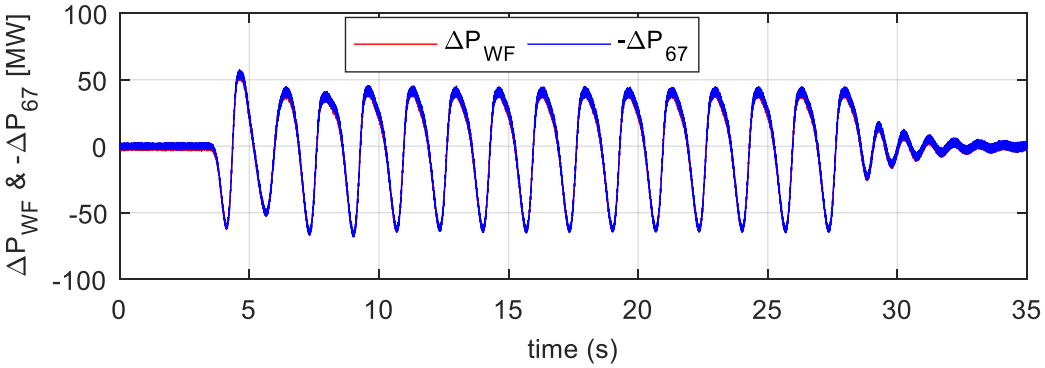

(b) ΔP_{WF} and $-\Delta P_{67}$ under the proposed control.

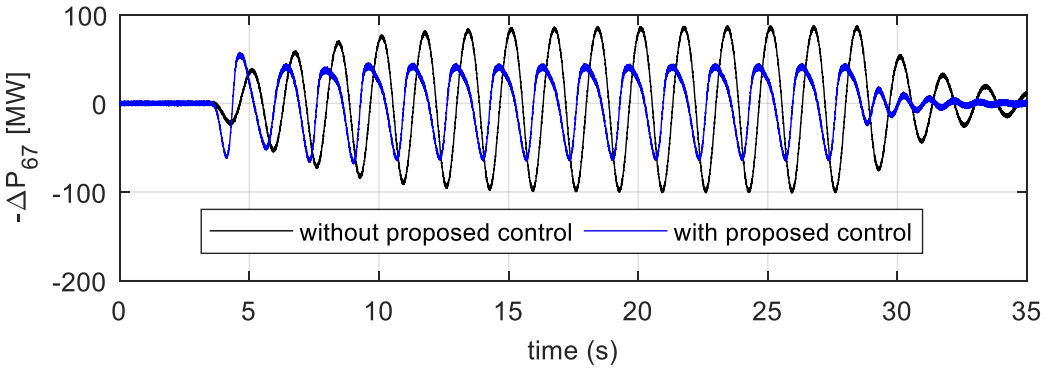

(c) $-\Delta P_{67}$ with and without the proposed control.

Figure 4-8 Simulation results under Case 2.

The simulation results of Case 3 are shown in Figure 4-9 and Figure 4-10. Figure 4-9(a) and Figure 4-9(b) shows that P_{79} is well smoothed under the proposed control when both the areas are excited forced oscillations. In other words, the wind farm protects the tie-lines from experiencing oscillations and act as a wall of isolation for the forced oscillations from both the areas. Figure 4-10 shows that the forced oscillations in both the areas are greatly reduced using the proposed method.

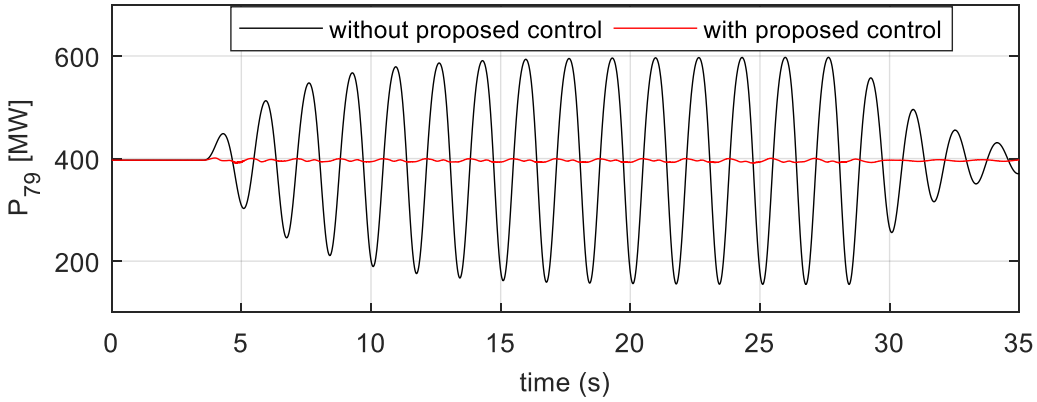

(a) P_{79} with and without the proposed control.

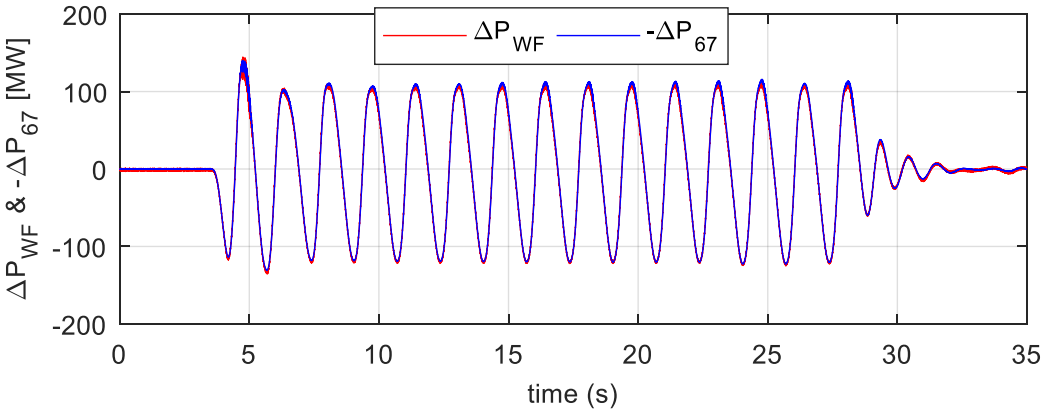

(b) ΔP_{WF} and $-\Delta P_{67}$ under the proposed control.

Figure 4-9 Simulation results under Case 3.

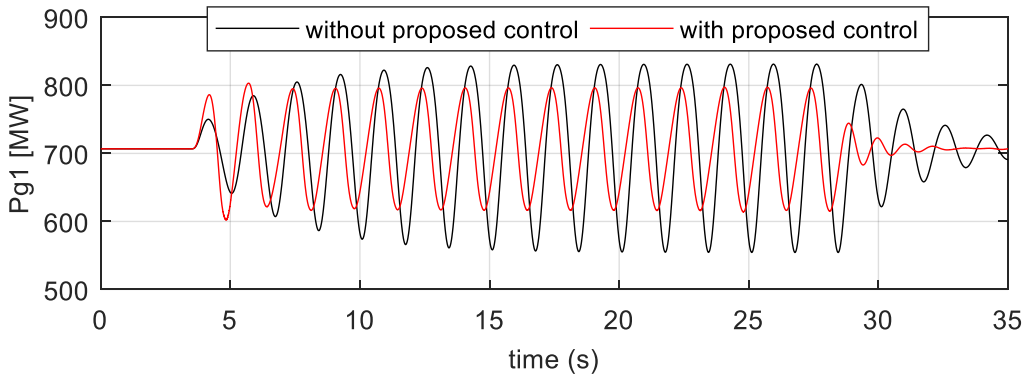

(a) The active power output of G1.

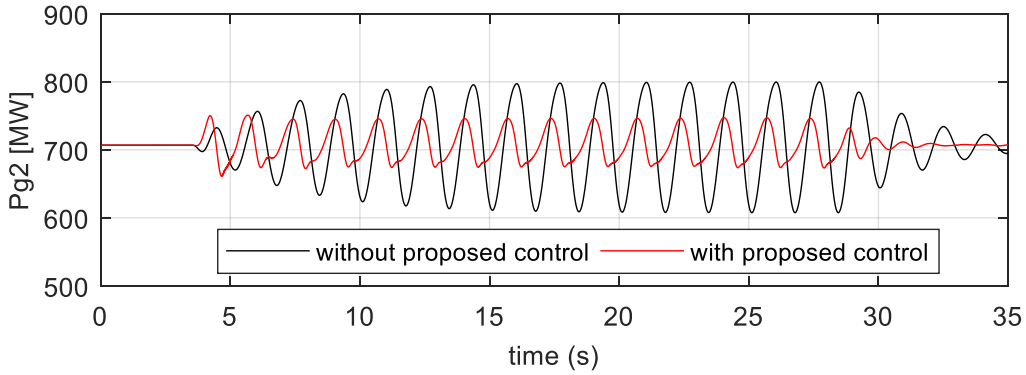

(b) The active power output of G2.

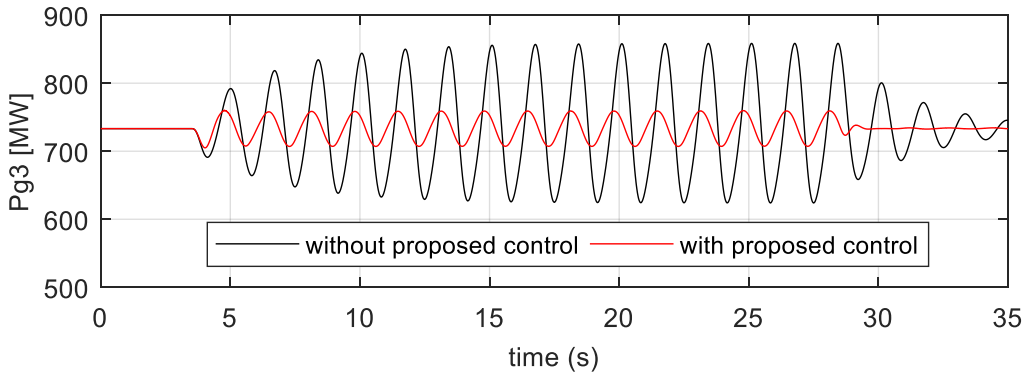

(c) The active power output of G3.

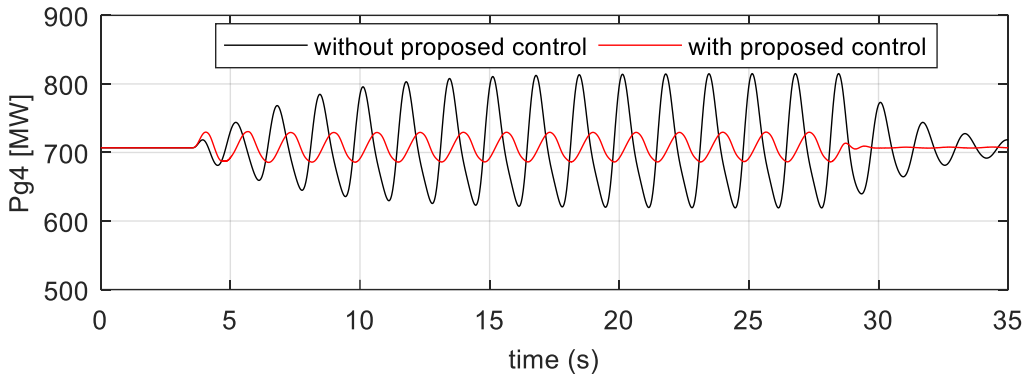

(d) The active power output of G4.

Figure 4-10 Active power output of G1, G2, G3 and G4 with and without the proposed control in Case 3.

The simulation results of Case 4 are shown in Figure 4-11. Figure 4-11(a) shows the simulated real-time wind speeds. Figure 4-11(b) shows that P_{79} is well smoothed with the proposed control even under varying wind speeds. Figure 4-11(c) shows that the captured wind power under the proposed control is close to that under the MPPT control.

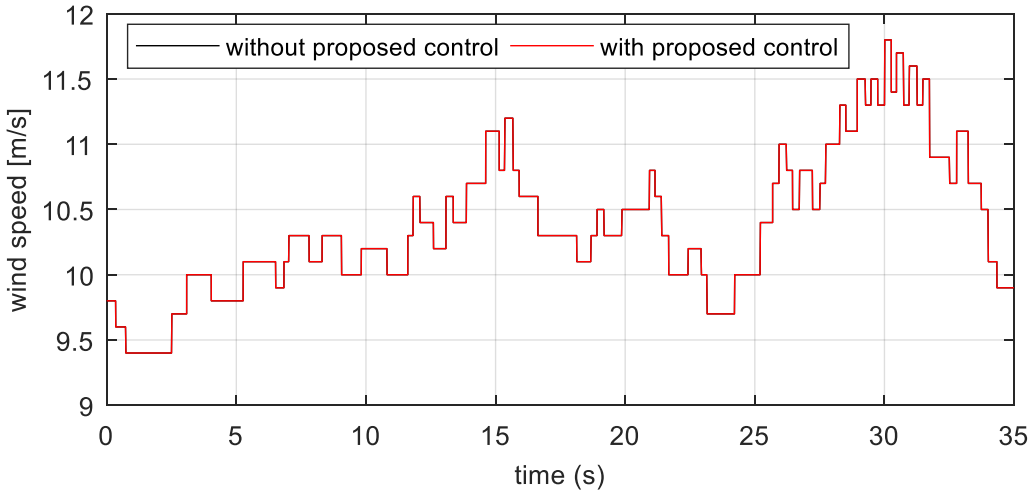

(a) Simulated real-time wind speeds.

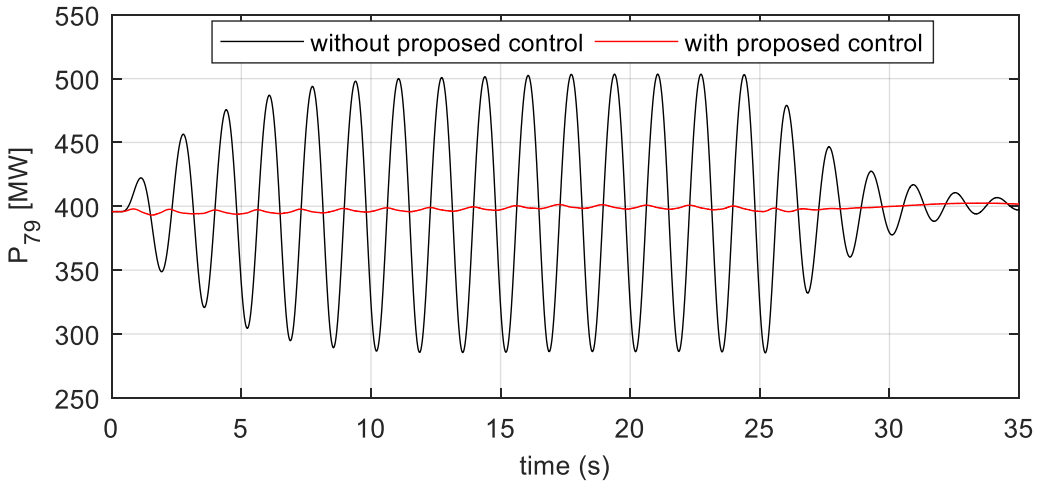

(b) P_{79}.

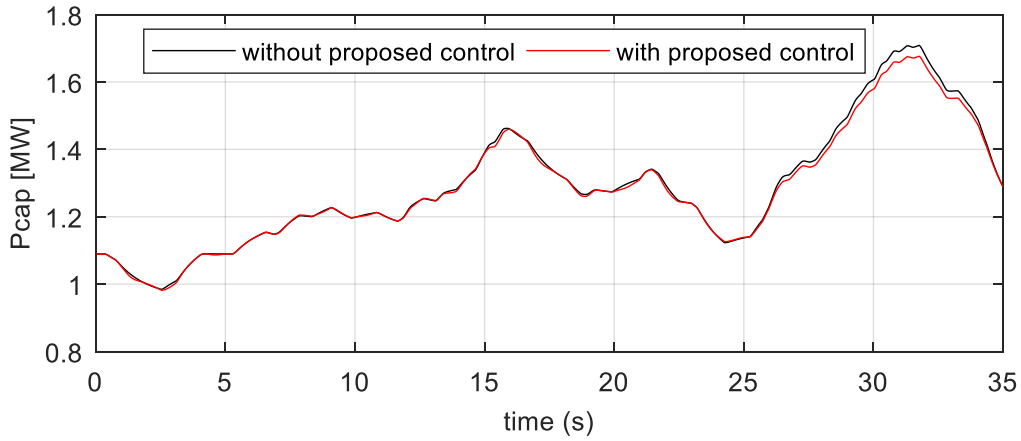

(c) The captured wind power of a single WTS.

Figure 4-11 Comparative simulation results with and without the proposed control under Case 4.

4.4.3 Impact of Wind Farm Location

Case 5: Case 5 is the same as Case 1, except that the location of the wind farm is moved from bus 7 to bus 5. In this case, the wind farm is controlled to inject active power opposite to ΔP_{15}, aiming to reduce the oscillation in P_{56} to zero. Simulation results of Case 5 are compared with those of Case 1 for better illustration.

The simulation results of Case 5 are shown in Figure 4-12 and Figure 4-13. Figure 4-12 shows that when the wind farm is connected to bus 5 with the proposed control scheme, the oscillating component of P_{56} is well reduced. Thus, bus 5 becomes an isolation wall through which the forced oscillation excited by the external perturbation on G1 cannot propagate further. This outcome is also verified by Figure 4-13(a) which shows the oscillation of the active power output by G2 decreases, and by Figure 4-13(b) which shows that P_{79} is well smoothed.

When the transmission line between bus 5 and bus 6 becomes an isolation wall, the forced oscillation is restricted within a smaller area compared with that in Case 1; thus, the magnitude of the oscillation with the proposed control in theory (as illustrated in Section 4.3.1) should be reduced more than that in Case 1. This outcome is verified by comparing the blue and read lines in Figure 4-13(a) and Figure 4-13(c), where oscillations of active power from G2 and G1 are smaller than those in Case 1. It further leads to a smaller compensating power from the wind farm as seen from Figure 4-13(d).

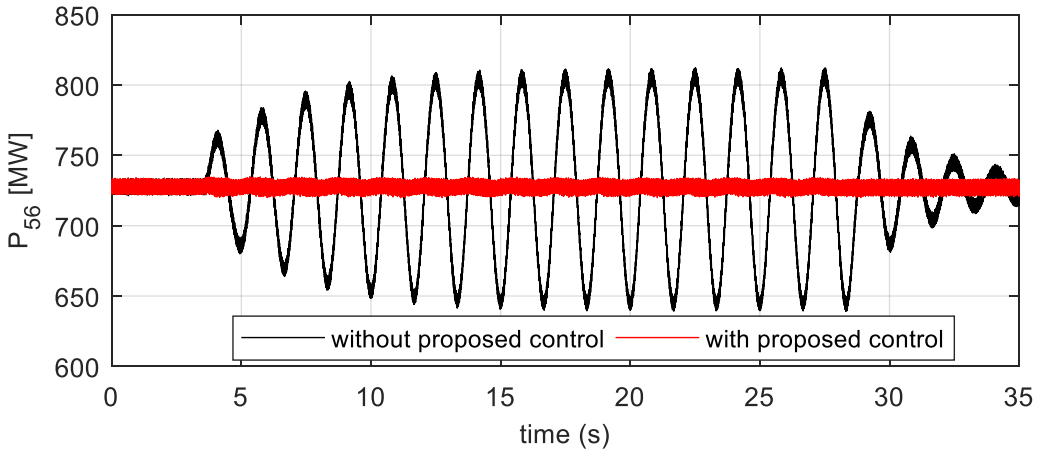

Figure 4-12 P_{56} with and without the proposed control under Case 5.

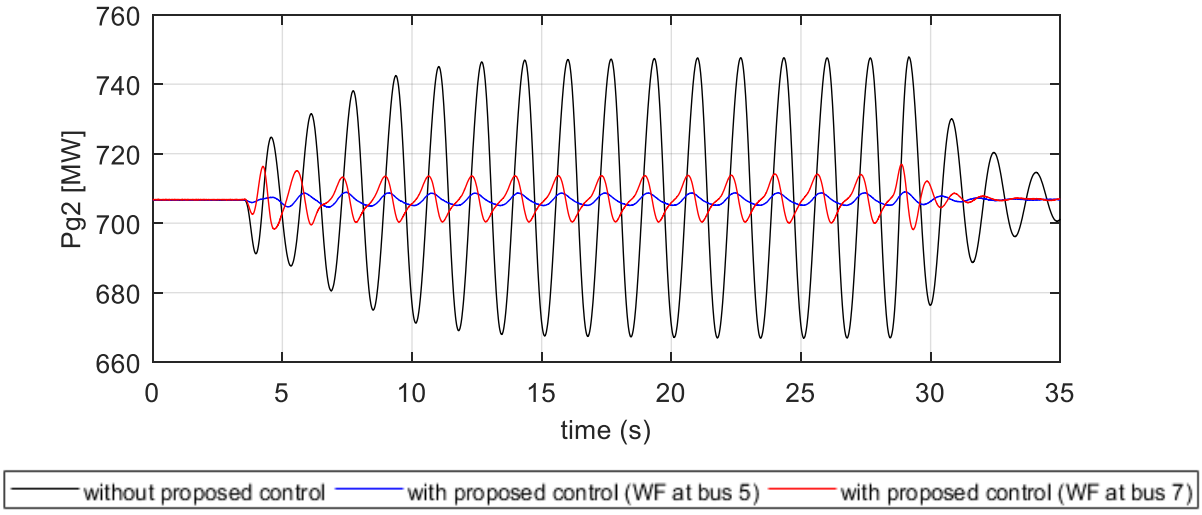

(a) Active power output of G2.

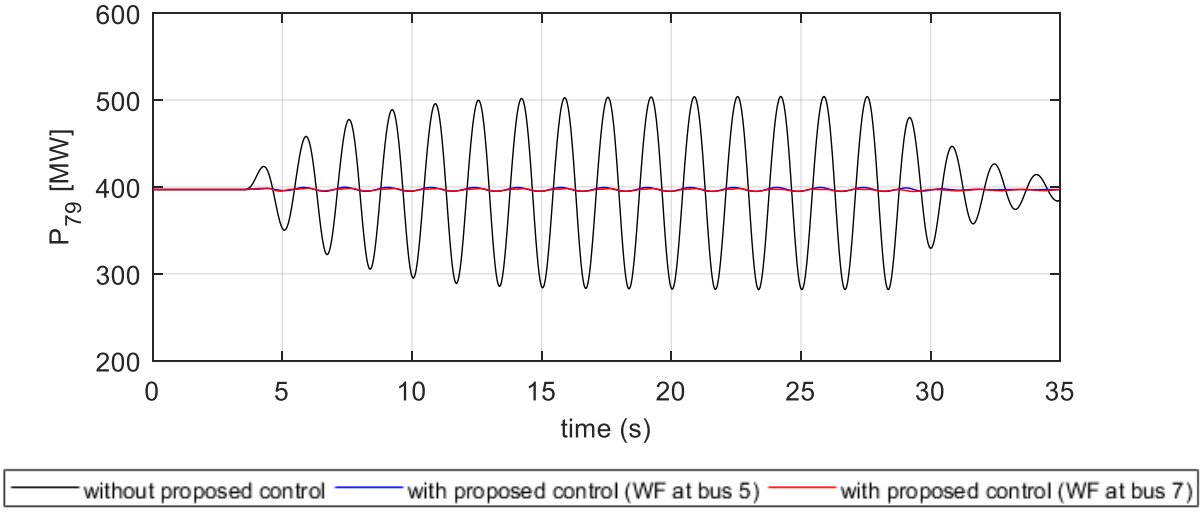

(b) P_{79}.

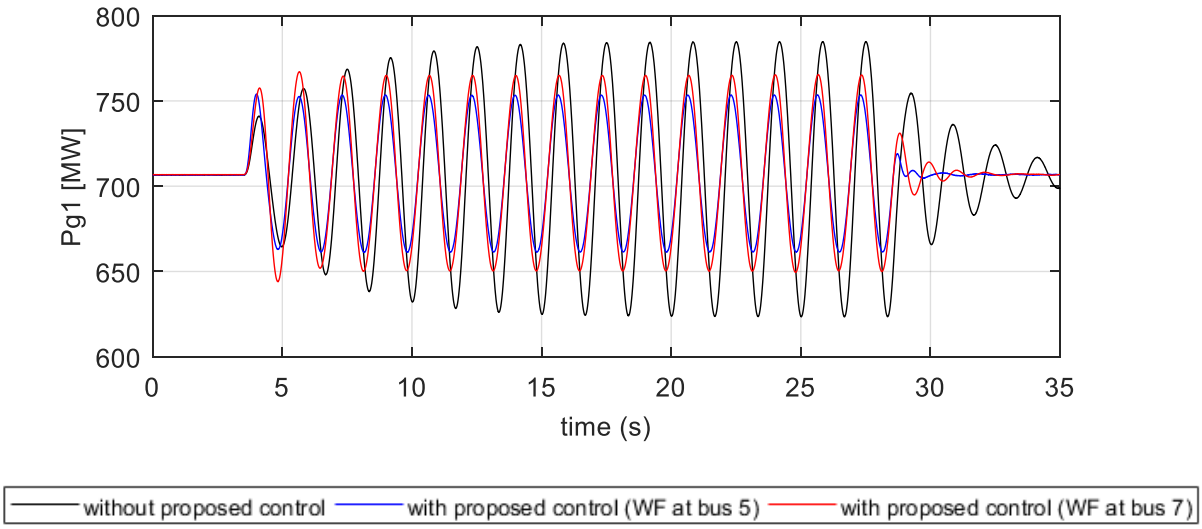

(c) Active power output of G1.

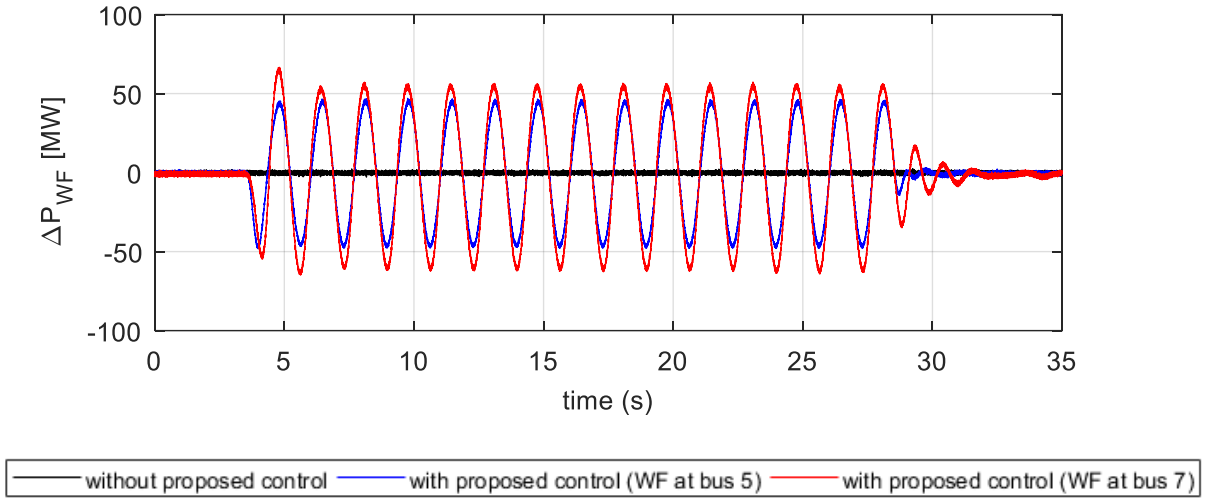

(d) ΔP_{WF}.

Figure 4-13 Comparative simulation results of Case 5 and Case 1 under the proposed control and under the proposed control when the wind farm is connected at bus 5 and bus 7.

4.4.4 Suppression of Inter-Area Oscillations

Case 6: This case is considered to verify that the proposed method can also help to damp inter-area oscillations. To excite an inter-area oscillation, a 0.02 $p.u.$ voltage step with a duration of 500 ms ([163]) is added to the exciter of G1. The wind farm is installed at bus 7.

The simulation results of Case 6 are shown in Figure 4-14. Figure 4-14(a) and Figure 4-14(b) show that by using the proposed control method, the inter-area oscillation is damped. Moreover, the wind farm has nearly zero loss of wind power capture as demonstrated by Figure 4-14(c), although the active power output from the wind farm is varying dramatically as seen from Figure 4-14(d).

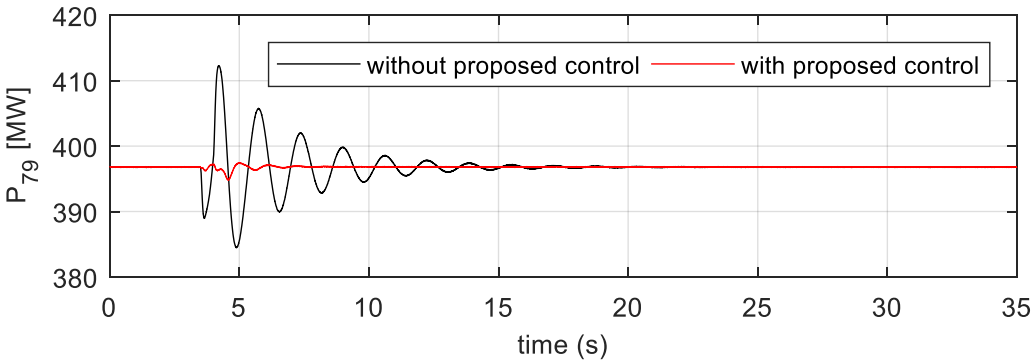

(a) Active power P_{79} on tie-lines.

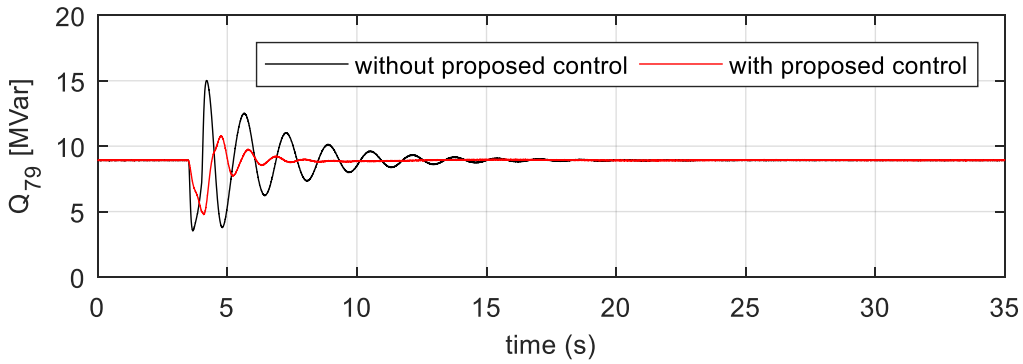

(b) Reactive power Q_{79} on tie-lines.

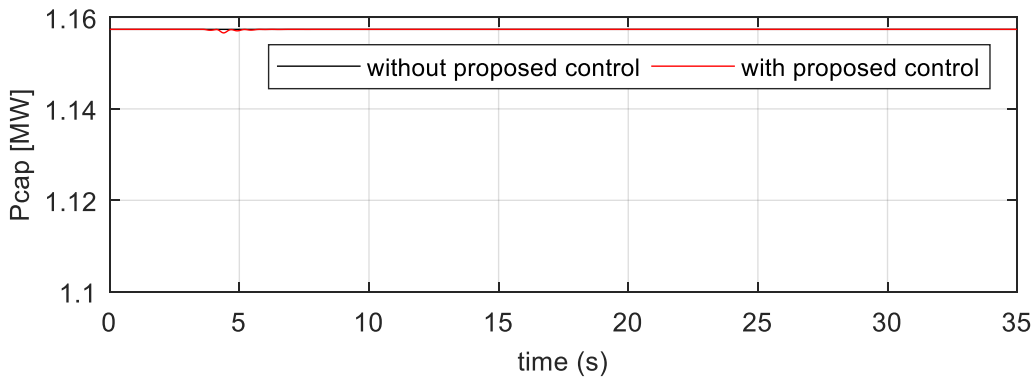

(c) Captured wind power of a single WTS.

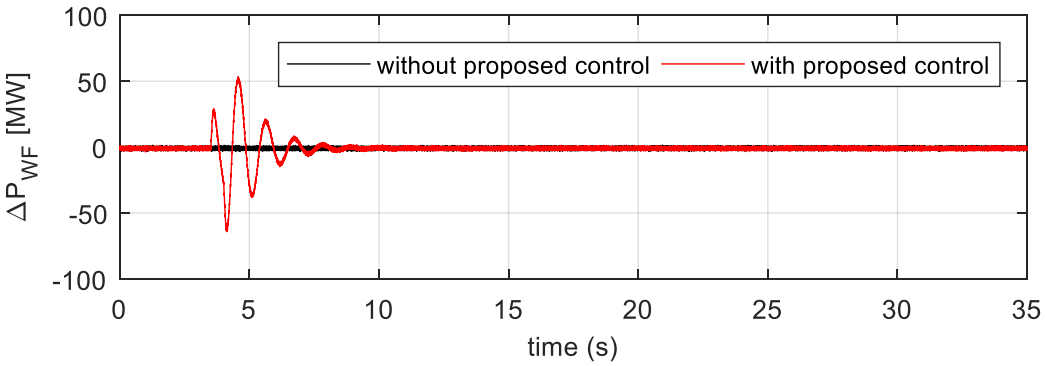

(d) ΔP_{WF}.

Figure 4-14 Comparative simulation results under Case 6 with and without the proposed control of forced oscillations isolation and suppression.

4.5 Summary

This Chapter presented a proposed isolation and suppression strategy for forced oscillations based on the use of the large rotor inertia of the WTSs in wind farms. By controlling the WTSs in a wind farm to timely release or absorb active power opposite to the oscillating power from the disturbed area(s), the forced oscillations can be isolated within the disturbed areas and hence are prevented from propagating to the rest of the system. Meanwhile, the forced oscillations excited in the disturbed areas are also reduced and suppressed because the active power output of the synchronous generators in the disturbed areas are affected by the injected active power of the wind farm. Unlike the other forced oscillations suppression methods, the proposed strategy does not require the installation of extra energy storage and power electronic devices, and a prior knowledge of the oscillations frequencies. Furthermore, the proposed method can be implemented with slight loss of wind power capture.

The two-area power system with a DFIG-based wind farm was simulated using RTDS. The simulation results under different scenarios demonstrated that the proposed method can well isolate and suppress forced oscillations, and damp inter-area oscillations as well.

CHAPTER 5 CONCLUSIONS AND FUTURE WORK

5.1 Conclusions

Because of concerns of fossil fuels depletion, air pollution and global warming, renewable generation has been developed rapidly, and will become the main source of heat and electricity generation in the future. However, most of the renewable generation is fluctuating in nature. Fluctuating power will bring many side-effects if directly transmitted to power grids, e.g. forced oscillations. This thesis focuses on smoothing fluctuating wave and wind power, and isolating and suppressing forced oscillations. The main work that has been done can be summarized in the following three parts.

5.1.1 Smoothing Wave Power

It is reviewed in Chapter 1 that wave energy generation has sparked a surge attention in the world and many different types of WEC devices have been designed. However, the electrical wave power generated by most of the WECs fluctuates from zero to several times of the average at typical periods of 5~12 s. If the fluctuating wave power is directly transmitted to power grids without being smoothed, it will cause many problems. In order to avoid these problems, many wave power smoothing methods have been proposed. However, the existing smoothing methods either are limited in specific ocean environment by particularly designing physical components or arranging the geometrical layout of the WECs in a wave farm, or have high installation and maintenance costs by using extra energy storage devices.

Considering the many advantages brought by a combined exploitation of offshore wave and wind energy, in Chapter 2 a new wave power smoothing method is proposed by using the inherent large amount of inertial energy of nearby offshore WTSs. The smoothing principle is

that the WTSs are controlled to release or absorb power which is opposite to the wave power fluctuations, so that the wave power is smoothed. However, the control challenge is that on one hand, the rotor speeds of the WTSs have to be controlled according to the kinetic energy storage requirement to smooth the wave power. On the other hand, they have to be controlled to follow wind speeds changes to maximize wind power capture, which is, however, irrelevant to the kinetic energy storage requirement. Thus, by using DCC, the WTSs cannot output fluctuating power exactly opposite to wave power fluctuations. Therefore the wave power cannot be well smoothed. However, by adding a supplementary integral torque term into DCC, the proposed ICC can generate power waveform which is exactly opposite to the fluctuating component of the wave power so that the wave power is smoothed. The contributions of the proposed wave power smoothing strategy are summarized as:

- The proposed smoothing strategy does not require any additional energy storage systems or changes to the existing devices in the offshore WTSs.

- The design is applicable to all kinds of WEC technologies since the smoothing is based on the total electrical power output of a wave farm.

- The smoothing control has minor effect on wind power capture. The conducted quantitative analysis results show that the standard deviation of the output power flowing on the system bus in a wave-wind farm can be decreased by $10\sim20$ times using the proposed ICC, with less than 1% wind power capture loss.

In order to further reduce wind power capture loss, a coordination algorithm of multi-WTSs is proposed in a wind farm. With the coordination algorithm, the required compensation power can be dynamically allocated to each WTS according to the square of their average rotor speeds. In this way, those WTSs with higher rotor speeds are allocated with more wave power to

smooth. And those with lower rotor speeds are allocated with less. Thus, the loss of wind power capture is less than the case when each individual WTS is evenly allocated with the same amount of compensation power.

The effectiveness of ICC is verified by simulation results of a DFIG-based WTS and a PMSG-based WTS with both steady wind speeds and varying wind speeds in RTDS. Then the performance of the coordination algorithm is validated by a two-DFIG-based wind farm with variable wind speeds.

In order to quantify the conflicts between the wave power smoothing effect and wind power capture efficiency, the index $\xi = \overline{P_{wind}}/\sigma_{P_{wave}}$ is defined as wave-wind ratio. For a given level of wave power fluctuations, it indicates how many WTSs are needed to achieve a required wave power smoothing effect. Based on this index and simulation results, related quantitative analysis is then carried out.

5.1.2 Smoothing Wind Power

It is described in Chapter 1 that wind energy generation is projected to account for the worldwide biggest renewable generation except hydropower in the future. However, due to the high variability and limited predictability of wind power, wind energy generation brings a series of technical and economic problems to power systems, especially with high wind power integration.

This thesis only focuses on smoothing wind power with variations less than tens of seconds. As reviewed in Chapter 1, it is attracting to self-smooth wind power by controlling the wind turbines large amount of inertial energy. Because this type of methods does not need extra energy storage systems and has the problems of the pitch angle control and using the DC-link capacitors in the full-rated converters. However, the existing control methods for this type are

still needed to be improved because the wind power smoothing and high energy capture efficiency cannot be achieved simultaneously.

Based on this background, Chapter 3 proposes a new wind power self-smoothing approach through controlling the rotating kinetic energy of the WTSs in a wind farm by adopting the structure of the power reference of ICC in Chapter 2. The coefficient of the proposed power reference is reduced in a way different from that of ICC, due to in the specific wind power self-smoothing situation. Moreover, different from that in ICC to smooth wave power, the required compensation power to smooth wind power cannot be measured. Thus an easily implemented estimation method is proposed to obtain the compensation power. Finally, the given power reference of the proposed wind power smoothing control includes two parts. The first part can approximately recover the original power trajectory of the MPPT control. And the second part can compensate the fluctuations of the former. In this way, wind power smoothing can be achieved with slightly loss of wind power capture. Furthermore, for a wind farm, a coordinated control of multiple WTSs is proposed, similar to wave power smoothing. However, the coordinated control for wind power smoothing has different advantages. Those advantages include: (1) Less wind power needs to be smoothed; (2) Less loss of wind power capture can be achieved; and (3) Less possibilities of rotor speed will drop to the minimum.

Compared with the existing work, the proposed wind power smoothing control can have the merits shown below at the same time:

- It can smooth wind power output variations within tens of seconds and still keep a high efficiency of wind power capture. Simulation results show that by using the proposed wind power smoothing control c_v of the output power of the two-DFIG-based wind farm is reduced by 36.11% while less than1% wind energy capture is lost with a real varying wind speed profile.

- It can maintain stabilities of WTSs under variable wind velocities;
- It can mitigate mechanical stress of a wind turbine by giving a smoother torque reference compared with the that of MPPT control, thus extending wind turbines lifetime;
- It is easily implemented because no modification of the existing devices and no installation of extra energy storage systems are needed;
- It can smooth wind power from a wind farm instead of from the individual WTSs. This can reduce wind power capture loss, because a wind farm has an inherent power smoothing effect and the WTSs in the wind farm have different wind velocities.

A DFIG-based WTS, a PMSG-based WTS and a wind farm composing of two DFIG-based WTSs are simulated in RTDS. The simulation results validate the performances of the proposed wind smoothing control and the coordinated control algorithm.

Quantitative analysis of a single WTS about the relationship between wind power smoothing effect and capture efficiency under different MAF window time are conducted. It shows that c_v of the output power can be reduced by 5% - 40% with less than 2% loss of wind power capture. The quantitative analysis also gives a guidance for the chosen of MAF window time.

5.1.3 Isolating and Suppressing Forced Oscillations

Forced oscillation is a resonance in a power system, which has been found in Canada, US, and China. It can be excited when there exist periodic external perturbations in a power system at frequencies that are close or equal to the natural frequencies of the system modes. Since forced oscillations still occur for a system with good damping performance and they can be eliminated only by removing the external periodic perturbations, countermeasures to eliminate or mitigate

them are significantly different from those for natural oscillations. As reviewed in Chapter 1, new methods to isolate and suppress forced oscillations are still remained open.

Since wind energy generation will take a predominant position in the future energy generation, using the inherent large amount of inertial energy of these controllable WTSs to suppress short periodic forced oscillations is proposed in Chapter 4. Controlling the inertial energy of WTSs has been proposed to suppress inter-area oscillations before, but not for forced oscillations. Besides, the state-space based methods have limited applicability since they are subject to fixed system structures. Unlike the existing methods, by adopting ICC described in Chapter 2 the proposed strategy to isolate and suppress forced oscillations is achieved by controlling wind farms to timely release or absorb power opposite to the oscillating power from the perturbation area(s). Thus, the forced oscillations can be prevented from propagating to the rest of power grid (isolated) and at the same time the oscillating power in the disturbed area(s) is also reduced (suppressed). Specifically, the proposed strategy has the following four main advantages:

- Wind farms are used to isolate and suppress forced oscillations with minor effect on wind power capture efficiency.

- It is easy in practical implementation based on measurement of the oscillating power from disturbed area(s), while a prior knowledge of the frequencies of the forced oscillations is not required.

- The controller is universal which is not subject to fixed system structures. However, the existing state-space based control methods are subject to fixed control structures and specific power systems.

- Although the strategy is to suppress forced oscillations, it can also help to damp inter-area oscillations.

RTDS simulation results of a DFIG- based wind farm in a modified two-area test power system under different scenarios demonstrate that the proposed method can isolate and suppress forced oscillations with minor loss of wind power capture. Meanwhile inter-area oscillations can also be damped as well.

5.2 Further Discussions of the Proposed Methods

5.2.1 Smoothing Wave Power

To well smooth the wave power, it is important to obtain the real-time electrical power from the wave farm. According to the data shown in [164-166], the total delay caused by the synchronized measurements and transmission based on phasor measurement units (PMU) and optical fibres, respectively, ranges from 60 ms to 80 ms. In the proposed wave-wind farm system, in order to realize the proposed wave power smoothing scheme, the related measurement and transmission infrastructures have to be installed. Since in the proposed design these devices are only used for the smoothing operation, therefore the delays happened in the wide-area measurement systems, such as queuing delays, will not happen in this specific smoothing situation. Thus, in the wave-wind farm, the delay due to communication is much less than $60ms$ and is also fixed. Then using lead-lag components can well compensate the phase and amplitude caused by the communication delay. Therefore, obtaining the accurate wave power is not a problem in the proposed smoothing scheme.

Another issue in the proposed wave power smoothing is the possibility that a resonant phenomenon would happen in the wind turbine when the generator is controlled to generate oscillating power opposite to the fluctuations of the wave power. This needs to be checked before using the proposed scheme, by taking into account of the proximity between the oscillating frequency of the wave power and the frequency of the oscillating modes of the WTS.

The third issue is that the rated capacity of the AC generator in a WTS would be increased, when the proposed wave power smoothing method is implemented. However, this is not a concern since an AC generator can endure several times its rated current.

The forth issue is the rated capacity of the power electronic converters in a WTS has to be increased, since the usually used VSC converters have little capability to endure overrated current. However, compared with other existing methods, such as using flywheels and supercapacitors, the proposed smoothing scheme is much more economic. For example, if an equivalent flywheel system is installed to smoothing the wave power, at least extra installation costs for the generator is required. As for supercapacitor-based energy storage, full-rated converters have to be used. The costs for the full-rated converters is nearly 4 times that of the extra capacity of the converter in DFIG-based WTSs. Moreover, DFIG-based WTSs are still the most popular wind energy conversion technology [39].

The last issue should be taken into account is the fatigue of wind turbine shafts caused by the smoothing action. This should be further studied.

5.2.2 Smoothing Wind Power

Similar to the proposed wave power smoothing, it is also critical that the measured signals are accurate without delay in the wind power self-smoothing situation. This is not an issue when each WTS smooths its own output power, since the signals are measured and transferred within a WTS. In the case when the wind power smoothing is taken place within a wind farm by the coordination control of multiple WTSs, the delay should be considered. However, this also depends on the size of the wind farm. Assuming a wind farm has a radius of 500 km, and the signals are transferred by optical fibers (whose transmission speed is $2 \times 10^8 m/s$), the total delay is 5 ms (both data sending and receiving are considered) when the data collecting center is installed in the center of the wind farm. This delay is sufficiently small and can be ignored. Therefore, the delay is also not a problem in the wind power self-smoothing situation as that in Chapter 2.

Other issues happened in the proposed wave power smoothing situation are not problems anymore in the proposed wind power smoothing situation. Because after the output wind power is smoothed, the capacity of power electronic converters can be reduced, and the fatigue of wind turbine shafts can be improved.

5.2.3 Isolating and Suppressing Forced Oscillations

To isolate and suppress forced oscillations by wind farm, it is also essential that the accurate signals of forced oscillating power on the transmission lines are obtained. Unlike the wave power smoothing in Chapter 2 and wind power self-smoothing in Chapter 3 where the measurement and transmission devices are particularly installed and the delay is not a problem, the communication delay in this situation should be carefully dealt with. Because from a system point of view the measurement and transmission devices would not be particularly installed only for this one purpose, so the delay in this case is bigger than that in the wave and wind power smoothing situations and it is changing [164-166]. Therefore, the designed lead-lag components which are used for compensation of phase and amplitude caused by the delay should be able to tolerate a certain range of change of delay.

Similar to the wave power smoothing, in this case the capacity of converters should be increased. However, following the analysis similar to that of the wave power smoothing, the proposed strategy is more economic than the existing methods.

The last issue is about wind turbine shafts fatigue. Unlike the wave power smoothing, this issue does not need to be considered in the isolation and suppression of forced oscillations. This is because forced oscillations and inter-area oscillations neither happen frequently nor last too long. Thus, the extra fatigue caused by the proposed oscillations isolation and suppression scheme has little impact on a WTS compared with the lifetime fatigues during normal operation.

5.3 Future Research

The following is a list of the possible future works:

1. The proposed coordinated control for smoothing wave power or wind power is merely based on the square of the rotor speed average of the participated WTSs. It would be interesting to investigate other methods to achieve a better coordination within a wind farm.

2. In this thesis, the quantitative analysis of the relationship between the wave power smoothing effect and wind power capture loss based on the index $\xi = \overline{P_{wind}}/\sigma_{P_{wave}}$ has been done. However, one thing that has not been investigated is what value of ξ is good enough in a real situation. Hence, it would be interesting to explore the optimal choice of ξ in practice.

3. In this thesis the isolation and suppression of forced oscillations is performed based on a single aggregated wind farm. Further work can be carried out on the choice of the optimal locations and coordination of multiple wind farms in the context of a bigger power system.

APPENDIX A

Table A-1 Simulation parameters of the DFIGs [44]

Symbol	QUANTITY	Value
Sb	Rated MVA	2.2 MVA
Vb	Rated Stator Voltage (line-to-line RMS)	0.69 kV
fb	Rated Frequency	60 Hz
Rs	Stator Resistance	$0.00462\ p.u.$
Rr	Rotor Resistance	$0.0060\ p.u.$
Xs	Stator Leakage Reactance	$0.102\ p.u.$
Xr	Rotor Leakage Reactance	$0.08596\ p.u.$
Lm	Unsaturated Magnetizing Reactance	$4.348\ p.u.$
H	Integrated Inertia Constant	5.05 s
Cd	DC-link Capacitance of the Rotor-side Converters	10 mF
Li	Grid-side Inductance of the Rotor-side Converters	100 μH
Ri	Grid-side Resistance of the Rotor-side Converters	0.0015 Ω
Twye	Three-winding Transformer Turn Ratio	$22/0.69/0.69$

Table A-2 Simulation parameters of the PMSGs [167]

Symbol	QUANTITY	Value
Sb	Rated MVA	2.0 MVA
Vb	Rated Stator Voltage (line-to-line RMS)	4 kV
fb	Rated Frequency	3.77 Hz
Xs	Stator Leakage Reactance	$0.1\ p.u.$
Xmd	D-axis Unsaturated Magnetizing Reactance	$0.65\ p.u.$
Xld	D-axis Damper Leakage Reactance	$2.5\ p.u.$
Xmq	Q-axis Magnetizing Reactance	$1.0\ p.u.$
Xlq	Q-axis Damper Leakage Reactance	$2.5\ p.u.$
Rs	Stator Resistance	$0.01\ p.u.$
Rd	D-axis Damper Resistance	$2.0\ p.u.$
Rq	Q-axis Damper Resistance	$2.0\ p.u.$
Psim	Magnetic Strength	$1.3\ Norm$
H	Inertia Constant	5.05 s
Cd	DC-link Capacitance of the Rotor-side Converters	5 mF
Tratio	Transformer Turn Ratio	$33/4$

Table A-3 Simulation parameters of the FSIGs [168]

Symbol	QUANTITY	Value
Sb	Rated MVA	0.4 MVA
Vb	Rated Stator Voltage (line-to-line RMS)	0.825 kV
fb	Rated Frequency	60 Hz
Xr	Stator Resistance	$0.00365\ p.u.$
Xs	Stator Leakage Reactance	$0.06\ p.u.$
Lm	Unsaturated Magnetizing Reactance	$3.0\ p.u.$
Rfd	First Cage Rotor Resistance	$0.0039\ p.u.$
Xfd	First Cage Rotor Leakage Reactance	$0.1203\ p.u.$

LIST OF PUBLICATIONS & OUTCOMES

1. **Xianxian Zhao**, Zuanhong Yan, and Xiao-Ping Zhang, "A wind-wave farm system with self-energy storage and smoothed power output," *IEEE Access*. vol. 4, pp. 8634-8642, Nov. 2016.

2. **Xianxian Zhao**, Zuanhong Yan, Ying Xue, and Xiao-Ping Zhang, "Wind Power Smoothing by Controlling the Inertial Energy of Turbines With Optimized Energy Yield," *IEEE Access*, vol. 5, pp. 23374-23382, Sep. 2017.

3. **Xianxian Zhao**, Ying Xue, and Xiao-Ping Zhang, "Isolation and Suppression of Forced Oscillations by Controlling Wind Farm Inertial Energy," *IEEE Transactions on Sustainable Energy,* under review.

REFRENCES

[1] B. Harris. How climate change threatens food security [Online]. Available: http://climateandcapitalism.com/2009/01/22/how-climate-change-threatens-food-security/ accessed on 24th Feb, 2018

[2] S. Chu, Y. Cui, and N. Liu, "The path towards sustainable energy," *Nature materials*, vol. 16, no. 1, p. 16, 2017.

[3] M. Höök and X. Tang, "Depletion of fossil fuels and anthropogenic climate change—a review," *Energy Policy*, vol. 52, pp. 797-809, 2013.

[4] International Energy Agency (IEA). CO2 emissions from fuel combustion—2017 edition [Online]. Available: https://www.iea.org/publications/freepublications/publication/CO2EmissionsfromFuelCombustionHighlights2017.pdf accessed on 24th Feb, 2018

[5] International Energy Agency (IEA). World energy outlook 2017 [Online]. Available: https://www.iea.org/weo2017/ accessed on 24th Feb, 2018

[6] International Panel on Climate Change (IPCC). Climate change 2014-mitigation of climate change: working group III contribution to the fifth assessment report (Chapter 7) [Online]. Available: http://www.ipcc.ch/pdf/assessment-report/ar5/wg3/ipcc_wg3_ar5_chapter7.pdf accessed on 24th Feb, 2018

[7] N. Stern, "The economics of climate change," *American Economic Review*, vol. 98, no. 2, pp. 1-37, 2008.

[8] D. P. van Vuuren *et al.*, "Energy, land-use and greenhouse gas emissions trajectories under a green growth paradigm," *Global Environmental Change*, vol. 42, pp. 237-250, 2017.

[9] X. Liang, "Emerging power quality challenges due to integration of renewable energy sources," *IEEE Transactions on Industry Applications*, vol. 53, no. 2, pp. 855-866, 2017.

[10] Electricity Networks Strategy Group. ENSG 'Our electricity transmission network: a vision for 2020' [Online]. Available: https://www.gov.uk/government/uploads/system/uploads/attachment_data/file/48274/4263-ensgFull.pdf accessed on 24th Feb, 2018

[11] U.S. Energy Information Administration (EIA). Annual energy outlook 2018 with projections to 2050 [Online]. Available: https://www.eia.gov/outlooks/aeo/pdf/AEO2018_FINAL_PDF.pdf accessed on 24th Feb, 2018

[12] K. Gunn and C. Stock-Williams, "Quantifying the global wave power resource," *Renewable Energy*, vol. 44, pp. 296-304, 2012.

[13] International Energy Agency (IEA). Key world energy statistics [Online]. Available: http://www.iea.org/publications/freepublications/publication/kwes.pdf accessed on 24th Feb, 2018

[14] T. K. Brekken, H. T. Ozkan-Haller, and A. Simmons, "A methodology for large-scale ocean wave power time-series generation," *IEEE Journal of Oceanic Engineering*, vol. 37, no. 2, pp. 294-300, 2012.

[15] M. Lehmann, F. Karimpour, C. A. Goudey, P. T. Jacobson, and M.-R. Alam, "Ocean wave energy in the United States: Current status and future perspectives," *Renewable and Sustainable Energy Reviews,* vol. 74, pp. 1300-1313, 2017.

[16] A. Clément *et al.*, "Wave energy in Europe: current status and perspectives," *Renewable and Sustainable Energy Reviews,* vol. 6, no. 5, pp. 405-431, 2002.

[17] L. Ran *et al.*, "Power conversion and control for a linear direct drive permanent magnet generator for wave energy," *IET Renewable Power Generation,* vol. 5, no. 1, pp. 1-9, 2011.

[18] B. Drew, A. R. Plummer, and M. N. Sahinkaya, "A review of wave energy converter technology," in *Proceedings of the Institution of Mechanical Engineers, Part A: Journal of Power and Energy*, vol. 223, pp. 887–902, 2009.

[19] D. Zhang, W. Li, and Y. Lin, "Wave energy in China: current status and perspectives," *Renewable Energy,* vol. 34, no. 10, pp. 2089-2092, 2009.

[20] R. Henderson, "Design, simulation, and testing of a novel hydraulic power take-off system for the Pelamis wave energy converter," *Renewable Energy,* vol. 31, no. 2, pp. 271-283, 2006.

[21] F. Wu, X.-P. Zhang, P. Ju, and M. J. Sterling, "Modeling and control of AWS-based wave energy conversion system integrated into power grid," *IEEE Transactions on Power Systems,* vol. 23, no. 3, pp. 1196-1204, 2008.

[22] H. Polinder and M. Scuotto, "Wave energy converters and their impact on power systems," in *International Conference on Future Power Systems*, vol. 18, pp. 618–623, 2005.

[23] S. Ceballos, J. Rea, I. Lopez, J. Pou, E. Robles, and D. L. O'Sullivan, "Efficiency optimization in low inertia wells turbine-oscillating water column devices," *IEEE Transactions on Energy Conversion*, vol. 28, no. 3, pp. 553-564, 2013.

[24] A. Blavette, D. L. O'Sullivan, R. Alcorn, T. W. Lewis, and M. G. Egan, "Impact of a medium-size wave farm on grids of different strength levels," *IEEE Transactions on Power Systems,* vol. 29, no. 2, pp. 917-923, 2014.

[25] M.-F. Hsieh, I.-H. Lin, D. G. Dorrell, M.-J. Hsieh, and C.-C. Lin, "Development of a wave energy converter using a two chamber oscillating water column," *IEEE Transactions on Sustainable Energy,* vol. 3, no. 3, pp. 482-497, 2012.

[26] S. Armstrong, E. Cotilla-Sanchez, and T. Kovaltchouk, "Assessing the impact of the grid-connected pacific marine energy center wave farm," *IEEE Journal of Emerging and Selected Topics in Power Electronics,* vol. 3, no. 4, pp. 1011-1020, 2015.

[27] E. Lejerskog, C. Boström, L. Hai, R. Waters, and M. Leijon, "Experimental results on power absorption from a wave energy converter at the Lysekil wave energy research site," *Renewable Energy,* vol. 77, pp. 9-14, 2015.

[28] T. Kovaltchouk, A. Blavette, J. Aubry, H. B. Ahmed, and B. Multon, "Comparison between centralized and decentralized storage energy management for Direct Wave Energy Converter Farm," *IEEE Transactions on Energy Conversion,* vol. 31, no. 3, pp. 1051-1058, 2016.

[29] R. Salim, M. Oleskovicz, and R. Ramos, "Power quality of distributed generation systems as affected by electromechanical oscillations–definitions and possible solutions," *IET Generation, Transmission & Distribution,* vol. 5, no. 11, pp. 1114-1123, 2011.

[30] P. K. Ray, S. R. Mohanty, and N. Kishor, "Classification of power quality disturbances due to environmental characteristics in distributed generation system," *IEEE Transactions on sustainable energy*, vol. 4, no. 2, pp. 302-313, 2013.

[31] M. Prodanovic and T. C. Green, "High-quality power generation through distributed control of a power park microgrid," *IEEE Transactions on Industrial Electronics*, vol. 53, no. 5, pp. 1471-1482, 2006.

[32] M. Rahm, O. Svensson, C. Boström, R. Waters, and M. Leijon, "Experimental results from the operation of aggregated wave energy converters," *IET Renewable Power Generation*, vol. 6, no. 3, pp. 149-160, 2012.

[33] E. Tedeschi and M. Santos-Mugica, "Modeling and control of a wave energy farm including energy storage for power quality enhancement: the bimep case study," *IEEE Transactions on Power Systems*, vol. 29, no. 3, pp. 1489-1497, 2014.

[34] J. F. DeCarolis and D. W. Keith, "The costs of wind's variability: is there a threshold?," *The Electricity Journal*, vol. 18, no. 1, pp. 69-77, 2005.

[35] Global Wind Energy Council. Global wind statistics 2017 [Online]. Available: http://gwec.net/wp-content/uploads/vip/GWEC_PRstats2017_EN-003_FINAL.pdf accessed on 24th Feb, 2018

[36] Global Wind Energy Council. Global wind energy outlook 2014 [Online]. Available: https://www.gwec.net/wp-content/uploads/2014/10/GWEO2014_WEB.pdf accessed on 24th Feb, 2018

[37] U.S. Energy Information Administration (EIA). International energy outlook 2017 [Online]. Available: https://www.eia.gov/outlooks/ieo/pdf/0484(2017).pdf accessed on 24th Feb, 2018

[38] G. Ren, J. Liu, J. Wan, Y. Guo, and D. Yu, "Overview of wind power intermittency: Impacts, measurements, and mitigation solutions," *Applied Energy*, vol. 204, pp. 47-65, 2017.

[39] V. Yaramasu, B. Wu, P. C. Sen, S. Kouro, and M. Narimani, "High-power wind energy conversion systems: State-of-the-art and emerging technologies," *Proceedings of the IEEE*, vol. 103, no. 5, pp. 740-788, 2015.

[40] G. Abad, J. Lopez, M. Rodriguez, L. Marroyo, and G. Iwanski, *Doubly fed induction machine: modeling and control for wind energy generation*. John Wiley & Sons, 2011.

[41] H. Li and Z. Chen, "Overview of different wind generator systems and their comparisons," *IET Renewable Power Generation*, vol. 2, no. 2, pp. 123-138, 2008.

[42] Y. Duan and R. G. Harley, "Present and future trends in wind turbine generator designs," in *Proceedings of IEEE Power Electronics and Machines in Wind Applications*, pp. 1-6, 2009.

[43] D. J. Trudnowski, A. Gentile, J. M. Khan, and E. M. Petritz, "Fixed-speed wind-generator and wind-park modeling for transient stability studies," *IEEE Transactions on Power Systems*, vol. 19, no. 4, pp. 1911-1917, 2004.

[44] R. Pena, J. Clare, and G. Asher, "Doubly fed induction generator using back-to-back PWM converters and its application to variable-speed wind-energy generation," *IEE Proceedings-Electric Power Applications*, vol. 143, no. 3, pp. 231-241, 1996.

[45] N. R. Ullah, T. Thiringer, and D. Karlsson, "Temporary primary frequency control support by variable speed wind turbines—Potential and applications," *IEEE Transactions on Power Systems*, vol. 23, no. 2, pp. 601-612, 2008.

[46] J. M. Mauricio, A. Marano, A. Gómez-Expósito, and J. L. M. Ramos, "Frequency regulation contribution through variable-speed wind energy conversion systems," *IEEE Transactions on Power Systems,* vol. 24, no. 1, pp. 173-180, 2009.

[47] G. Lalor, A. Mullane, and M. O'Malley, "Frequency control and wind turbine technologies," *IEEE Transactions on Power Systems,* vol. 20, no. 4, pp. 1905-1913, 2005.

[48] L. Xie *et al.*, "Wind integration in power systems: Operational challenges and possible solutions," *Proceedings of the IEEE,* vol. 99, no. 1, pp. 214-232, 2011.

[49] J. Morren, S. W. De Haan, W. L. Kling, and J. Ferreira, "Wind turbines emulating inertia and supporting primary frequency control," *IEEE Transactions on Power Systems,* vol. 21, no. 1, pp. 433-434, 2006.

[50] J. Morren, J. Pierik, and S. W. De Haan, "Inertial response of variable speed wind turbines," *Electric Power Systems Research,* vol. 76, no. 11, pp. 980-987, 2006.

[51] S. Wang, J. Hu, X. Yuan, and L. Sun, "On inertial dynamics of virtual-synchronous-controlled DFIG-based wind turbines," *IEEE Transactions on Energy Conversion,* vol. 30, no. 4, pp. 1691-1702, 2015.

[52] Q.-C. Zhong, Z. Ma, W.-L. Ming, and G. C. Konstantopoulos, "Grid-friendly wind power systems based on the synchronverter technology," *Energy Conversion and Management,* vol. 89, pp. 719-726, 2015.

[53] B. C. Ummels, M. Gibescu, E. Pelgrum, W. L. Kling, and A. J. Brand, "Impacts of wind power on thermal generation unit commitment and dispatch," *IEEE Transactions on Energy Conversion,* vol. 22, no. 1, pp. 44-51, 2007.

[54] P. Sorensen *et al.*, "Power fluctuations from large wind farms," *IEEE Transactions on Power Systems,* vol. 22, no. 3, pp. 958-965, 2007.

[55] P. P. Barker and R. W. De Mello, "Determining the impact of distributed generation on power systems. I. Radial distribution systems," in *Proceedings of IEEE Power Engineering Society Summer Meeting*, vol. 3, pp. 1645-1656, 2000.

[56] Q. Jiang and H. Wang, "Two-time-scale coordination control for a battery energy storage system to mitigate wind power fluctuations," *IEEE Transactions on Energy Conversion,* vol. 28, no. 1, pp. 52-61, 2013.

[57] D. S. Dolan and P. W. Lehn, "Simulation model of wind turbine 3p torque oscillations due to wind shear and tower shadow," *IEEE Transactions on Energy Conversion,* vol. 21, no. 3, pp. 717-724, 2006.

[58] F. M. Hughes, O. Anaya-Lara, G. Ramtharan, N. Jenkins, and G. Strbac, "Influence of tower shadow and wind turbulence on the performance of power system stabilizers for DFIG-based wind farms," *IEEE Transactions on Energy Conversion,* vol. 23, no. 2, pp. 519-528, 2008.

[59] W. Meng, Q. Yang, Y. Ying, Y. Sun, Z. Yang, and Y. Sun, "Adaptive power capture control of variable-speed wind energy conversion systems with guaranteed transient and steady-state performance," *IEEE Transactions on Energy Conversion,* vol. 28, no. 3, pp. 716-725, 2013.

[60] T. Sun, Z. Chen, and F. Blaabjerg, "Flicker study on variable speed wind turbines with doubly fed induction generators," *IEEE Transactions on Energy Conversion,* vol. 20, no. 4, pp. 896-905, 2005.

[61] A. Larsson, "Flicker emission of wind turbines during continuous operation," *IEEE transactions on Energy Conversion,* vol. 17, no. 1, pp. 114-118, 2002.

[62] W. Hu, C. Su, and Z. Chen, "Impact of wind shear and tower shadow effects on power system with large scale wind power penetration," in *Proceedings of IEEE 37th Annual Conference on IEEE Industrial Electronics Society*, pp. 878-883, 2011.

[63] C. Su, W. Hu, Z. Chen, and Y. Hu, "Mitigation of power system oscillation caused by wind power fluctuation," *IET Renewable Power Generation,* vol. 7, no. 6, pp. 639-651, 2013.

[64] M. Chowdhury, N. Hosseinzadeh, and W. Shen, "Smoothing wind power fluctuations by fuzzy logic pitch angle controller," *Renewable Energy*, vol. 38, no. 1, pp. 224-233, 2012.

[65] R. Teodorescu, F. Blaabjerg, S. Munk-Nielsen, L. Helle, T. Abeyasekera, and P. Rodriguez, "An overview of the reliability prediction related aspects of high power IGBTs in wind power applications," *Microelectronics Reliability,* vol. 51, no. 9-11, pp. 1903-1907, 2011.

[66] C. Luo, H. G. Far, H. Banakar, P.-K. Keung, and B.-T. Ooi, "Estimation of wind penetration as limited by frequency deviation," *IEEE Transactions on Energy Conversion,* vol. 22, no. 3, pp. 783-791, 2007.

[67] C. Luo and B.-T. Ooi, "Frequency deviation of thermal power plants due to wind farms," *IEEE Transactions on Energy Conversion,* vol. 21, no. 3, pp. 708-716, 2006.

[68] M. Magdy and F. Coowar, "Frequency domain analysis of power system forced oscillations," *IEE Proceedings-Generation, Transmission and Distribution*, vol. 137, no. 4, pp. 261-268, 1990.

[69] C. Vournas, N. Krassas, and B. Papadias, "Analysis of forced oscillations in a multimachine power system," in *Control 1991. Control'91., International Conference on*, 1991, pp. 443-448: IET.

[70] H. Ye, Y. Liu, P. Zhang, and Z. Du, "Analysis and detection of forced oscillation in power system," *IEEE Transactions on Power Systems,* vol. 32, no. 2, pp. 1149-1160, 2017.

[71] S. Feng, X. Wu, P. Jiang, L. Xie, and J. Lei, "Mitigation of power system forced oscillations: an E-STATCOM approach," *IEEE Access*, 2017.

[72] J. Ma, P. Zhang, H.-j. Fu, B. Bo, and Z.-y. Dong, "Application of phasor measurement unit on locating disturbance source for low-frequency oscillation," *IEEE Transactions on Smart Grid,* vol. 1, no. 3, pp. 340-346, 2010.

[73] L. Vanfretti *et al.*, "Application of ambient analysis techniques for the estimation of electromechanical oscillations from measured PMU data in four different power systems," *International Transactions on Electrical Energy Systems,* vol. 21, no. 4, pp. 1640-1656, 2011.

[74] M. Ghorbaniparvar, "Survey on forced oscillations in power system," *Journal of Modern Power Systems and Clean Energy*, vol. 5, no. 5, pp. 671-682, 2017.

[75] P. Kundur, N. J. Balu, and M. G. Lauby, *Power system stability and control*. McGraw-hill New York, 1994.

[76] K. R. Rao and L. Jenkins, "Studies on power systems that are subjected to cyclic loads," *IEEE transactions on power systems*, vol. 3, no. 1, pp. 31-37, 1988.

[77] J. Pinneilo and J. Van Ness, "Dynamic response of a large power system to a cyclic load produced by a nuclear accelerator," *IEEE Transactions on Power Apparatus and Systems,* no. 4, pp. 1856-1862, 1971.

[78] J. Van Ness, "Response of large power systems to cyclic load variations," *IEEE Transactions on Power Apparatus and Systems,* no. 7, pp. 723-727, 1966.

[79] N. Rostamkolai, R. Piwko, and A. Matusik, "Evaluation of the impact of a large cyclic load on the LILCO power system using time simulation and frequency domain techniques," *IEEE transactions on power systems,* vol. 9, no. 3, pp. 1411-1416, 1994.

[80] W. Xuanyin, L. Xiaoxiao, and L. Fushang, "Analysis on oscillation in electro-hydraulic regulating system of steam turbine and fault diagnosis based on PSOBP," *Expert Systems with Applications,* vol. 37, no. 5, pp. 3887-3892, 2010.

[81] T. J. Larsen and T. D. Hanson, "A method to avoid negative damped low frequent tower vibrations for a floating, pitch controlled wind turbine," in *Journal of Physics: Conference Series*, 2007, vol. 75, no. 1, p. 012073: IOP Publishing.

[82] S. A. N. Sarmadi, V. Venkatasubramanian, and A. Salazar, "Analysis of November 29, 2005 western American oscillation event," *IEEE Transactions on Power Systems,* vol. 31, no. 6, pp. 5210-5211, 2016.

[83] M. Xiao and Z. Liang, "Analysis on the forced oscillation failure in China Southern Power Grid and its handling measures," *Nanfang Dianwang Jishu,* vol. 6, no. 2, pp. 51-54, 2012.

[84] F. d. O. Antonio, "Modelling and control of oscillating-body wave energy converters with hydraulic power take-off and gas accumulator," *Ocean engineering,* vol. 34, no. 14-15, pp. 2021-2032, 2007.

[85] M. Ruellan, H. BenAhmed, B. Multon, C. Josset, A. Babarit, and A. Clement, "Design methodology for a SEAREV wave energy converter," *IEEE Transactions on Energy Conversion,* vol. 25, no. 3, pp. 760-767, 2010.

[86] N. Hodgins, O. Keysan, A. S. McDonald, and M. A. Mueller, "Design and testing of a linear generator for wave-energy applications," *IEEE Transactions on Industrial Electronics,* vol. 59, no. 5, pp. 2094-2103, 2012.

[87] J. K.-H. Shek, D. E. Macpherson, M. A. Mueller, and J. Xiang, "Reaction force control of a linear electrical generator for direct drive wave energy conversion," *IET renewable power generation,* vol. 1, no. 1, pp. 17-24, 2007.

[88] M. Alberdi, M. Amundarain, A. Garrido, I. Garrido, O. Casquero, and M. De la Sen, "Complementary control of oscillating water column-based wave energy conversion plants to improve the instantaneous power output," *IEEE Transactions on Energy Conversion,* vol. 26, no. 4, pp. 1021-1032, 2011.

[89] F. Wu, X. Zhang, and P. Ju, "Application of the battery energy storage in wave energy conversion system," in *Sustainable Power Generation and Supply, 2009. SUPERGEN'09. International Conference on*, 2009, pp. 1-4: IEEE.

[90] T. Kovaltchouk, B. Multon, H. B. Ahmed, J. Aubry, and P. Venet, "Enhanced aging model for supercapacitors taking into account power cycling: Application to the sizing of an energy storage system in a direct wave energy converter," *IEEE Transactions on Industry Applications,* vol. 51, no. 3, pp. 2405-2414, 2015.

[91] D. B. Murray, J. G. Hayes, D. L. O'Sullivan, and M. G. Egan, "Supercapacitor testing for power smoothing in a variable speed offshore wave energy converter," *IEEE Journal of Oceanic Engineering,* vol. 37, no. 2, pp. 301-308, 2012.

[92] G. Brando, A. Dannier, A. Del Pizzo, L. P. Di Noia, and C. Pisani, "Grid connection of wave energy converter in heaving mode operation by supercapacitor storage technology," *IET Renewable Power Generation,* vol. 10, no. 1, pp. 88-97, 2016.

[93] T. Yoshida, M. Sanada, S. Morimoto, and Y. Inoue, "Study of flywheel energy storage system for power leveling of wave power generation system," in *Electrical Machines and Systems (ICEMS), 2012 15th International Conference on*, 2012, pp. 1-5: IEEE.

[94] Z. Nie, X. Xiao, Q. Kang, R. Aggarwal, H. Zhang, and W. Yuan, "SMES-battery energy storage system for conditioning outputs from direct drive linear wave energy converters," *IEEE Transactions on Applied Superconductivity*, vol. 23, no. 3, pp. 5000705-5000705, 2013.

[95] H. Zhang *et al.*, "Design and simulation of SMES system using YBCO tapes for direct drive wave energy converters," *IEEE Transactions on Applied Superconductivity*, vol. 23, no. 3, pp. 5700704-5700704, 2013.

[96] M. Rahm, C. Boström, O. Svensson, M. Grabbe, F. Bülow, and M. Leijon, "Offshore underwater substation for wave energy converter arrays," *IET Renewable Power Generation*, vol. 4, no. 6, pp. 602-612, 2010.

[97] A. M. Howlader, N. Urasaki, A. Yona, T. Senjyu, and A. Y. Saber, "A review of output power smoothing methods for wind energy conversion systems," *Renewable and Sustainable Energy Reviews*, vol. 26, pp. 135-146, 2013.

[98] M. H. Qais, H. M. Hasanien, and S. Alghuwainem, "Output power smoothing of grid-connected permanent magnet synchronous generator driven directly by variable speed wind turbine: a review," *Journal of Engineering*, 2017.

[99] F. Díaz-González, A. Sumper, O. Gomis-Bellmunt, and R. Villafáfila-Robles, "A review of energy storage technologies for wind power applications," *Renewable and Sustainable Energy Reviews*, vol. 16, no. 4, pp. 2154-2171, 2012.

[100] M. Jannati, S. Hosseinian, B. Vahidi, and G.-J. Li, "A survey on energy storage resources configurations in order to propose an optimum configuration for smoothing fluctuations of future large wind power plants," *Renewable and Sustainable Energy Reviews*, vol. 29, pp. 158-172, 2014.

[101] T. Ayodele and A. Ogunjuyigbe, "Mitigation of wind power intermittency: Storage technology approach," *Renewable and Sustainable Energy Reviews*, vol. 44, pp. 447-456, 2015.

[102] N. A. Ahmed, M. Miyatake, and A. Al-Othman, "Power fluctuations suppression of stand-alone hybrid generation combining solar photovoltaic/wind turbine and fuel cell systems," *Energy Conversion and Management*, vol. 49, no. 10, pp. 2711-2719, 2008.

[103] X. Li, "Fuzzy adaptive Kalman filter for wind power output smoothing with battery energy storage system," *IET Renewable Power Generation*, vol. 6, no. 5, pp. 340-347, 2012.

[104] X. Li, D. Hui, and X. Lai, "Battery energy storage station (BESS)-based smoothing control of photovoltaic (PV) and wind power generation fluctuations," *IEEE Transactions on Sustainable Energy*, vol. 4, no. 2, pp. 464-473, 2013.

[105] S. Muyeen, R. Takahashi, M. H. Ali, T. Murata, and J. Tamura, "Transient stability augmentation of power system including wind farms by using ECS," *IEEE Transactions on Power Systems*, vol. 23, no. 3, pp. 1179-1187, 2008.

[106] S. Muyeen, R. Takahashi, T. Murata, and J. Tamura, "Integration of an energy capacitor system with a variable-speed wind generator," *IEEE Transactions on Energy Conversion*, vol. 24, no. 3, pp. 740-749, 2009.

[107] C. Abbey and G. Joos, "Supercapacitor energy storage for wind energy applications," *IEEE Transactions on Industry Applications*, vol. 43, no. 3, pp. 769-776, 2007.

[108] M. Ammar and G. Joós, "A short-term energy storage system for voltage quality improvement in distributed wind power," *IEEE Transactions on Energy Conversion,* vol. 29, no. 4, pp. 997-1007, 2014.

[109] S. I. Gkavanoudis and C. S. Demoulias, "A combined fault ride-through and power smoothing control method for full-converter wind turbines employing Supercapacitor Energy Storage System," *Electric Power Systems Research,* vol. 106, pp. 62-72, 2014.

[110] H. M. Hasanien, "A set-membership affine projection algorithm-based adaptive-controlled SMES units for wind farms output power smoothing," *IEEE Transactions on Sustainable Energy,* vol. 5, no. 4, pp. 1226-1233, 2014.

[111] T. Kinjo, T. Senjyu, N. Urasaki, and H. Fujita, "Terminal-voltage and output-power regulation of wind-turbine generator by series and parallel compensation using SMES," *IEE Proceedings Generation, Transmission and Distribution,* vol. 153, no. 3, pp. 276-282, 2006.

[112] S. Nomura, Y. Ohata, T. Hagita, H. Tsutsui, S. Tsuji-Iio, and R. Shimada, "Wind farms linked by SMES systems," *IEEE Transactions on Applied Superconductivity,* vol. 15, no. 2, pp. 1951-1954, 2005.

[113] F. Zhou, G. Joós, C. Abbey, L. Jiao, and B. T. Ooi, "Use of large capacity SMES to improve the power quality and stability of wind farms," in *Proceedings of IEEE Power Engineering Society General Meeting*, pp. 2025-2030, 2004.

[114] S.-S. Chen, L. Wang, W.-J. Lee, and Z. Chen, "Power flow control and damping enhancement of a large wind farm using a superconducting magnetic energy storage unit," *IET Renewable Power Generation,* vol. 3, no. 1, pp. 23-38, 2009.

[115] F. Díaz-González, A. Sumper, O. Gomis-Bellmunt, and F. D. Bianchi, "Energy management of flywheel-based energy storage device for wind power smoothing," *Applied Energy,* vol. 110, pp. 207-219, 2013.

[116] F. Diaz-Gonzalez, F. D. Bianchi, A. Sumper, and O. Gomis-Bellmunt, "Control of a flywheel energy storage system for power smoothing in wind power plants," *IEEE Transactions on Energy Conversion,* vol. 29, no. 1, pp. 204-214, 2014.

[117] A. K. Arani, H. Karami, G. Gharehpetian, and M. Hejazi, "Review of Flywheel Energy Storage Systems structures and applications in power systems and microgrids," *Renewable and Sustainable Energy Reviews,* vol. 69, pp. 9-18, 2017.

[118] R. Cárdenas, R. Peña, G. Asher, and J. Clare, "Power smoothing in wind generation systems using a sensorless vector controlled induction machine driving a flywheel," *IEEE Transactions on Energy Conversion,* vol. 19, no. 1, pp. 206-216, 2004.

[119] G. O. Cimuca, C. Saudemont, B. Robyns, and M. M. Radulescu, "Control and performance evaluation of a flywheel energy-storage system associated to a variable-speed wind generator," *IEEE Transactions on Industrial Electronics,* vol. 53, no. 4, pp. 1074-1085, 2006.

[120] G. Suvire and P. Mercado, "Active power control of a flywheel energy storage system for wind energy applications," *IET Renewable Power Generation,* vol. 6, no. 1, pp. 9-16, 2012.

[121] W. Li, G. Joós, and J. Bélanger, "Real-time simulation of a wind turbine generator coupled with a battery supercapacitor energy storage system," *IEEE Transactions on Industrial Electronics,* vol. 57, no. 4, pp. 1137-1145, 2010.

[122] P. D. Lund, J. Lindgren, J. Mikkola, and J. Salpakari, "Review of energy system flexibility measures to enable high levels of variable renewable electricity," *Renewable and Sustainable Energy Reviews*, vol. 45, pp. 785-807, 2015.

[123] M. Liserre, R. Cardenas, M. Molinas, and J. Rodriguez, "Overview of multi-MW wind turbines and wind parks," *IEEE Transactions on Industrial Electronics*, vol. 58, no. 4, pp. 1081-1095, 2011.

[124] Z. Qin, F. Blaabjerg, and P. C. Loh, "A rotating speed controller design method for power leveling by means of inertia energy in wind power systems," *IEEE Transactions on Energy Conversion*, vol. 30, no. 3, pp. 1052-1060, 2015.

[125] T. Senjyu, R. Sakamoto, N. Urasaki, T. Funabashi, H. Fujita, and H. Sekine, "Output power leveling of wind turbine generator for all operating regions by pitch angle control," *IEEE Transactions on Energy Conversion*, vol. 21, no. 2, pp. 467-475, 2006.

[126] M. Q. Duong, F. Grimaccia, S. Leva, M. Mussetta, and E. Ogliari, "Pitch angle control using hybrid controller for all operating regions of SCIG wind turbine system," *Renewable Energy*, vol. 70, pp. 197-203, 2014.

[127] Y. Zhang, Z. Chen, W. Hu, and M. Cheng, "Flicker mitigation by individual pitch control of variable speed wind turbines with DFIG," *IEEE Transactions on Energy Conversion*, vol. 29, no. 1, pp. 20-28, 2014.

[128] W. Hu, Z. Chen, Y. Wang, and Z. Wang, "Flicker mitigation by active power control of variable-speed wind turbines with full-scale back-to-back power converters," *IEEE Transactions on Energy Conversion*, vol. 24, no. 3, pp. 640-649, 2009.

[129] A. Abedini and A. Nasiri, "Output power smoothing for wind turbine permanent magnet synchronous generators using rotor inertia," *Electric Power Components and Systems*, vol. 37, no. 1, pp. 1-19, 2008.

[130] S. G. Varzaneh, G. Gharehpetian, and M. Abedi, "Output power smoothing of variable speed wind farms using rotor-inertia," *Electric Power Systems Research*, vol. 116, pp. 208-217, 2014.

[131] A. Uehara *et al.*, "A coordinated control method to smooth wind power fluctuations of a PMSG-based WECS," *IEEE Transactions on Energy Conversion*, vol. 26, no. 2, pp. 550-558, 2011.

[132] A. M. Howlader, T. Senjyu, and A. Y. Saber, "An integrated power smoothing control for a grid-interactive wind farm considering wake effects," *IEEE Systems Journal*, vol. 9, no. 3, pp. 954-965, 2015.

[133] B. G. Rawn, P. W. Lehn, and M. Maggiore, "Control methodology to mitigate the grid impact of wind turbines," *IEEE Transactions on Energy Conversion*, vol. 22, no. 2, pp. 431-438, 2007.

[134] L. Ran, J. Bumby, and P. Tavner, "Use of turbine inertia for power smoothing of wind turbines with a DFIG," in *Proceeding of IEEE International Conference on Harmonics and Quality of Power*, pp. 106-111, 2004.

[135] C. Luo, H. Banakar, B. Shen, and B.-T. Ooi, "Strategies to smooth wind power fluctuations of wind turbine generator," *IEEE Transactions on Energy Conversion*, vol. 22, no. 2, pp. 341-349, 2007.

[136] S. De Rijcke, J. Driesen, and J. Meyers, "Power smoothing in large wind farms using optimal control of rotating kinetic energy reserves," *Wind Energy*, vol. 18, no. 10, pp. 1777-1791, 2015.

[137] C. Huang, F. Li, T. Ding, Z. Jin, and X. Ma, "Second-order cone programming-based optimal control strategy for wind energy conversion systems over complete operating regions," *IEEE Transactions on Sustainable Energy*, vol. 6, no. 1, pp. 263-271, 2015.

[138] X. Wang and K. Turitsyn, "Data-driven diagnostics of mechanism and source of sustained oscillations," *IEEE Transactions on Power Systems*, vol. 31, no. 5, pp. 4036-4046, 2016.

[139] T. R. Nudell, S. Nabavi, and A. Chakrabortty, "A real-time attack localization algorithm for large power system networks using graph-theoretic techniques," *IEEE Transactions on Smart Grid*, vol. 6, no. 5, pp. 2551-2559, 2015.

[140] L. Chen, Y. Min, and W. Hu, "An energy-based method for location of power system oscillation source," *IEEE Transactions on Power Systems*, vol. 28, no. 2, pp. 828-836, 2013.

[141] S. A. N. Sarmadi and V. Venkatasubramanian, "Inter-area resonance in power systems from forced oscillations," *IEEE Transactions on Power Systems*, vol. 31, no. 1, pp. 378-386, 2016.

[142] J. Tan, X. Wang, T. Wang, and Y. Zhang, "Alleviation of oscillations power of wind farm using flywheel energy storage," in *Proceedings of IEEE PES General Meeting| Conference & Exposition*, pp. 1-5, 2014.

[143] I. Erlich, F. Shewarega, C. Feltes, F. W. Koch, and J. Fortmann, "Offshore Wind Power Generation Technologies," *Proceedings of the IEEE*, vol. 101, no. 4, pp. 891-905, 2013.

[144] B. Snyder and M. J. Kaiser, "Ecological and economic cost-benefit analysis of offshore wind energy," *Renewable Energy*, vol. 34, no. 6, pp. 1567-1578, 2009.

[145] C. Pérez-Collazo, D. Greaves, and G. Iglesias, "A review of combined wave and offshore wind energy," *Renewable and Sustainable Energy Reviews*, vol. 42, pp. 141-153, 2015.

[146] S. Astariz and G. Iglesias, "Output power smoothing and reduced downtime period by combined wind and wave energy farms," *Energy*, vol. 97, pp. 69-81, 2016.

[147] E. D. Stoutenburg and M. Z. Jacobson, "Reducing offshore transmission requirements by combining offshore wind and wave farms," *IEEE Journal of Oceanic Engineering*, vol. 36, no. 4, pp. 552-561, 2011.

[148] E. Tedeschi, E. Robles, M. Santos, O. Duperray, and F. Salcedo, "Effect of energy storage on a combined wind and wave energy farm," in *Proceedings of IEEE Energy Conversion Congress and Exposition*, pp. 2798-2804, 2012.

[149] Y. Kim, M. Kang, E. Muljadi, J.-W. Park, and Y. C. Kang, "Power smoothing of a variable-speed wind turbine generator in association with the rotor-speed-dependent gain," *IEEE Transactions on Sustainable Energy*, vol. 8, no. 3, pp. 990-999, 2017.

[150] M. Wang-Hansen, R. Josefsson, and H. Mehmedovic, "Frequency controlling wind power modeling of control strategies," *IEEE Transactions on Sustainable Energy*, vol. 4, no. 4, pp. 954-959, 2013.

[151] Y. Wang, J. Meng, X. Zhang, and L. Xu, "Control of PMSG-based wind turbines for system inertial response and power oscillation damping," *IEEE Transactions on Sustainable Energy*, vol. 6, no. 2, pp. 565-574, 2015.

[152] J. L. Domínguez-García, O. Gomis-Bellmunt, F. D. Bianchi, and A. Sumper, "Power oscillation damping supported by wind power: A review," *Renewable and Sustainable Energy Reviews*, vol. 16, no. 7, pp. 4994-5006, 2012.

[153] C. Zhang, D. Ke, Y. Sun, C. Chung, J. Xu, and F. Shen, "Coordinated Supplementary Damping Control of DFIG and PSS to Suppress Inter-Area Oscillations with Optimally Controlled Plant Dynamics," *IEEE Transactions on Sustainable Energy*, vol. 9, no. 2, pp. 780-791, 2018.

[154] L. Fan, H. Yin, and Z. Miao, "On active/reactive power modulation of DFIG-based wind generation for interarea oscillation damping," *IEEE Transactions on Energy Conversion*, vol. 26, no. 2, pp. 513-521, 2011.

[155] M. Singh, A. J. Allen, E. Muljadi, V. Gevorgian, Y. Zhang, and S. Santoso, "Interarea oscillation damping controls for wind power plants," *IEEE Transactions on Sustainable Energy*, vol. 6, no. 3, pp. 967-975, 2015.

[156] Y. Liu, J. R. Gracia, T. J. King, and Y. Liu, "Frequency regulation and oscillation damping contributions of variable-speed wind generators in the US eastern interconnection (EI)," *IEEE Transactions on Sustainable Energy*, vol. 6, no. 3, pp. 951-958, 2015.

[157] X. Zhao, Z. Yan, and X.-P. Zhang, "A wind-wave farm system with self-energy storage and smoothed power output," *IEEE Access*, vol. 4, pp. 8634-8642, 2016.

[158] R. Cardenas, R. Peña, S. Alepuz, and G. Asher, "Overview of control systems for the operation of DFIGs in wind energy applications," *IEEE Transactions on Industrial Electronics*, vol. 60, no. 7, pp. 2776-2798, 2013.

[159] D. Woodford, "Determination of main Parameters for a Doubly Fed Induction Generator for a Given Turbine Rating," *Technical Report, Electranix Corporation*, Winnipeg, Canada, 2004.

[160] Mathworks, "MATLAB SimPowerSystems documentation: Wind turbine," 2004.

[161] National Renewable Energy Laboratory (NREL). An aeroelastic computer-aided engineering tool for horizontal axis wind turbines [Online]. Available: https://nwtc.nrel.gov/FAST accessed on 19th Mar, 2015

[162] X. Zhao, Z. Yan, Y. Xue, and X.-P. Zhang, "Wind power smoothing by controlling the inertial energy of turbines with optimized energy yield," *IEEE Access*, vol. 5, pp. 23374-23382, 2017.

[163] C. Li, J. Deng, and X.-P. Zhang, "Coordinated design and application of robust damping controllers for shunt FACTS devices to enhance small-signal stability of large-scale power systems," *CSEE Journal of Power and Energy Systems*, vol. 3, no. 4, pp. 399-407, 2017.

[164] National Renewable Energy Laboratory (NREL). An aeroelastic computer-aided engineering tool for horizontal axis wind turbines [Online]. Available: https://nwtc.nrel.gov/FAST accessed on 19th Mar, 2015

[165] P. Kansal and A. Bose, "Bandwidth and latency requirements for smart transmission grid applications," *IEEE Transactions on Smart Grid*, vol. 3, no. 3, pp. 1344-1352, 2012.

[166] X. Zhang, C. Lu, S. Liu, and X. Wang, "A review on wide-area damping control to restrain inter-area low frequency oscillation for large-scale power systems with increasing renewable generation," *Renewable and Sustainable Energy Reviews*, vol. 57, pp. 45-58, 2016.

[167] N. P. Strachan and D. Jovcic, "Stability of a variable-speed permanent magnet wind generator with weak AC grids," *IEEE Transactions on Power Delivery*, vol. 25, no. 4, pp. 2779-2788, 2010.

[168] A. Feijóo, J. Cidrás, and C. Carrillo, "A third order model for the doubly-fed induction machine," *Electric Power Systems Research*, vol. 56, no. 2, p. 121, 2000.